Aus der Abt. Vaskuläre Biologie und Tumorangiogenese
der Medizinischen Fakultät Mannheim
European Center for Angioscience
(Direktor: Prof. Dr. Hellmut Augustin)

The accumulated acrolein in *akr1a1a* zebrafish mutants promotes insulin resistance leading to hyperglycemia and retina vessels alteration.

Inauguraldissertation
zur Erlangung des medizinischen Doktorgrades
der
Medizinischen Fakultät Mannheim
der Ruprecht-Karls-Universität
zu
Heidelberg

vorgelegt von
Haozhe Qi

aus
(Chengdu, China)
(2021)

Dekan: Prof. Dr. med. Sergij Goerdt
Referent(in): Prof. Dr. Jens Kroll

凡是过去，皆为序章。

莎士比亚

"What's past is prologue."

William Shakespeare

CONTENTS

Page

ABBREVIATIONS

C	Degree Celsius
∞	Forever
µl	Microliter
µm	Micrometre
µM	Micromolar
%	Percent
ACR	Acrolein
AGE	Advanced glycation end product
AKR	Aldo keto reduktase
AKT	Protein kinase B
ALDH	Aldehyde dehydrogenase
bp	Base pairs
BSA	Bovine serum albumin
Cas9	CRISPR associated protein 9
CEMA	N-acetyl-S-(carboxyethyl)-L-cysteine
cDNA	Complementary deoxyribonucleic acid
CKD	chronic kidney disease
cm	Centimetre
Con	Control
CoA	Co-enzymeA
CRISPR	Clustered regularly-interspaced short pa
DM	Diabetes
DME	Diabetic macular edema
DLAV	Dorsal longitudinal anastomotic vessel
DKFZ	German Cancer Research Center
DR	Diabetic retinopathy
DN	Diabetic nephropathy
DNA	Deoxyribonucleic acid
dpf	Days after post fertilization
DR	Diabetic retinopathy
EGFP	Enhanced green fluorescent protein
ESRD	End-stage renal disease
ER	Endoplasmic reticulum
eNOS	endothelial nitric oxide synthase
fli1	Friend leukemia integration1
FDP-lysine	acrolein-lysine adduct
g	Gram
GBM	Glomerular basement membrane
GC-MS	Gas chromatography-mass spectrometry
GDM	Gestational diabetes
Glo1	Glyoxalase1
Glut	Glucose transporter
Gly	Glycine
gRNA	Guide RNA
GSEA	Gene set enrichment analysis
GST	glutathione S-transferase
h	Hours
H2O	water

HbA1C	Glycated hemoglobin
HIF1	Hypoxia-inducible transcription factor 1
HK	hexokinase
hpf	Hours after post fertilization
HPLC	High performance liquid chromatography
Hz	Hertz
kb	Kilo bases
KCl	Potassium chloride
l	Litre
IDDM	Insulin-dependent diabetes mellitus
IFG	Impaired fasting glycaemia
IGT	Impaired glucose tolerance
Ins	Preproinsulin
Insb	Preproinsulin b
Insra	Insulin receptor a
Insrb	Insulin receptor b
IOC	Inner optic circle
ISV	Intersegment vessel
LB	Lysogeny broth
LC-MS/MS	Liquid chromatography-tandem mass spectometry
LD50	Median lethal dose
Leu	Leucine
LRP	LDL receptor-related protein
Lys	Lysine
M	Molar
MARD	mild age-related diabetes
MAPK	Mitogen-activated Protein Kinase
MDA	Malondialdehyde
MEF	Mouse Embryonic Fibroblasts
MG	Methylglyoxal
mg	Milligram
min	Minutes
ml	Millilitre
mM	Millimolar
MO	Morpholino
MOD	mild obesity-related diabetes
MODY	maturity onset diabetes of the young
mTORC1	mammalian target of rapamycin complex 1
mRNA	Messenger RNA
n	Number of samples
NaCl	Sodium chloride
NADH	Nicotinamide adenine dinucleotide
NADPH	Nicotinamide adenine dinucleotide phosphate
NCBI	National Center for Biotechnology Information
NDM	Neonatal diabetes mellitus
NF	Normal feeding
NPDR	non-proliferative diabetic retinopathy
nl	Nanolitre
nm	Nanometre
nmol	Nanomole
NOX	NADPH oxidase

OCT	Optical coherence tomography
OGTT	Oral glucose tolerance test
OF	Overfeeding
Orn	Ornithine
p	p-value
PAM	Protospacer adjacent motif
PAS	Periodic acid Schiff
PBS	Phosphate buffered saline
PCA	Principal component analysis
PCR	Polymerase chain reaction
PCOS	polycystic ovary syndrome
PDR	Proliferative diabetic retinopathy
Pdx1	Pancreatic and duodenal homeobox 1
PFA	Paraformaldehyde
PFK	phosphofructokinase
Phe	Phenylalanine
PI3K	Phosphatidylinositol-3-Kinase
PK	pyruvate kinase
PKC	Protein kinase C
PKM2	Pyruvate kinase M2
pmol	Picomol
PNDM	permanent neonatal diabetes mellitus
Pro	Proline
PTU	Phenylthiourea
p70-S6K	ribosomal protein S6 kinase
PUFAs	Polyunsaturated fatty acids
RAS	Renin angiotensin system
RAAS	Renin-angiotensin-aldosterone system
RCS	Reactive carbonyl species
ROS	Reactive-oxygen species
RPE	Retinal pigmented epithelium
rpm	Rounds per minute
RT-PCR	Reverse transcription polymerase chain reaction
RT-qPCR	Real time-quantitative polymerase chain reaction
SAID	Severe autoimmune diabetes
SA	segmental artery
SB	Splice blocking
SNO-CoA	S-nitroso-CoA
SCoR	SNO-CoA reductase
SD	Standard deviation
SDS	Sodium dodecyl sulfate
Ser	Serine
SIDD	Severe insulin-deficient diabetes
SIRD	severe insulin-resistant diabetes
SNOs	S-nitrosothiols
SV	Segmental vein
T1DM	Type 1 diabetes
T2DM	Type 2 diabetes
TCA	Tricarboxylic acid
Tg	Transgenic
Thr	Threonie

Tris	Tris-aminomethan
Tyr	Tyrosine
UCP2	Ultra-performance liquid chromatography with
UPLC-FSR	fluorescence detection
UV	Ultraviolet
Val	Valine
VEGF	Vascular endothelial growth factor
4-HNE	4-Hydroxynonenal
3-HPMA	N-acetyl-S-(3-hydroxypropyl)-L-cysteine
3DG	3-deoxyglucosone

1 INTRODUCTION

1.1 Diabetes mellitus and clinical classifications

Diabetes mellitus (DM), commonly known as diabetes, is a group of metabolic disorders characterized by a high blood glucose level over a prolonged period of time. Lasted high-level blood glucose, which is named hyperglycemia, is usually driven by relatively reduced insulin secretion or insulin resistance due to it is the unique hypoglycemic hormone in vivo. If left untreated, diabetes can cause a series of complications, including but not limited to retinopathy, nephropathy, cardiovascular disease, chronic neural injury, and functional loss(Zheng, Ley, & Hu, 2018). More than 463 million people have been diagnosed with diabetes in total so far, and this worldwide disease led to approximately 4.2 million deaths in 2019. It's estimated that the number of patients will be rising to 700 million in 2045(Saeedi et al., 2019).

According to the WHO diabetes diagnostic criteria, a human with one of the following criteria could be confirmed as a diabetic patient: Fasting plasma glucose level ≥ 7.0 mmol/L (126 mg/dL), Plasma glucose ≥ 11.1 mmol/L (200 mg/dL) in a glucose tolerance test (OGTT) or Glycated hemoglobin (HbA1C) ≥ 48 mmol/mol (≥ 6.5 DCCT %) ("Summary of revisions for the 2010 Clinical Practice Recommendations," 2010). Regarding the different primary etiologies, DM could be grouped into three subgroups, type 1 diabetes, type 2 diabetes, and gestational diabetes. Besides, regarding a newly published study, a refined classification was utilized to identify diabetes into five subgroups: severe autoimmune diabetes (SAID), severe insulin-deficient diabetes (SIDD), severe insulin-resistant diabetes (SIRD), mild obesity-related diabetes (MOD), mild age-related diabetes (MARD)(Ahlqvist et al., 2018). This new substratification may provide a useful tool to individualize treatment regimens and distinguish individuals with a higher risk of complications at diagnosis.

Type 1 diabetes, also known as juvenile diabetes or insulin-dependent diabetes, results from an autoimmune disorder destroying insulin-producing beta-cells in the pancreas usually appears during childhood or adolescence, and the patients have to be managed with insulin daily to maintain regular blood glucose level. Type 2 diabetes mainly displays an inadequate response of several glucose-consuming tissues to insulin, namely, insulin resistance, along with gradually functional loss of

pancreas and relatively reduced insulin secretion. The prevalence of type 2 diabetes in the past few decades has risen critically due to changes in lifestyle and behavior like over nutrition, western diet, and physiological inactivity leading to an increase in risk factors such as obesity, sedentary lifestyle, and some specific medical conditions, such as polycystic ovary syndrome(PCOS)(Zheng et al., 2018). In addition to dyslipidemia, obesity, and environmental issues, some genetic alterations are also linked to the initiation and progression of type 2 diabetes(McCarthy, 2010). Interferences at the early stage of insulin resistance via redressing these factors could alleviate or even reverse the risk of developing into type 2 diabetes afterward, while the potential mechanisms are still missing. Gestational diabetes is the third main form and occurs when women without a previous diabetes history develop high blood glucose levels during pregnancy. Although most cases could get back into normal after giving birth, it still can affect a baby's health and raise the risk of getting type 2 diabetes later in life. The potential mechanism is also relevant to reduced insulin and insulin resistance.

1.2 Insulin signaling pathway and insulin resistance

The regular insulin signal transduction pathway begins with the binding between insulin and insulin receptors, mainly located at the membrane of liver cells, muscular cells, erythrocytes, brain cells, and adipose cells(De Meyts, 2000). So far, it has been figured out that the insulin receptor has an extracellular domain made up of two α-subunits and an intracellular catalytic domain made up of two β-subunits. The α-subunits act as insulin binding domain and the insulin molecule acts as a ligand. Together, they form a receptor-ligand complex(Boucher, Kleinridders, & Kahn, 2014). The insulin receptor (INSR) belongs to tyrosine kinase receptors, which locates at the cell surface. A single gene *insr* encoded the insulin receptor in mammals, and *insr* can be translated into two alternative splice variants, IR-A and IR-B, distinguished by the inclusion of exon 11(Belfiore et al., 2017). However, in zebrafish, the genome is duplicated during evolution and possesses two *insr* genes: *insra* and *insrb*, correspondingly encoded proteins share 68.3% and 65.1% sequence similarity in contrast to human INSR, respectively(Toyoshima et al., 2008). Meanwhile, similar to INSRA and INSRB in human, Insra and Insrb are also widely expressed in zebrafish.

Afterward, tyrosine kinase domains on each β-subunit will be activated and cause auto-phosphorylation of several tyrosine residues in the β-subunit(Kasuga, Karlsson, & Kahn, 1982). Once the tyrosine kinase is activated, it triggers the activation of the docking proteins, also called insulin receptor substrate1-4(IRS) and then following the activation of the Phosphatidylinositol-3-Kinase (PI3K) and Mitogen-activated Protein Kinase (MAPK), which are responsible for promoting the mitogenic and metabolic actions of insulin respectively(Cusi et al., 2000; Draznin, 2006). Specifically, the activation of MAPK leads to the completion of mitogenic functions like cell growth and gene expression, while the activation of PI3K leads to crucial metabolic functions like the synthesis of lipids, proteins, and glycogen(Cusi et al., 2000). Most importantly, the PI3K pathway is responsible for the distribution of glucose for essential cell functions. The activation of PI3K furtherly leads to the activation of PKB (p-AKT), which possesses a critical role in enrolling glucose transporters (GLUT4) to translocate to the cell membrane and promote the transportation of glucose into the intracellular medium(Sano et al., 2003).

Furthermore, AKT could activate the mammalian target of rapamycin complex 1 (mTORC1) pathway(Avruch et al., 2006), and one crucial downstream effector of mTORC1 is the 70 kDa ribosomal protein S6 kinase (p70-S6K)(Bahrami, Ataie-Kachoie, Pourgholami, & Morris, 2014). P70-S6K phosphorylates S6 protein within the 40S ribosomal subunit and regulates proteins' translation, essential for protein synthesis and cell proliferation(Byfield, Murray, & Backer, 2005). In addition to the activation by insulin receptor signaling, mTORC1, and subsequently, p70-S6K can be activated by amino acids through pVps34, a class 3 PI3K(Byfield et al., 2005). Hence, insufficient activation of p70-S6K is associated with insulin resistance development through the subsequent insulin signaling inhibition(Shah, Wang, & Hunter, 2004; Zhang, Gao, Yin, Quon, & Ye, 2008). Theoretically, the issues in any step of the insulin signal cascade might cause an inappropriate response to insulin, which finally turns to insulin resistance.

1.3 Diabetic retinopathy and diabetic nephropathy

Diabetic retinopathy (DR) is a common microvascular diabetic complication that is becoming the fifth leading cause of moderate to severe visual impairment(Bourne et al., 2013). According to the severity of DR, it could be classified into several stages,

non-proliferative diabetic retinopathy (NPDR) and proliferative diabetic retinopathy (PDR) in the presence or absence of macular edema (DME). The global prevalence of DR between 2015 and 2019 was 25.2% for NPDR, 1.4% PDR, and 4.6% DME in diabetic crowds(Thomas, Halim, Gurudas, Sivaprasad, & Owens, 2019). The lowest prevalence was in Europe at 20.6% and South East Asia at 12.5%, and highest in Africa at 33.8%, Middle East and North Africa at 33.8%, and the Western Pacific region at 36.2%(Thomas et al., 2019; Yau et al., 2012).

Caused by the damage to the retinal blood vessels, DR may lead to no symptoms or only mild vision problems, which are quite easily neglected at the very beginning. While without treatment over time, DR is prone to result in blindness eventually. At the stage of NPDR, microaneurysms protrude from the weakened vessel walls of the smaller vessels. Larger retinal vessels begin to dilate and become irregular in diameter(Heng et al., 2013). NPDR can progress from mild to severe as more blood vessels become blocked. Additionally, nerve fibers in the retina may begin to swell at the same time(Cohen & Gardner, 2016).

In contrast, when it comes to proliferative diabetic retinopathy, damaged blood vessels get congested, causing the growth of new, abnormal blood vessels in the retina(Kusuhara, Fukushima, Ogura, Inoue, & Uemura, 2018). Once the new blood vessels interfere with the normal flow of fluid out of the eye, pressure may build up in the eyeball and further injure the nerve that carries images from eye to brain (optic nerve), resulting in glaucoma(Cheung, Mitchell, & Wong, 2010). Finally, scar tissue stimulated by new blood vessels' growth may cause the retina to detach from the eye.

Over the years, DR's risk factors highly concentrate on the duration of diabetes, poor control of blood sugar level, high blood pressure, high cholesterol, pregnancy, and tobacco use (Cheung et al., 2010; Yau et al., 2012). While recent studies identified even under great control of blood sugar level, DR still kept processing, which implies that some unnoticed factors promote the DR's development in advance of the glycemic alteration(Whitehead, Wickremasinghe, Osborne, Van Wijngaarden, & Martin, 2018). Further studies unveiled that etiopathogenesis behind DR is tightly connected to several biochemical, hemodynamic, and endocrine mechanisms with a

preponderant initial role assumed by polyol pathways, accumulation of advanced glycation end products (AGE), reaction from reactive carbonyl species (RCS), activation of inflammation, activation of the renin-angiotensin-aldosterone system (RAAS), and leukostasis(Capitao & Soares, 2016; Csosz, Deak, Kallo, Csutak, & Tozser, 2017; Fuloria et al., 2020; Steckelings, Rompe, Kaschina, & Unger, 2009).

Diabetic nephropathy (DN) is another serious diabetic complication related to kidney disease and is characterized by unreversed damage on the glomerulus and tubulus, also called diabetic kidney disease. Diabetic nephropathy is one of the leading causes of chronic kidney disease (CKD) and end-stage renal disease (ESRD) globally. DN affects approximately a third of patients with type 1 and type 2 diabetes mellitus and contributes to a third of ESRD cases worldwide, and an even larger fraction in the developed countries(Zimmet, Alberti, & Shaw, 2001).

The onset of symptoms is commonly 5 to 10 years after the DM begins. A usual first symptom is frequent urination at night, nocturia. The following symptoms include tiredness, headaches, a general feeling of illness, nausea, vomiting, frequent daytime urination, lack of appetite, itchy skin, and leg swelling(Kowalski, Krikorian, & Lerma, 2015). The clinical presentation of DN is characterized by proteinuria, hypertension, and progressive loss of kidney function(Freedman, Bostrom, Daeihagh, & Bowden, 2007). Affected individuals with end-stage kidney disease often require hemodialysis or kidney transplantation to replace the failed kidney(Wang et al., 2019).

Not all patients with diabetes go on to develop diabetic nephropathy. The main risk factors that increase the likelihood of developing diabetic nephropathy are poorly controlled blood glucose, uncontrolled high blood pressure, type 1 diabetes mellitus, with onset before age 20, past or current cigarette use, a family history of diabetic nephropathy specific genes have been identified that are associated with DN(Kowalski et al., 2015). Additionally, several molecular mechanisms correlating with the development of DN have been clarified involving glomerular insulin resistance, endoplasmic reticulum (ER) stress, autophagy and Reactive Oxygen Species (ROS) in recent studies, which are expected to provide new strategies for DN treatment(Gnudi, Coward, & Long, 2016).

Accompanied by long-term poorly controlled blood glucose levels, multiple changes in the kidneys' filtration units gradually show up. Initially, here comes the constriction of the efferent arterioles and dilation of afferent arterioles, with the following results of glomerular capillary hypertension and hyperfiltration. Some unexpected changes in the glomerular show up, encompassing a thickening of the basement membrane, a widening of the slit membranes, an increase in the number of mesangial cells, and an increase in the mesangial matrix. The matrix could invade the glomerular capillaries and produce deposits called Kimmelstiel-Wilson nodules. With time passing by, the mesangial cells and matrix progressively expand and consume the entire glomerulus, shutting off filtration, which turns out to hypofiltration(Schlondorff & Banas, 2009).

Since the progression of the DN is hardly reversed, the clinical treatments now mainly aim to slow the deterioration of kidney function. Management of DN currently centers over four main areas: Cardiovascular risk reduction, glycemic control, blood pressure control, and inhibition of the RAAS system(J. Li et al., 2019).

1.4 Reactive carbonyl species and acrolein in diabetes

Reactive carbonyl species (RCS) is a type of molecule that is continuously produced *in vivo* with highly reactive carbonyl groups. Typically, the steady-state concentration of RCS is maintained in a certain range. However, changes occurring in RCS production and/or detoxification procedure by its corresponding enzymes properly, such as aldehyde dehydrogenase (ALDH), aldo keto reductase (AKR), and glutathione S-transferase (GST), may lead to their damaging effects on proteins, nucleic acids, and lipids(Bellier et al., 2019). RCS has drawn significant attention over the last years due to its contribution to aging, the pathogenesis of metabolic syndrome, chronic complications associated with diabetes and renal failure, neurodegenerative, and other disorders(Brownlee, 2001; Chang & Wu, 2006; Forman et al., 2008; Gugliucci, 2000; Lovell, Xie, & Markesbery, 2001; Uchida, 2000). Typical and well-studied RCS are acrolein (ACR), 4-hydroxy-(E)-2-nonenal (HNE), 4-oxo-(E)-2-nonenal, and malondialdehyde (MDA).

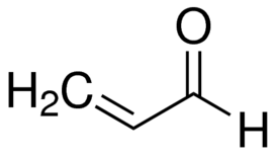

Fig.1 Chemical structure of acrolein

Acrolein is the simplest unsaturated aldehyde and the major reactive component of cigarette and wood smoke. It could be generated during heating foods, from carbohydrates, vegetable oils, animal fats, and amino acids. The main endogenous origins of acrolein are myeloperoxidase-mediated degradation of threonine, amine oxidase-mediated degradation of spermine and spermidine, and lipid peroxidation of polyunsaturated fatty acids(PUFAs)(Stevens & Maier, 2008). In specific, unsaturated fatty acids are prone to oxidation by reactive oxygen species (ROS), and the resultant lipid peroxidation products mostly contain aldehyde groups. Among lipid-derived aldehydes, 4-HNE and malondialdehyde are abundantly produced as peroxidation products(Sultana, Perluigi, & Butterfield, 2013). Although acrolein is produced to a lesser extent under oxidative conditions, it exerts the most substantial cytotoxicity(Moretto, Volpi, Pastore, & Facchinetti, 2012).

The cytotoxic effects of acrolein are mediated by the modification of a variety of molecules, including proteins and nucleic acids(Aldini, Orioli, & Carini, 2011). Recent studies have indicated that the formation of DNA adduct with acrolein leads to mutagenesis and, finally, tumorigenesis(Tang et al., 2011). Acrolein also exerts its cytotoxicity by triggering mitochondrial damage and endoplasmic reticulum (ER) stress in pulmonary cells(Kitaguchi et al., 2012) and endothelial cells(Haberzettl, Vladykovskaya, Srivastava, & Bhatnagar, 2009), in the liver(Mohammad et al., 2012), and in other cell lines(Hengstermann & Muller, 2008).

ACR is known to form four different types of adducts, namely aldimine-, propanal-, methylpyridinium (MP)- and formyl-dehydropiperidino (FDP)-type adducts(Furuhata et al., 2003; Furuhata, Nakamura, Osawa, & Uchida, 2002; Kaminskas, Pyke, & Burcham, 2007; Uchida, Kanematsu, Morimitsu, et al., 1998; Uchida, Kanematsu, Sakai, et al., 1998). Several clinical studies have identified that acrolein-lysine adduct(FDP-lysine) accumulates in both type 1 and type 2 diabetic patients' urine, and even more in diabetic patients with microalbuminuria(Daimon et al., 2003; Tsukahara et al., 2003). Additionally, Kaori et al. indicated that there was not only a higher concentration of FDP-lysine but also free acrolein in plasma of renal failure patients(Sakata et al., 2003). Furthermore, Eisei et al. figured out that in end-stage renal disease, the FDP-lysine level of those patients with type 2 diabetes was significantly higher than the non-DM group(Noiri et al., 2002), which implies FDP-

lysine has a strong connection with diabetic nephropathy. It has also pointed out that FDP-lysine level could be utilized as a biomarker for the severity of diabetic retinopathy(X. Zhang et al., 2008). Another research suggested diabetes as well as insulin resistance were positively associated with acrolein metabolites, such as N-acetyl-S-(3-hydroxypropyl)-L-cysteine (3-HPMA) and N-acetyl-S-(carboxyethyl)-L-cysteine (CEMA) with evidence of a dose-response relationship(Feroe, Attanasio, & Scinicariello, 2016).

Although studies identified an apparent link between acrolein and DM, investigators believed that increasing acrolein as a “marker” under DM condition mostly results from oxidative stress. Recent studies gradually indicated that acrolein might play an important role right before the onset of DM. A report claimed that acrolein has a modification behavior on insulin B chain directly. Exclusive formation of an adduct between insulin and acrolein could destroy both the hypoglycemic effect of the hormone in rats and glucose uptake in 3T3 adipocytes (Medina-Navarro, Guzman-Grenfell, et al., 2007). Jeffery et al. reported that acrolein has a toxic effect on the ARPE-19 cells exposed to hyperglycemic media by reducing viability conducted through the TGFβ signaling pathway (Grigsby, Betts, Vidro-Kotchan, Culbert, & Tsin, 2012). However, studies regarding acrolein as the “maker” in insulin resistance are still restricted. An appropriate model is necessary for the next *in vivo* exploration.

1.5 Aldo-keto reductase superfamily and Akr1a1

The Aldo-Keto reductase (AKR) superfamily is a family of several enzymes that catalyze redox substances involved in biosynthesis, metabolism, and detoxification. More than 190 members of this family have been described. These proteins are found in all phyla ranging from prokaryotes, protozoans, and yeasts to plants, animals, and humans. This superfamily can be subdivided into 16 categories, including several related monomeric NADPH-dependent oxidoreductases, such as aldehyde reductase, aldose reductase, prostaglandin F synthase, xylose reductase, rho crystallin, and many others. Members of each family share more than 40% homology and less than 40% with any other families. Mammalian AKRs fall within three well-defined families (AKR1, 6, and 7), while zebrafish AKRs only involve 2 families (AKR1 and 7) and 4 members in total. These proteins are widely distributed in tissues, and most cells express several AKRs simultaneously. In humans, 13

different AKR proteins have been identified that fall within the three prominent families of mammalian AKR. While in zebrafish, only four members exist, including AKR1a1a, AKR1a1b, AKR1b1, and AKR7a3(Barski, Tipparaju, & Bhatnagar, 2008; Penning, 2015).

The superfamily's substrates include glucose, steroids, glycosylation end products, lipid peroxidation products, and environmental pollutants. Due to their broad substrate specificity, AKRs also play an essential role in the Phase II detoxification of many pharmaceuticals, drugs, and xenobiotics. As ancient proteins, Aldo-keto reductases share a common chemical structure. A distinguishing feature of the structure is the active site's presence at the C-terminus. It can be utilized to bind redox-active cofactors and metals to oligomerize into quaternary arrangements that can form active site interfaces, or it could be used as a gated barrel for channeling reaction intermediates(Amaro, Tajkhorshid, & Luthey-Schulten, 2003; Vega, Lorentzen, Linden, & Wilmanns, 2003; Wise, Yew, Babbitt, Gerlt, & Rayment, 2002).

Up to now, the AKRs have been implicated in several diseases. It is known that AKR1A1, AKR1B10, and AKR1C1–C3 are well involved in tobacco-induced carcinogenesis(Liu, Wen, & Cao, 2009; L. Zhang et al., 2008). AKR1B1 and AKR1B10 regulate the development and progression of human liver, breast, and lung cancers through detoxifying reactive carbonyls, retinoic acid homeostatic regulation, and lipid metabolism(Diez-Dacal et al., 2011). AKR7A protects the liver from acetaminophen-induced hepatotoxicity by enhancing hepatocellular antioxidant defense(Ahmed et al., 2011). Through mediating oxidative stress-induced inflammatory signals, AKR1B1 plays a role in inflammation-related diseases such as sepsis and colon cancer(Ramana, 2011). Besides, several *in vivo* studies claimed the inhibition of AKR1B1 could alleviate diabetic complications, such as cataractogenesis, retinopathy, nephropathy, and neuropathy(Cogan et al., 1984; He et al., 2019; Q. R. Li et al., 2016; Lou, Xu, Zigler, & York, 1996; Toyoda et al., 2014). Hence, AKR1B1 inhibitors were regarded as potent drugs for alleviating or even reversing diabetic complications in past decades. However, a series of clinical trials were turned out to be failed due to the high incidence of side effects and ineffectiveness(Suzen & Buyukbingol, 2003). One probable reason might be the AKR1B1 inhibitors also impede AKR1A1 exerting functions in several tissues(El-

Kabbani & Podjarny, 2007). Therefore, a better understanding of the *akr1a1* gene's regulation under physiological and pathological conditions is necessary and urgently needed for helping us develop novel therapeutic approaches.

The first discovered AKRs, AKR1A1, is a cytosolic, NADPH-dependent, monomeric oxidoreductase with a compulsory ordered substrate binding and product release. The enzyme is ubiquitously expressed in most tissues, with the highest in kidney proximal tubules(Barski, Papusha, Ivanova, Rudman, & Finegold, 2005). AKR1A1 owns a broad substrate spectrum, and it prefers carboxyl-group containing negatively charged substrates(Wermuth & Monder, 1983). In addition to detoxifying reactive carbonyl species(RCS) such as 3-deoxyglucosone(3DG), glyoxal, and methylglyoxal(MG), AKR1A1 also reacts with some lipid peroxidation end-products, including acrolein(ACR), malondialdehyde(MDA), and 4-hydroxynonenal(HNE). Kurahashi et al. reported that the detoxification of toxic aldehydes, e.g., acrolein, is a principal role for AKR1A, and overexpression of AKR1A alleviates the Tg MEF's(transgenic Mouse Embryonic Fibroblasts) sensitivity to acrolein(Kurahashi et al., 2014).

Lately, a new study implied that besides acting as a metabolic enzyme, AKR1A1 also plays a vital role in the way of protein post-translational modification, S-nitrosylation(Stomberski et al., 2019). Briefly, nitric oxide (NO)-based cellular signaling is generally mediated by protein S-nitrosylation, the oxidative modification of Cys residues to form S-nitrosothiols (SNOs). While classic metabolic intermediate Co-enzymeA (CoA) serves as an endogenous source of SNOs through its conjugation with NO to form S-nitroso-CoA (SNO-CoA), and that its cognate denitrosylase governs S-nitrosylation of proteins by SNO-CoA, SNO-CoA reductase (SCoR). Furtherly, the study identified AKR1A1 as a new critical endogenous SCoR(Stomberski et al., 2019). Therefore, AKR1A1 could modify specific proteins by reducing the S-nitrosylation level. Moreover, inhibitory S-nitrosylation of pyruvate kinase M2 (PKM2) by the SNO-CoA-AKR1A1 system can balance fuel utilization (through glycolysis) with redox protection (through the pentose phosphate shunt) and transduces the activity of endothelial nitric oxide synthase (eNOS) in reprogramming intermediary metabolism, thereby protecting kidneys against acute kidney injury(Zhou et al., 2019). In parallel to this study, another study in our lab showed

loss of Akr1a1b could inhibit gluconeogenesis via regulating the S-nitrosylation level of cPEPCK, implying that Akr1a1b might be the counterpart of AKR1A1 in regulating the S-nitrosylation level of proteins(X. Li et al., 2020).

1.6 Aim of the thesis

Previous research in our lab suggested that hyperglycemia-induced formation of MG was identified as a cause for early vascular alterations in zebrafish embryos via targeting the VEGF receptor signaling cascade(Jorgens et al., 2015). Apart from MG, there are also several reactive metabolites such as ACR, MDA, and 4-HNE being involved in diabetes and corresponding complications. While, how does ACR, one of the most active RCS contribute to diabetes and relevant complications and whether AKR1A1 benefits via detoxfying ACR *in vivo* remains unknown.

Besides, rare previous studies focused on the functions of AKR1A1 in metabolomics, vacular angiogenesis and diabetes with its complications. Moreover, in zebrafish, the available data have only reported the existance of the Akr1a1 enzyme system with two homologues, Akr1a1a and Akr1a1b. Although previous study in our lab has revealed that Akr1a1b might be the counterpart of AKR1A1 in regulating the S-nitrosylation level of proteins, foundamental function and properties of Akr1a1a in organ development and disease processes is still unclear.

Therefore, the thesis mainly aims to investigate the function of Akr1a1a via knockout strategy *in vivo* by using zebrafish as a model organism. The objective was to generate an Akr1a1a zebrafish knockout line, to investigate the characteristics of metabolic state and alterations of vascular system and kidneys. And to address the toxic effects of ACR and if loss of Akr1a1a could aggravate these toxic effects *in vivo*. The working hypothesis was: 1. Loss of Akr1a1a leads to the detoxification and accumulation of ACR in zebrafish. 2. The accumulated ACR *in vivo* contributes to metabolic alterations, hyperglycemia, vasular alterations and results in diabetic complications subsequently.

2 MATERIALS AND METHODS

If not mentioned otherwise, all materials and methods used during the experiments are according to the standard protocols of AG Kroll's Lab, which may be modified from the methods section of the enclosed papers(Lodd et al., 2019; Schmohl et al., 2019; Wiggenhauser et al., 2020).

2.1 Materials

If not mentioned otherwise, all materials and methods used during the experiments are according to the standard protocols of AG Kroll's Lab, which may be modified from the methods section of the enclosed papers(Lodd et al., 2019; Schmohl et al., 2019; Wiggenhauser et al., 2020).

2.1.1 Equipment

Product	**Company**
Agarose gel chamber	Peqlab Biotechnologie GmbH
Bench top centrifuge (Rotina 420R)	Hettich
BioPhotometer D30	Eppendorf
Dry bath incubator	Major Science
Electronic balance	Kern & Sohn GmbH
Electrophoresis power supply	Consort
Glucometer Freedom Lite	Abbott (FreeStyle)
Hamilton syringe (Glastight® #1705)	Hamilton
Heating/Shaking block	HLC
Jun-Air 3-4 Quiet Running Compressor (11l / min at 8 bar)	Jun-Air
Leica HI1210 water bath	Leica
Leica RM2235 microtome	Leica
QuantStudio 3 Real-Time-PCR-System	Applied Biosystems
Microcentrifuge Mikro 200R	Hettich
PCR cycler	BioRad
pH-meter ProfiLine 197i	WTW ProfiLine
See-saw rocker	Stuart
Table centrifuge	Carl Roth GmbH

UV transilluminator	INTAS
Vertical Micropipette Puller P30	Sutter instruments Co.
Water Bath	Seelbach

2.1.2 Chemicals

If not indicated especially, all chemicals used during the experiments were purchased from the following companies: Carl Roth GmbH & Co. KG, Merck AG, Roche Diagnostics GmbH, Sigma-Aldrich Chemie GmbH and Thermo Fisher Scientific Inc.

2.1.3 Consumables

Product	**Company**
0.22 µm syringe filter	Millex
Blood glucose test stripes	Abbott (FreeStyle Lite)
Conical tubes (15 ml, 50 ml)	Falcon
Dumont Tweezers No. 5	NeoLabs
Feather disposable scalpel No.10	Feather
Glass culture cyl. (14 mm I.D. x 5 mm)	Biotechs
Microscope slides (76x26 mm)	IDL
Needle 20G x1 ½” nr.1	BD Microlance
Nitrile Gloves	Semperguard
Pasteur Pipettes	Hirschmann
PCR tubes (0.2 ml)	Star Labs
Petri dishes (10cm and quadratic)	Greiner
Pipette filter tips (1000, 100, 20 and 10 µl)	Nerbe plus GmbH
Pipette tip refills (1000, 200, 10 µl)	TipOne Star Labs
Pipettes (P1000, P200, P20 and P2)	Gilson/Eppendorf
Quantitative PCR 96-well reaction plate	Axon
Safe-Lock tubes (0.5, 1.5 and 2.0 ml)	Eppendorf

Stainless steel beads (5 mm)	Qiagen
Syringes (1 ml, 30 ml)	BD Plastipak
Tissue culture plate (6 and 96 well)	Falcon

2.1.4 Buffers and Solutions

2.1.4.1 Gel electrophoresis

50x TAE buffer	232 g Tris 57.1 ml conc. acetic acid 100 ml 0.5 M EDTA, pH 8.6 ad 1 l deionized water
1x TAE buffer	100 ml 50x TAE buffer ad 5 l deionized water
Denaturing agarose gel sample loading buffer	75 µl deionized formamide 75 µl 10x MOPS buffer 120 µl 37% formaldehyde 90 µl sterile deionized water 50 µl glycerin a spatula's tip bromophenoblue

2.1.4.2 Western blot

5x Electrophoretic buffer:	15.1g Tris base 94g Gly 50ml 10%SDS (10g SDS+100ml ddH2O) ad deionized water to 1L When using: 100ml 5X Electrophoretic solution ad deionized water to 500ml
10x blotting buffer	30.3g Tris base 144g Gly add deionized water to 1L When using: 50ml 10X Transfer Solution 100ml Methanol add deionized water to 500ml
5x Laemmli buffer	8.34 ml Tris/HCl, pH 6.8 5 g SDS 0.25 g bromophenol blue 25 ml glycerol

	3.45 g DTT ad 50 ml MilliQ water
TRIS/HCl pH 6.8	90.86 g Tris pH 6.8 ad 500 ml MilliQ water
TRIS/HCl pH 8.8	90.86 g Tris pH 8.8 ad 500 ml MilliQ water
NP40 lysis buffer	0.87 g NaCl 5 ml 1M Tris/HCl, pH 7.4 1.8 ml 0.5 M Na2EDTA, pH 8 1 bottle Proteinase inhibitor cocktail 10 ml 10% Nonidet P40 solution 10 ml Glycerol ad 100 ml MilliQ water

2.1.4.3 Histology

Hematoxylin staining solution	1 g Hematoxylin 100 ml MilliQ water 200 mg Sodium iodat 50 g Potassium alum 50 g Chloral hydrate 1 g Citric acid

2.1.4.4 Zebrafish maintenance and work

E3 (“eggwater”)	3 g Red Sea Salt ad 10 l MilliQ water
0.1M KCl	0.745 g KCl ad 100 ml MilliQ water
1-phenyl-2-thiourea (PTU, 10x stock)	304 mg PTU ad 1 l MilliQ water
10x PBS	400 g NaCl 10 g KCl 57.5 g Na2HPO4 10 g KH2PO4 ad 5 l MilliQ water
Lysis buffer	133 µl of 1.5 M Tris/HCl, pH8 40 µl 0.5 M EDTA 60 µl Tween 60 µl Glycerol

	ad 20 ml MilliQ water
Tricaine (3-amino benzoic acidethylester)	400 mg Tricaine powder 97.9 ml MilliQ water ~2.1 ml 1 M Tris (pH 9) adjust to pH ~7 100 ml total volume
Tris/HCl, pH 7.8	181.17 g Tris Adjust pH to 7.8 with HCl Ad 1 l MilliQ water
4% PFA	4 g PFA dissolved in 100 ml 1xPBS

2.1.5 Kits and Reagents

Product	**Company**
Acrolein (ACR) ELISA Kit	MyBioSource Inc
Acrolein-S-11030F1-1ML	Chem Service Inc
Biotin Switch Assay Kit (S-Nitrosylation)	abcam
DAB Peroxidase (HRP) Substrate Kit (with Nickel)	vector laboratories
Gene Ruler DNA ladder mix (0.5 µg/µl)	Thermo Fisher Scientific
Glucose Assay Kit CBA086	Merck
GoTaq® Green Master Mix	Promega
Maxima First Strand cDNA Synthesis Kit with dsDNase	molecular biology by thermo scientific
Power SYBR™ Green PCR Master Mix Kit	Applied Biosystems
QIAquick PCR Purification Kit	QIAGEN
RNeasy Mini Kit	QIAGEN
Tricaine (3-amino benzoic acidethylester)	Sigma-Aldrich
Trypsin/EDTA solution (25200-056)	Gibco

2.1.6 Enzymes and buffers

All restriction enzymes and buffers, including BamHI-HF, BglII, NEB Buffer 3, NEB CutSmart Buffer, SalI, SmaI, T4 DNA Ligase Buffer, T4 Ligase, T7 endonuclease, XbaI were purchased from New England Biolabs GmbH. Proteinase K was purchased from Roche.

2.1.7 Oligonucleotides

CRISPR-construct	**Oligonucleotide sequence (5‘ to 3‘)**
Akr1a1a-CRISPR#1-for	TAGGTCAGAGGATGCCAACGGT
Akr1a1a-CRISPR#1-rev	AAACACCGTTGGCATCCTCTGA

Genotyping primer	**Primer sequence (5‘ to 3‘)**
Akr1a1a-Crisp#1_Genotype_neu-for:	TCATTTGGGCAGGAAAACGT
Akr1a1a-Crisp#1_Genotype_neu-rev:	GTAGCCACAGTCTAAAGCTGC

qPCR primer name	**Primer sequence**
b2m-qPCR-for	ACTGCTGAAGAACGGACAGG
b2m-qPCR-rev	GCAACGCTCTTTGTGAGGTG
ins-qPCR-for	GGTCGTGTCCAGTGTAAGCA
ins-qPCR-rev	GGAAGGAAACCCAGAAGGGG
insb-qPCR-for	CCTGGAGACCTTGCTGGCTTTG
insb-qPCR-rev	CCAGGTGGTAGATGGTGCAGG
Insra-qPCR-for	AGAGGCCAGCGAGCTCTAC
Insra-qPCR-rev	CACTTGTGTGGGGGCTCT
Insrb-qPCR-for	GCCTCTGCGGATCACTACAT
Insrb-qPCR-rev	CTCCTGCGTGGTCTTGAAC
PFK-La-qPCR-for	ACTGCCACTCCAGCGTTAAA
PFK-La-qPCR-rev	CAGAGCTGGAGTTCACCCTC
PFK-Lb 2-qPCR-for	GCCGTTCAACATTCACGACC
PFK-Lb-qPCR-rev	TGCAGTCGAACACTCCTTGG
PFK-ma-qPCR-for	CTCTGTGTAATCGGCGGTGA
PFK-ma-qPCR-rev	ATGGAGCCAACCATACCCAC
PFK-mb-qPCR-for	ACTGTCGGTTTGCTGTACTC

PFK-mb-qPCR-rev	GCTCGAACAGCAGCATTCAT
PK-L-qPCR-for	TCCTGGAGCATCTGTGTCTG
PK-L-qPCR-rev	GTCTGGCGATGTTCATTCCT
PK-M-qPCR-for	TGGGCTTATTAAGGGCAGTG
PK-M-qPCR-rev	TGCACCACCTTTGTGATGTT
HK-qPCR-for	ATGATAGCGGCACAGCTTCT
HK-qPCR-rev	GTTGGTGTCTCGTGCCAATC
Glut1a-qPCR-for	TGACCGGCCCATACGTTTTC
Glut1a-qPCR-rev	ATCATCTCGGTTATATTTATCTGCC
Glut1b-qPCR-for	CCATTTCTCCTGGGCTTTACCTTTA
Glut1b-qPCR-rev	CAGATTTGGCTTTGCTTTCCTCGTT
Glut1c-qPCR-for	CATCCGTAATATTCAGGTGCTAGTG
Glut1c-qPCR-rev	ATTTTCAGCAGAGGTGGAAAGAG
Glut2-qPCR-for	GCAGAAGAACCCTCACTC
Glut2-qPCR-rev	TCTCCGCCACAATAAACC
Glut3-qPCR-for	TCGTCAATGTCTTGGCTCTG
Glut3-qPCR-rev	CAACATACATTGGCGTGAGG
Glut5-qPCR-for	TCTCTGGTTGCTGGATTTGGT
Glut5-qPCR-rev	CAAGAGGGTGAGGAGATTGTCC
Glut6-qPCR-for	TTGCTATTGCAGCCAGTTTG
Glut6-qPCR-rev	CAGGCCGTCTGTTAGGGTAA
Glut8-qPCR-for	CATTTTGTCTGGTGTCGTCATGT
Glut8-qPCR-rev	CCTGCAATGAAAAAGCCCAT
Glut9a-qPCR-for	GAGGCCGGAGCAGAGAAAGCGTTC
Glut9a-qPCR-rev	AGCATTCAGTCCACACAGCTGATA
Glut11a-qPCR-for	CCCTGGGAACTATCCCTCAT
Glut11a-qPCR-rev	TCCACTGATTGCCAACACAT

Glut11b-qPCR-for	AAGGATGAGTACTGGCCGATCCTC
Glut11b-qPCR-rev	AATGCCGAGAGCGCTGACCCTTTC
Glut11c-qPCR-for	ACTGTCCACACAATGTATATCTTG
Glut11c-qPCR-rev	GAGCCCAGCCGCACCGCTGAAAGC
Glut12-qPCR-for	GGGACAATCCTGGACCACTA
Glut12-qPCR-rev	ACATCCCAACCAGCATTCTC
Glut13.1-qPCR-for	AAAGCGTGACCATGAACTCC
Glut13.1-qPCR-rev	AACCACTCCGGTGTCATAGC

2.1.8 Morpholinos

All morpholinos were purchased from GENE TOOLS, LLC.

SB- insra-MO (exon3-intron3 junction)	5'-CACACAAGCAGCAGGGTACTTACGT-3'
SB- insrb-MO (exon7-intron7 junction)	5'-ACTGAAAGGACCACACTCACGCTTC-3'
Control-MO	5'-CCTCTTACCTCAGTTACAATTTATA-3'

2.1.9 Antibodies

Products	**Company**
Anti-Akr1a1a antibody (guinea pig)	Keyhole Limpet Hemocyanin and DKFZ
Anti-β-actin(rabbit)	Cell Signaling Technology (4967S)
Anti-rabbit IgG, HRP-linked Antibody	Cell Signaling Technology (7074S)

2.1.10 Zebrafish transgenic lines

Two transgenic zebrafish lines were used: *Tg(fli1:EGFP)* and *Tg(wt1b:EGFP)* for all the study of zebrafish (*Danio rerio*) experiments.

2.2 Methods

2.2.1 Animal studies

2.2.1.1 Ethics

Local government, Regierungspräsidium Karlsruhe and Medical Faculty Mannheim (license no: G-98/15, G-160/14 and I-19/02) authorized all the involving experimental

procedures on animals. All procedures carried out in accordance with the approved guidelines.

2.2.1.2 Zebrafish maintenance

Zebrafish lines were normally raised and staged under standard husbandry environment. Embryos/larvae were set in E3 media at 28.5 °C with/without PTU (2.5ml in 25 ml) treatment from 1dpf to suppress pigmentation formation till the time for performing experiments. Adult zebrafish were kept under 13 h light/11 h dark cycle and fed twice a day, with living shrimps in the morning and fish flake food in the afternoon.

2.2.1.3 Morpholino and CRISPR/Cas9-mRNA injection

Morpholino aliquots (8 or 16 µg/µl) were heated at 65°C for 5 minutes and diluted with 0.1 M KCl to 4 or 6 µg/µl right before using. CRISPR guide-RNA and Cas9 mRNA were each diluted to 200 ng/µl within 0.1 M KCl and mixed well. Fresh zebrafish eggs were collected and set in a 1% agarose ramp with a spot of E3 media. One nanoliter of morpholino or CRISPRguideRNA-Cas9mRNA-mix was injected into the yolk sack or the cell of one-cell staged embryos by using microneedle. 3-4 h later, the undamaged and fertilized eggs were sorted out and kept in Petri dish containing 20ml eggwater.

2.2.1.4 Incubation of zebrafish embryos/larvae

At 24 hours post fertilization(hpf), the chorion of zebrafish embryos was removed by using sharp forceps. Fertilized zebrafish embryos were transferred into 6-well plate, around 30 embryos per well with 5 ml eggwater containing 0,003% PTU and 10 µM acrolein till 5dpf. Medium were refreshed daily.

2.2.1.5 Microscopy and analysis of vascular and pronephric alterations in larvae

For in vivo imaging of the zebrafish trunk vasculature, *Tg(fli1:EGFP)* larvae were anesthetized in 0.0003% tricaine at 96hpf and transferred to transparent 96-well plates, lying on the side. Images were taken via a DM6000 B microscope with Leica TCS SP5 DS scanner with 600 Hz, 1024x1024 pixels and 1 µm thick z-stacks. For quantification of trunk vessels, the first 5 intersegment vessel (ISV) and dorsal longitudinal anastomotic vessel (DLAV) pairs of each zebrafish larvae were skipped and alterations in the following 17 pairs were counted. The development of new

blood vessels referred to ‘hyper branches’, and altered intersegment vessels that either miss connections to others or show slight malformations (thin, thick or wrong direction) were grouped as ‘abnormal ISVs’ and counted.

For in vivo imaging of the zebrafish retinal hyaloid vasculature, *Tg(fli1:EGFP)* larvae were anesthetized in 0.0003% tricaine at 120hpf, and fixed in 4% PFA/PBS overnight at 4°C. Fixed larvae were washed three times for 10 minutes per time in double distilled water (ddH2O) and incubated for 90 min at 37°C in 0.5% Trypsin/EDTA solution (25200-056, Gibco) buffered with 0.1 M TRIS (Nr. 4855.3, Roth) dilution and adjusted to pH 7.8 with 1 M HCl solution. Larval hyaloid vasculature was dissected under a stereoscope and displayed in PBS for visualization according to Jung’s protocol(Jung, Kim, Lee, & Kim, 2016). Confocal images for phenotype evaluation were acquired using a confocal microscope (DM6000 B) with a scanner (Leica TCS SP5 DS) utilizing a 20x0.7 objective, 1024 × 1024 pixels, 0.5 µm Z-steps. Vascular diameters were measured at two different positions by ImageJ, cross points of blood vessels were regarded as “branches” and small new blood vessels were counted and addressed as “sprouts” within the circumference of the hyaloid per sample.

For in vivo imaging of the zebrafish pronephros, *Tg(wt1b:EGFP)* embryos were anesthetized within 0.003% tricaine and mounted in 1% low melting point agarose (Promega) dorsally at 48hpf. Images were taken by Leica DFC420 C camera, attached to a Leica MZ10 F modular stereo microscope. Pronephric alterations were quantified by measuring the size of glomerular length, width, and neck length respectively by using Leica LAS V4.8 software.

2.2.1.6 Dissection of adult zebrafish

Adult zebrafish were transferred into single boxes one day before and fasted overnight. Sixteen hours later, fish were fed with 0.5 g flake food for 1 hour followed by refreshing water and 1hour postprandial experiment. Afterwards, fish were euthanized with 0.025% tricaine until the operculum movement disappeared entirely. Then blood was extracted from caudal vein and blood glucose was measured by a glucometer. Later on, fish were sacrificed by beheaded treatment and transferred into experimental platform covered with ice-cold PBS. Livers, muscles, were isolated, weighed, snap frozen in liquid nitrogen and stored at -80 °C for metabolomics, RT-qPCR and Elisa analysis. Kidneys were isolated, weighed and set into formalin

solution for histology and electronic microscopy analysis. The whole fish head was transferred into 4% PFA/PBS for 24 h at 4 °C for further retinal vasculature analysis.

2.2.1.7 Microdissection and visualization of retinal vasculature

Retina dissection and analysis was performed according to Wiggenhauser's protocol(Wiggenhauser, Kohl, Dietrich, Hammes, & Kroll, 2017). In brief, PFA fixed heads from adult zebrafish were transferred to agarose platform covered with 1xPBS and eyes were removed from the head as the first step. Retina was detached from eye and washed twice with 1xPBS. Washed retina was immersed in mounting media and covered with a cover slide. Images were taken by using DM6000 B confocal microscope with Leica TCS SP5 DS scanner. Parameter: 600 Hz, 1024x1024 pixels and 1.5 µm thick of z-stacks were utilized. Quantification of branch points and sprouts was performed by using GIMP and ImageJ in squares of 350*350 μm^2.

2.2.2 Molecular biology

2.2.2.1 Establishment of *akr1a1a* knockout zebrafish line via CRISPR/Cas9 technology

This part of work was completed by my colleague Dr. Felix Schmöhl, encompassing design of CRIRPR-oligonucleotides, restriction and ligation of gRNA-plasmids, transformation of E. coli, plasmid isolation and sequencing, and CRISPR-guideRNA and Cas9-mRNA in vitro transcription.

2.2.2.2 Isolation of genomic DNA

Whole zebrafish larvae or cut fins of adult zebrafish were set into 0.2ml PCR tubes and 20µl lysisbuffer was added. After incubation at 98 °C for 10 min, 10µl proteinase K was added following incubation at 55 °C overnight. Then flicked the tubes and incubated at 55 °C for another hour. Heated up to 98 °C for 10 min and genomic DNA was stored at -20 °C for long-term storage.

2.2.2.3 Polymerase chain reaction (PCR) and PCR purification

Polymerase chain reaction (PCR) was performed by using 12.5µl GreenTaq-mix, 1.5µl forward primer, 1.5µl reverse primer, 7.5µl sterile MilliQ water and 2µl DNA template. Following program was used:

Beginning denaturation	95 °C, 3 min
Denaturation	95 °C, 30 s
Annealing	Specific temperature according to the primer, 30 s
Elongation	72 °C, specific elongation time according to the PCR product size
From denaturation to elongation	35-cycle repetition were performed
Final elongation	72 °C, 10 min

For genotyping, the QIAGEN quick PCR Purification Kit was used and genotyping PCRs were purified according to the manufacturer's protocol.

2.2.2.4 DNA gel electrophoresis

An agarose gel (1-3% agarose in TAE buffer) was buildup for the DNA fragments separation. Using electrophoresis chambers, the gel was run at 120 V (100 ml gel) in TAE buffer up to 2h.

2.2.2.5 RNA isolation from larvae and adult zebrafish organs

Larvae from different developmental time point and/or treated with different drugs were anesthetized with 0.003% tricaine and the yolk sac was removed by pipetting embryos up and down and centrifuging for 5 min at 14000 rpm. The supernatant was discarded and the sediment was used for the following experiments. Adult zebrafish organs were collected during fish dissection and homogenized organs via tissuelyser. Lysis and purification of the larvae/adult zebrafish organs were performed with the RNeasy Mini Kit (Qiagen) according to the manufacturer's instruction. RNA concentration was measured with a photometer and checked on an 1% agarose gel for integrity. Then the samples were made into aliquots for RT-qPCR or RNA-seq and stored at -80 °C temporarily.

2.2.2.6 cDNA synthesis from total RNA (RT-PCR)

The Maxima First Strand cDNA Synthesis Kit was used for reverse transcription PCR (RT-PCR) to generate cDNA according to the manufacturer's protocol. One µg total RNA was utilized for template. The cDNA was made for aliquots and stored at -20 °C.

2.2.2.7 Real time quantitative PCR (RT-qPCR)

Primers (see in 2.1.7) were designed with the Primer-BLAST tool from NCBI using the transcript. All samples were mixed with Power SYBR™ Green PCR Master Mix Kit in 96-well reaction plates. The qPCR reaction proceeded with QuantStudio 3 RealTime-PCR-System.

A Primer-Mix was prepared for each gene: 10 µl of both forward and reverse primers Stock (100 µM) were mixed with 90 µl autoclaved MilliQ water.

Each well:	1 µl 5 µl 4µl	Primer Mix Power SYBR™ Green PCR Master Mix cDNA-autoclaved MilliQ water-Mix (containing 20 ng cDNA)

Total 10 µl

2.2.3 Biochemical analysis

2.2.3.1 Protein sequence alignment

The amino acid sequences of the akr1a1a proteins from zebrafish (Q6AZW2_DANRE), human (Akr1a1_HUMAN) and mouse (Akr1a1_MOUSE) were accessed from the UniProt Database (http://www.uniprot.org/). For the comparison, the genes were selected and aligned with the UniProt-own alignment tool (http://www.uniprot.org/align/).

2.2.3.2 Enzyme activity assay

Enzyme activity assay was performed by the laboratory of Prof. Dr. P. Nawroth (Department of Medicine I and Clinical Chemistry, Heidelberg University, Germany) 96 hpf old larvae were collected (50 larvae/sample) for the measurement. ALDH activity was assayed at 25 °C in 75 mM Tris-HCl (pH 9.5) containing 10 mM DL-2-amino-1propanol, 0.5 mM NADP and 5Mm Acetaldehyde by measuring the rate of NADP formation at 340 nm. Glo1-activity was determined spectrophotometrically monitoring the change in absorbance at 235nm caused by the formation of S-D-lactoylglutathione. AKR activity was determined by measuring the rate of reduction of NADPH at 340 nm, pH7.0, and 25°C. The assay mixture contained 100mM potassium phosphate, 0.1–2 mM methylglyoxal (MG) and 0.1mM NADPH.

2.2.3.3 Determination of methylglyoxal (MG), 3-Deoxyglucosone (3-DG), and glyoxal

The determination of MG, 3-DG and glyoxal was performed by stable isotopic dilution analysis via LC-MS by the laboratory of Prof. Dr. P. Nawroth (Department of Medicine I and Clinical Chemistry, Heidelberg University, Germany).
In brief, frozen Zebrafish larvae (50 larvae/sample) were treated with precipitation solution (Trichloracetic acid 20% w/v in 0.9% NaCl), incubated with an internal standard and derivatized with 1,2-Diaminobenzene. Quantification was carried out using a XEVO TQ-S tandem quadrupole mass spectrometer.

2.2.3.4 Metabolomic analysis

Detection was done in cooperation with the Metabolomics Core Technology Platform from the Centre of Organismal Studies Heidelberg by Gernot Poschet and Elena Heidenreich.
Zebrafish larvae at 96 hpf age were anesthetized with 0.003% tricaine. Adult zebrafish organs were collected during fish dissection. The detection was performed either by ultra-performance liquid chromatography with fluorescence detection (UPLC-FLR) or semi-targeted gas chromatography-mass spectrometry (GC/MS) analysis.

2.2.3.5 Whole-body glucose determination in zebrafish larvae

Zebrafish larvae were collected at 5dpf and snap frozen. Approximately 20-25 larvae per clutch were homogenized in glucose assay buffer by the ultrasonic homogenizer, 90% intensity, and 15 seconds for 2 times. Glucose content was determined according to manufacturer’s instruction (Glucose Assay Kit, CBA086, Sigma-Aldrich).

2.2.3.6 Acrolein determination in zebrafish larvae

Zebrafish larvae from 96hpf were collected and snap frozen. Approximately 40-50 larvae per clutch were homogenized in 1xPBS with by the ultrasonic homogenizer, 90% intensity, 15 seconds for 2 times. Acrolein amount was determined according to manufacturer’s instruction (Acrolein ELISA Kit, MBS7213206, MyBioSource Inc).

2.2.3.7 Measurement of adult zebrafish blood glucose

Adult zebrafish were transferred to single boxes the day before. The next day, the fish were either directly euthanized for blood sugar measurements under overnight fasting condition or fed with 0.5g flake food for postprandial condition. After feeding,

the zebrafish were euthanized in 250 mg/L tricaine, and blood glucose was measured.

2.2.4 Software

Analysis of retinal vasculature was carried out by using LAS AF Lite Software from Leica for taking screen shots, Gimp for image cutting and ImageJ for quantification. The “GCMS solution” software (Shimadzu®) was used for data processing of the GC/MS analysis. Statistics were calculated with GraphPad Prism 6.01 and 8.3.0.

2.2.5 Statistical analysis

Results are expressed as mean with standard deviation (mean ± SD). Statistical significance between different groups was analyzed using Student’s *t*-test and one-way ANOVA (followed by Tukey‘s multiple comparisons) in GraphPad Prism 6.01 or 8.3.0. p-values of 0.05 were considered as significant: *p<0.05, **p<0.01, ***p<0.001, ****p<0.0001.

3 RESULTS

3.1 Sequence alignment of Akr1a1a in different species and *akr1a1a* mRNA expression level in larvae and adult organs of zebrafish

Akr1a1 enzyme system does not only exist in humans and mice but also zebrafish. Yet, in zebrafish, two homologs, including Akr1a1a and Akr1a1b, appear. Since our research group has focused on Akr1a1b in another project before(X. Li et al., 2020), detailed information about Akr1a1b will not be involved in this thesis. The alignment comparing the amino acid sequence of Akr1a1 and Akr1a1a in humans, mice, and zebrafish showed that Akr1a1a in zebrafish shares a 60% and 58.154% similarity with Akr1a1 in humans and mice, respectively. Meanwhile, Akr1a1a and Akr1a1 possess the same active site and binding site among three different species, suggesting it is feasible to use zebrafish as a model animal to investigate the function of Akr1a1 (Fig.2A).

Akr1a1a mRNA level was determined by RT-qPCR in larvae and adult organs of zebrafish. The results showed ubiquitous *akr1a1a* expression throughout embryonic and larval stages with being highest expressed at 2dpf (Fig.2B). Besides, *akr1a1a* expression was mostly seen in the liver, more than two hundred-fold than the reference organ (heart), and to a less extent in the brain (8-fold), kidney (3-fold), and eye (3-fold) (Fig.2C). Altogether, these data imply that Akr1a1a distributes widely in the early developmental stages of zebrafish larvae and adult organs, and it may play an essential role in embryonic development and adulthood.

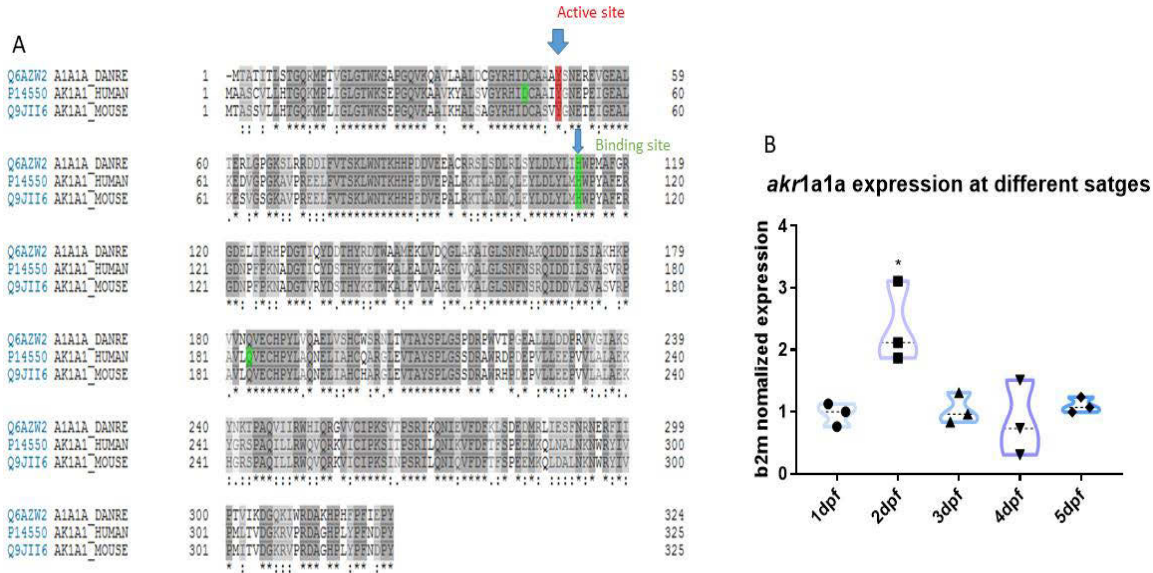

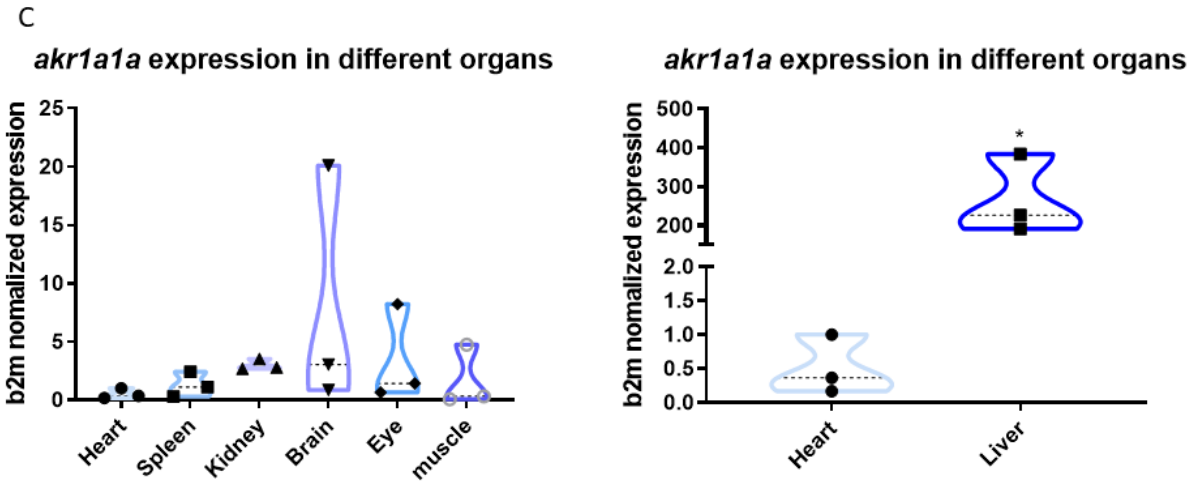

Fig.2 Sequence alignment of Akr1a1a across different species and *akr1a1a* mRNA expression in different embryonic and larval stages and adult organs of wild-type zebrafish.

(A) The amino acid alignment showed a high similarity between the different species in the active site (red frame) and binding site (green frame); first line: zebrafish Akr1a1a; second line: human Akr1a1; third line: mouse Akr1a1. (B) *akr1a1a* mRNA expression in wild-type zebrafish larvae showed a significant elevation at 2 dpf. (C) *akr1a1a* mRNA expressed mostly in liver of wild-type adult zebrafish (heart as reference organ). Expression of genes was determined by RT-qPCR and normalized to *b2m*. Larval stage: n=3 clutches with 30 larvae, adult organs: n=3 with one organ per sample. For statistical analysis one-way ANOVA followed by Tukey's multiple comparison test and Student's t-test were applied, *p<0.05. RT-qPCR, real-time quantitative polymerase chain reaction; dpf, day post fertilization; b2m, β2 microglobulin.

3.2 Generation and validation of Akr1a1a knockout in zebrafish

In order to explore the function of Akr1a1a in zebrafish, *akr1a1a*$^{-/-}$ line was generated by CRISPR/Cas9 technology as the first step(Konermann et al., 2015). I appreciate my colleague Dr. Felix Schmöhl, who completed this part of the work, including CRISPR-guide RNA (gRNA) design and mutant generation. Briefly, gRNA was designed targeting exon 2 of *akr1a1a*, and two various frame-shift mutants were identified and utilized for further studies, including a one base-pair insertion in the *Tg(fli1:EGFP)* reporter line and a five base-pair deletion in the *Tg(wt1b:EGFP)* reporter line (Fig.3A). The general morphology of larvae from 2dpf to 5dpf did not show any noticeable difference in mutants compared to the wild-type (Fig.3B). To evaluate whether the *akr1a1a* mutations cause the non-functional Akr1a1a protein after translation, we generated an antibody by collaborating with CF Unit Antibodies, DKFZ Heidelberg, Germany. Western blot was performed, afterwards. The result showed an ultimate loss of Akr1a1a in both five base-pair deletion and one base-pair

insertion mutants (Fig.3C). The percentage of *akr1a1a*$^{-/-}$ zebrafish growing into adulthood is about 21.21%, while 28.79% to wild type and 50% to heterozygous zebrafish which is consistent with Mendel's law of inheritance suggesting permanent loss of akr1a1a does not affect the survival of zebrafish (Fig.3D). Besides, AKR activity was measured by using DL-Glyceraldehyde as the substrate, which showed a 30% significant decline in *akr1a1a*$^{-/-}$ larvae (Fig.3E). All the above data have proven the successful generation of *akr1a1a* knockout mutants.

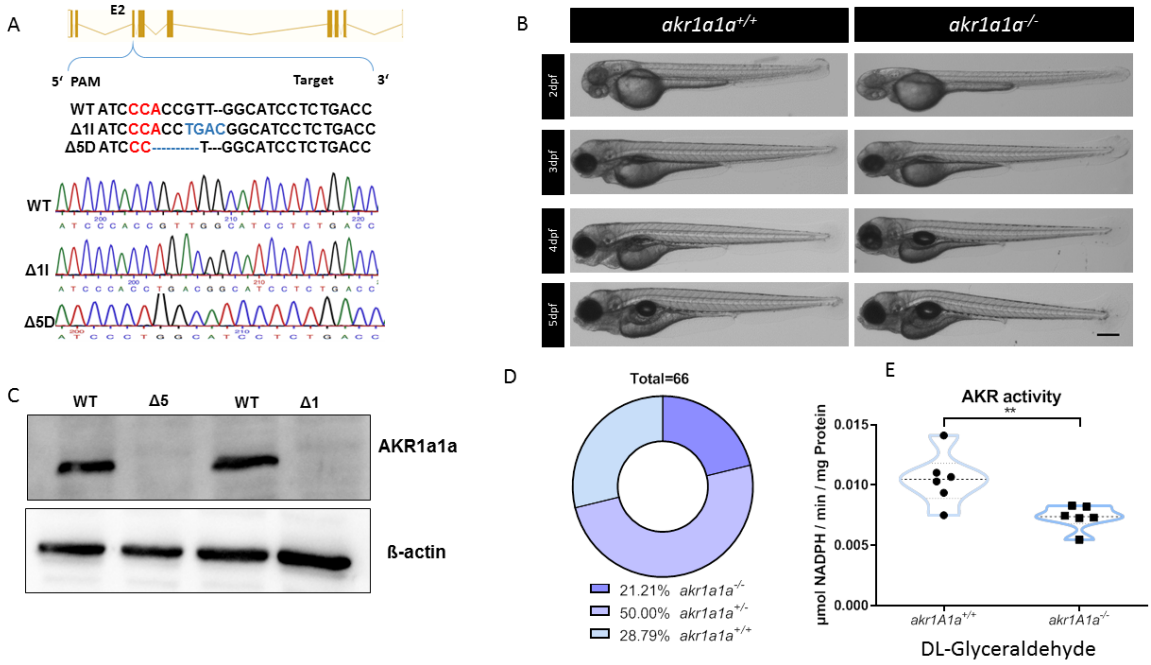

Fig.3 Generation of Akr1a1a knockout zebrafish by using CRISPR-Cas9 technology.
(A) Akr1a1a-CRISPR-target site was designed in exon 2 of *akr1a1a* and CRISPR/Cas9-induced insertion of one nucleotide and five deletion nucleotides, which were selected for further *akr1a1a* mutant line generation and maintenance. Genotype was analyzed using sequencing chromatograms of PCR-amplified *akr1a1a* region, containing the *akr1a1a* target site. Chromatogram shows *akr1a1a* wild type, one nucleotide insertion, and five nucleotides deletion homozygous sequencing results. Δ1I, one base-pair insertion. Δ5D, five base-pair deletion. (B) Microscopic images showed unaltered morphology of *akr1a1a*$^{-/-}$ larvae in comparison with *akr1a1a*$^{+/+}$ larvae from 2dpf to 5dpf. Black scale bar: 300 µm. (C) Western blot for Akr1a1a expression in adults' livers showed absent of Akr1a1a protein in both one base-pair insertion and the five base-pair deletion mutants. ß-actin served as loading control. n=3, each lane represents one liver sample from according adult fish. (D) Adult fish number among different genotypes was in line with *the Mendelian Inheritance* in the first generation of F2: *akr1a1a*$^{+/+}$ =19, *akr1a1a*$^{+/-}$ =30, *aldh3a1*$^{-/-}$ =11. (E) *akr1a1a*$^{-/-}$ zebrafish showed decreased enzyme activity (DL-Glyceraldehyde as substrate) measured by spectrophotometric analysis in zebrafish lysates at 96 hpf; n = 5-6 clutches with 50 larvae. For statistical analysis Student's t-test was applied, **p<0.01. PAM, protospacer-adjacent motif. dpf, day post fertilization. hpf, hour post fertilization

Enzyme-activity assays were performed by Dr. Jakob Morgenstern/Dr. Tomas Fleming.

3.3 Vascular and pronephric structure alters in *akr1a1a*$^{-/-}$ larvae

The vascular and pronephric structures were analyzed first by using *Tg(fli1: EGFP)* and *Tg(wt1b:EGFP)* reporter lines, respectively. *Tg(fli1:EGFP)* zebrafish reporter line was used to analyze vascular structure since enhanced green fluorescence protein (EGFP) expressed in endothelial cells enables the visualization of the vascular structure under the microscope(Lawson & Weinstein, 2002). To analyze the vasculature system including the trunk vasculature and hyaloid vasculature, zebrafish larvae were collected at 4dpf and 5dpf separately, and images were captured with a confocal microscope. Results showed the trunk vasculature rarely had a significant difference among *akr1a1a*$^{-/-}$ and *akr1a1a*$^{+/+}$ larvae at 4dpf (Fig.4). Nevertheless, I found increasing numbers of branches and sprouts in hyaloid vasculature of *akr1a1a*$^{-/-}$larvae compared to *akr1a1a*$^{+/+}$ larvae at 5dpf (Fig.5).

Besides, to evaluate kidney development, which may potentially be affected by the knockout of *akr1a1a*, the pronephric structure was analyzed by using *Tg(wt1b: EGFP)* zebrafish renal reporter line, which expresses EGFP under the wt1b promoter and enables the visualization of the glomerulus, the neck region and the tubule of the pronephros(Perner, Englert, & Bollig, 2007). 2dpf was chosen as the time point to analyze pronephros since the pronephros is already fully developed and starts its function as a blood filter at that time(Perner et al., 2007). The results showed that *akr1a1a*$^{-/-}$ larvae own slightly shorter neck, but the length and width of pronephros keep unaltered compared to *akr1a1a*$^{+/+}$ larvae (Fig.6).

Taken together, these results reveal that the loss of Akr1a1a leads to alterations of the hyaloid vessels and the pronephros at the larval stage of zebrafish.

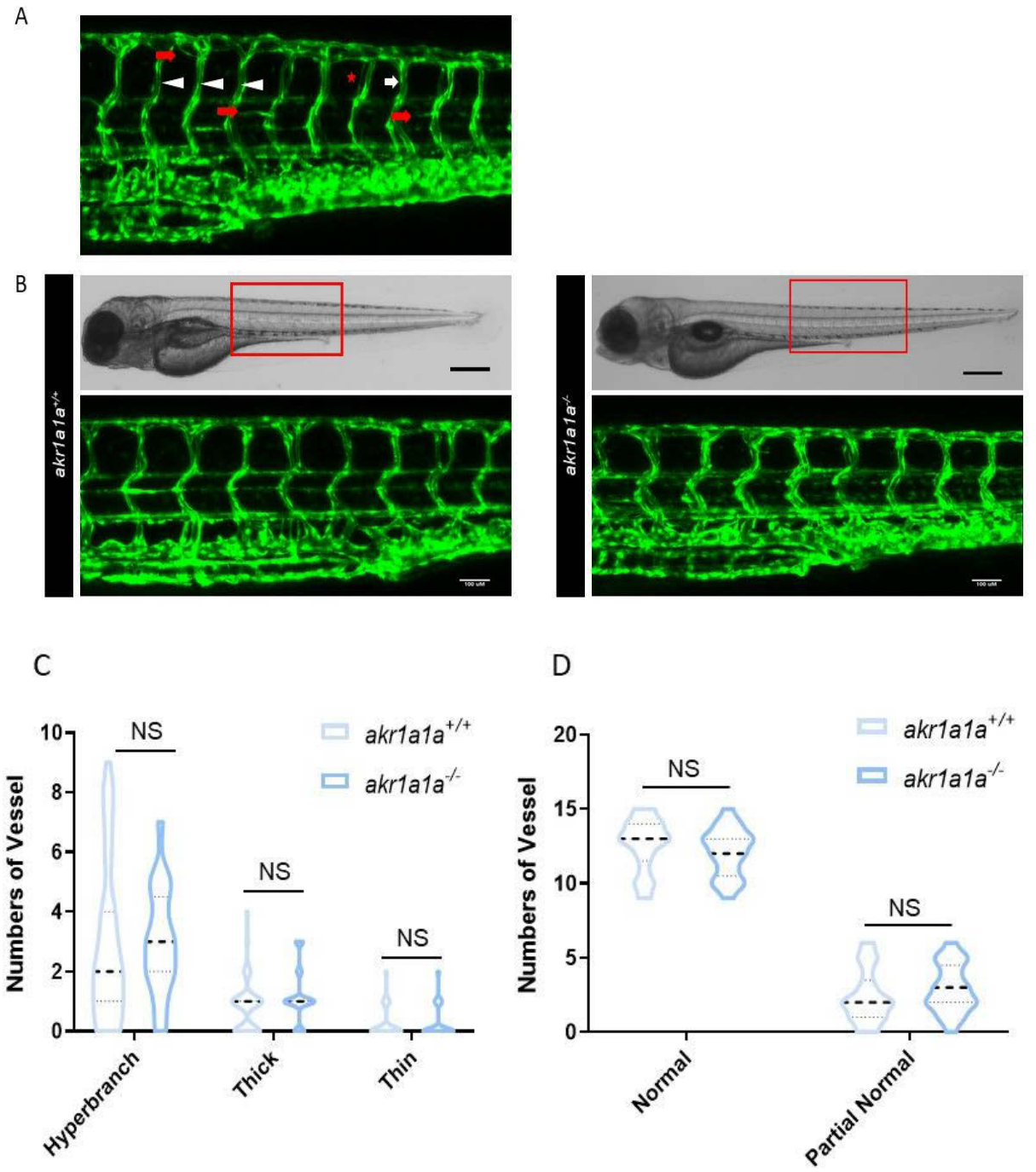

Fig.4 Trunk vasculature of *akr1a1a*$^{-/-}$ and *akr1a1a*$^{+/+}$ *Tg(fli1: EGFP)* zebrafish larvae.

(A) Representative confocal image to show normal ISV (white triangle), hyperbranch (red arrow), thin ISV (red pentastar) and thick ISV (white arrow). (B) Light microscopic images showed the gross morphology of zebrafish larvae and red boxes indicate the regions seen in the confocal images. White scale bar = 100 μm, black scale bar =300 μm. (C-D) Quantification of abnormal ISV and hyperbranch formation; n = 39 larvae (*akr1a1a*$^{+/+}$) and n = 34 larvae (*akr1a1a*$^{-/-}$). Mean± SD, for statistical analysis Student's t-test was applied. NS, not significant. ISV, intersegmental vessels.

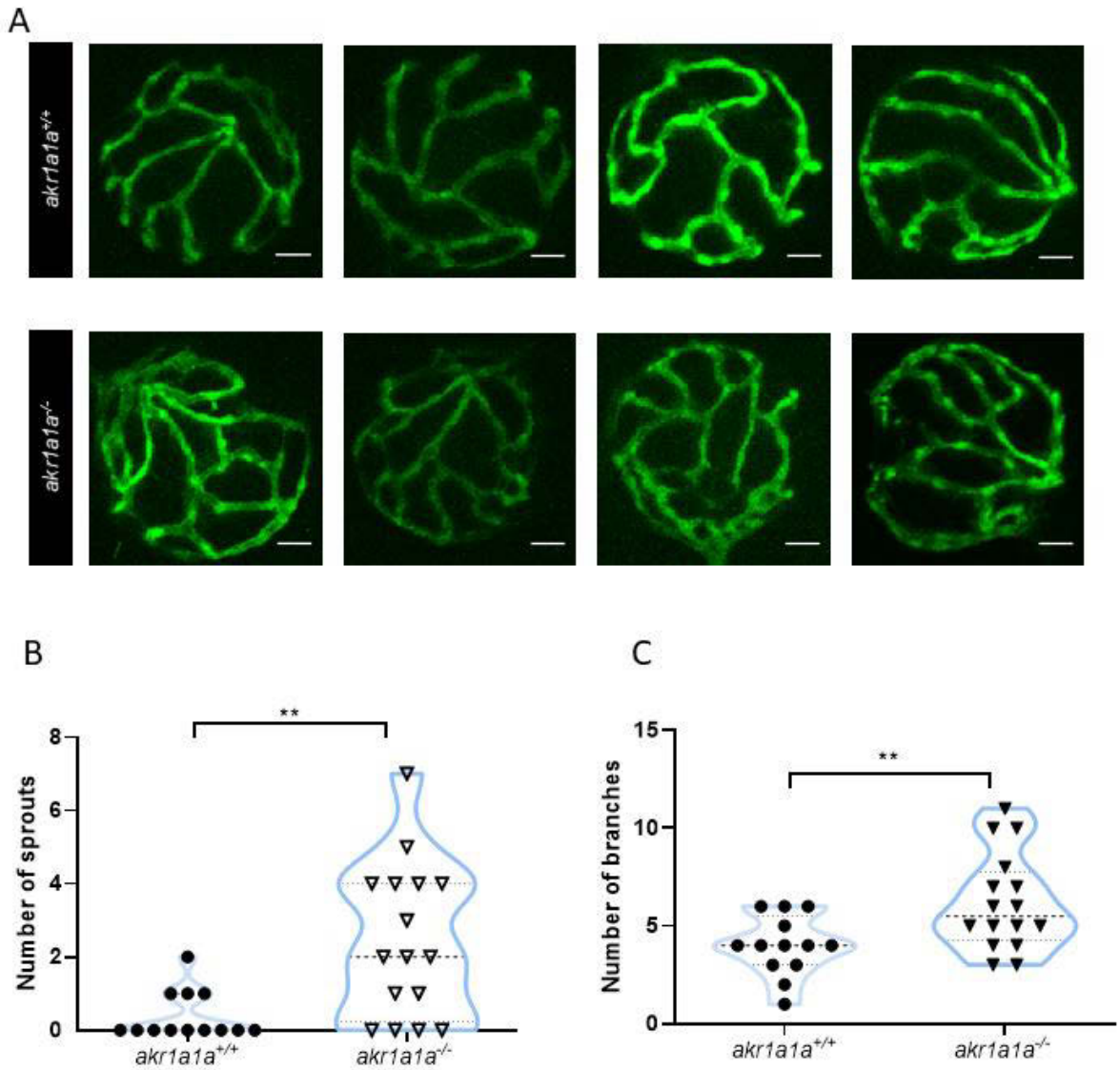

Fig.5 Retinal hyaloid vasculature alterations in *akr1a1a*$^{-/-}$ *Tg(fli1: EGFP)* zebrafish larvae.

(A) Representative confocal images of hyaloid vasculature. White scale bar = 20µm. (B-C) Quantification of the branches and sprouts formation, n=13-16 per group. Mean± SD, for statistical analysis Student's t-test was applied. **p<0.01.

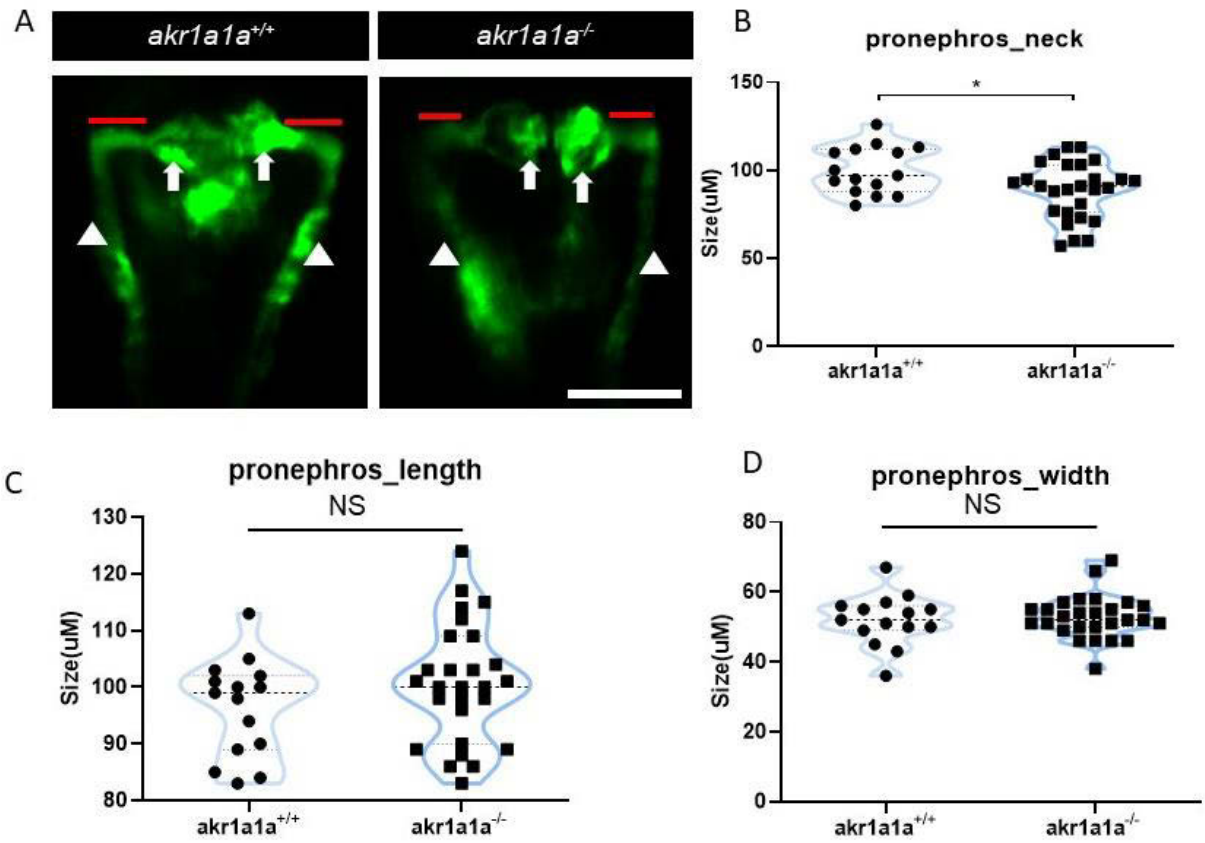

Fig.6 Akr1a1a knock-out in zebrafish caused alterations of the embryonic pronephros.
(A) Representative confocal images of the pronephros in *Tg(wt1b: EGFP)* embryo (48 hpf), visible from the dorsal view. The renal structure is composed of two tubules (white triangle) that are fused to form a single glomerulus (white arrow) via a neck (red line). White scale bar=0.1 mm. (B, C, D) Compared with *akr1a1b*$^{+/+}$ embryos (n=33, mean ± SD) at 48 hpf, *akr1a1b*$^{-/-}$ mutants (n=21, mean ± SD) displayed unaltered glomerulus but slightly shorten tubular neck. Mean± SD, for statistical analysis Student's t-test was applied. *p < 0.05. NS, not significant.

3.4 Insulin receptor signaling pathway is downregulated in *akr1a1a*$^{-/-}$ larvae

In order to investigate the mechanisms behind the alterations of hyaloid vasculature, gene-expression patterns were analyzed by genome RNA-Seq among *akr1a1a*$^{+/+}$ and *akr1a1a*$^{-/-}$ larvae at 5dpf. Principal component analysis (PCA) exhibited components of each sample by which showed that *akr1a1a*$^{+/+}$ and *akr1a1a*$^{-/-}$ plots are totally separated in the PC1 axis (Fig.7A). Volcano plot of statistically significant differentially expressed genes at p <0.05 identified around 2 thousand genes downregulated and 2 thousand genes upregulated in *akr1a1a*$^{-/-}$ zebrafish larvae (Fig.7B).

Then, gene set enrichment analysis (GSEA) was performed to better understand altered physiological signaling pathways reflected by the loss of Akr1a1a. GSEA revealed several altered biological pathways. Among them, the insulin receptor signaling pathway was significantly downregulated in *akr1a1a* mutants, suggesting the loss of Akr1a1a may induce imbalanced glucose homeostasis (Fig.7C, 7D).

A

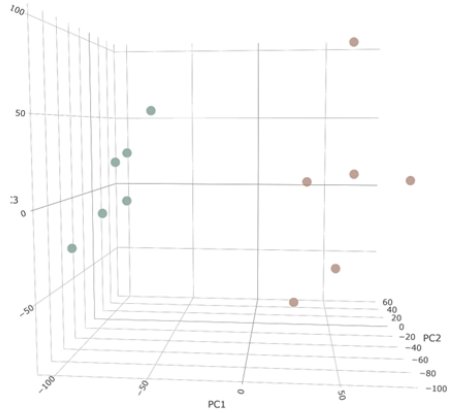

B

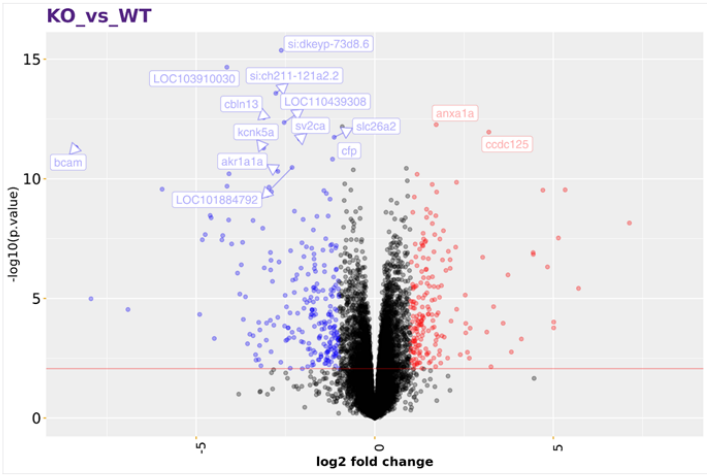

C

Pathway	Enrichment Score	NES	P.adjust	Q values
Insulin receptor signaling pathway	-0.542	-1.89	0.028	0.020

D

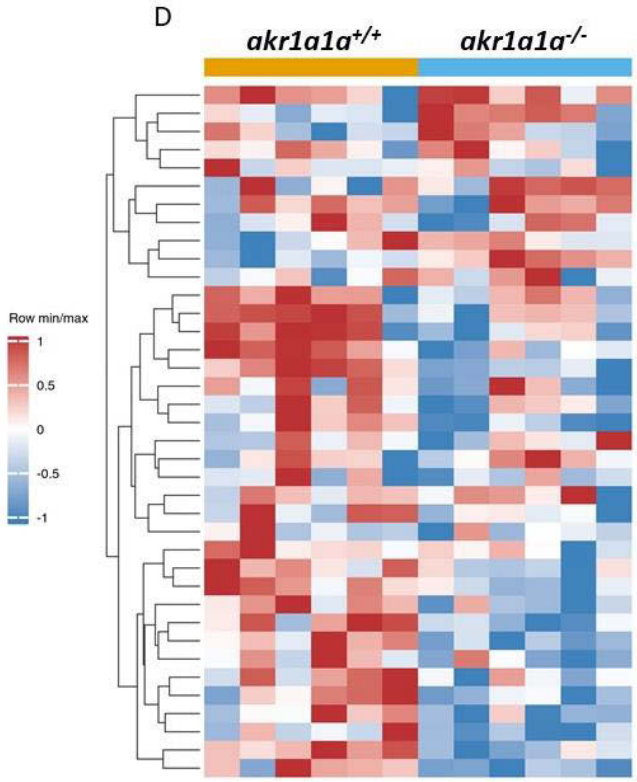

Fig.7 An overview of RNA sequence results and Insulin receptor signaling pathway decreased significantly by GESA analysis.

(A) Results of the quality control in gene expression analysis between *akr1a1a*$^{+/+}$ and *akr1a1a*$^{-/-}$ zebrafish larvae at 5dpf. Principal component 1,2 and 3 are on the axis. The plots showed the wild type(n=6) in brown and akr1a1a mutants(n=6) in green. (B) Volcano plot showed the down-regulated/upregulated between *akr1a1a*$^{+/+}$ and *akr1a1a*$^{-/-}$ zebrafish larvae at 5dpf. (C) Analysis result by GSEA. GESA, gene set enrichment analysis. (D) Heatmap showed relative mRNA expression in insulin receptor signaling pathway between *akr1a1a*$^{+/+}$ (n=6) and *akr1a1a*$^{-/-}$ (n=6). Higher and lower expression is displayed in red and blue, respectively.

RNA Sequence analysis was processed by Dr. Carsten Sticht

3.5 *Akr1a1a*$^{-/-}$ larvae display reduced *insra/insrb* mRNA expression and higher whole-body glucose at 5dpf

In order to confirm whether the insulin receptor signaling pathway is truly impaired in *akr1a1a*$^{-/-}$ larvae, insulin, and insulin receptor mRNA expression levels were analyzed by RT-qPCR, meanwhile, whole-body glucose was measured by glucose assay accordingly. Intriguingly, *preproinsulin (ins),* the main insulin-encoding gene involved in glucose homeostasis regulation in zebrafish, is unaltered in *akr1a1a*$^{-/-}$ larvae but insulin receptor a and b (*insra* and *insrb*) mRNA reduced significantly in *akr1a1a*$^{-/-}$ larvae at 5dpf (Fig.8B, C, D). In addition, *akr1a1a*$^{-/-}$ larvae exhibited 50% incremental glucose level in contrast to *akr1a1a*$^{+/+}$ larvae at 5dpf (Fig.8A). These data suggest the loss of Akr1a1a leads to impaired insulin receptor signaling pathway and imbalanced glucose homeostasis while downregulated insra and insrb mRNA expression might be the reason behind them.

Then a hypothesis came into my mind. Whether the abnormal hyaloid vasculature in *akr1a1a*$^{-/-}$ larvae result from reduced *insra/insrb* expression? In order to address this question, *insra* and *insrb* morpholinos (SB-insra-MO, SB-insrb-MO) were designed and used as tools to transiently and partially silence *insra* and *insrb* expression by the antisense approach. SB-insra-MO and SB-insrb-MO target exon3-intron3 and exon7-intron7 junctions of *insra/insrb* respectively (Fig.9A). Two/four nanograms of morpholinos were injected into the one-cell stage of wild-type zebrafish embryos. The efficiency of morpholinos was validated by RT-PCR gel, which showed decreased wild type insra/insrb but the elevated expression of morphant *insra/insrb* in the gel upon SB-insra-MO and SB-insrb-MO injection (Fig.9B). Hyaloid vessels were then analyzed after *insra/insrb* morpholino injection. Interestingly, similar to *akr1a1a*$^{-/-}$ larvae, either *insra* or *insrb* silencing could lead to alterations in wild-type larvae's hyaloid vessels. Besides, whole-body glucose increased significantly in both

insra/insrb silencing group at 5dpf (Fig.10). To sum up, these data indicate permanent loss of Akr1a1a results in downregulation of *insra* and *insrb* mRNA, which induce imbalanced glucose homeostasis and alterations in hyaloid vessels.

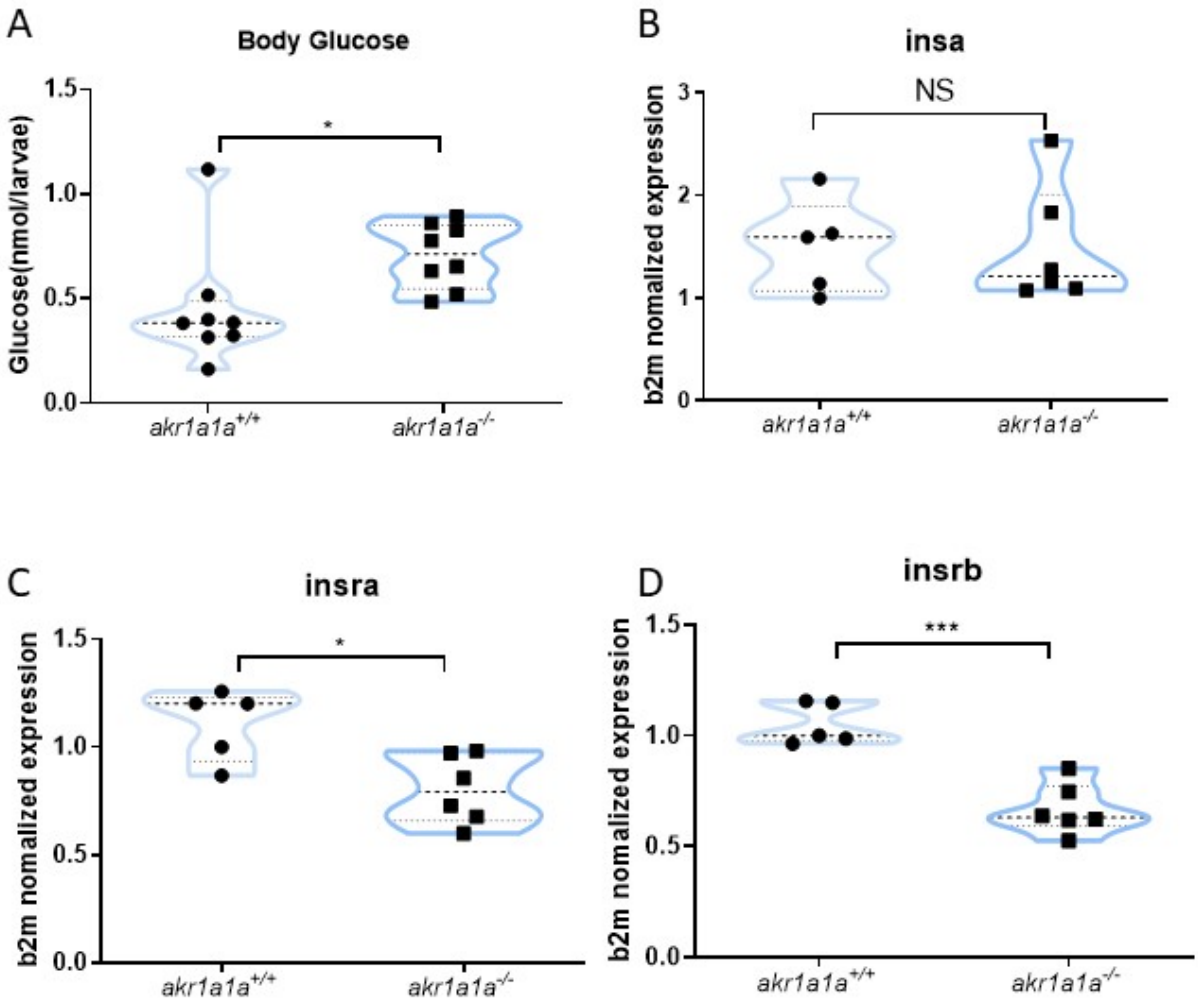

Fig.8 Whole-body glucose measurement and insulin relevant gene expression levels.
(A) *akr1a1a*$^{-/-}$ larvae owned obviously higher level of whole-body glucose compared with *akr1a1a*$^{+/+}$ larvae at 5dpf, n = 8 clutches with 20 larvae (B) *insa* gene expression level showed no alteration in *akr1a1a*$^{-/-}$ larvae at 5dpf. (C, D) Both *insra* and *insrb* mRNA expression were clear downregulated in *akr1a1a*$^{-/-}$ larvae at 5dpf, n = 5-6 clutches with 30 larvae, Mean ± SD, for statistical analysis Student's t-test was applied. *p < 0.05. ***p<0.001. NS, not significant.

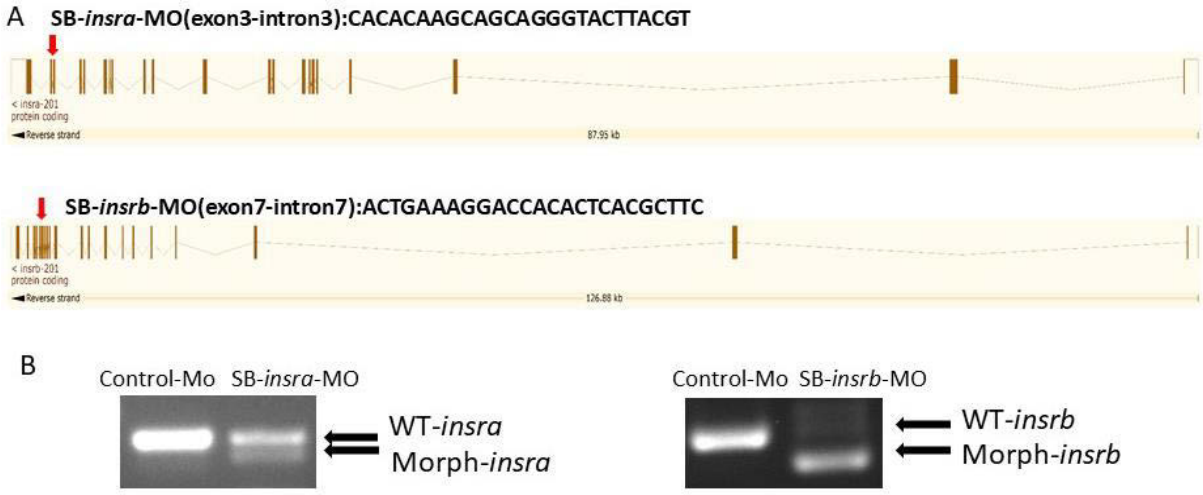

Fig.9 *Insra/insrb* morpholinos design and validation.
(A) SB-insra-MO and SB-insrb-MO target exon3-intron3 and exon7-intron7 junctions of *insra/insrb* respectively. (B) Validation of splice-blocking morpholinos: SB-insra-MO and SB-insrb-MO. RT-PCR of Control-MO, SB-insra-MO and SB-insrb-MO injected larvae showed wild type and generation of morphant insra/insrb signals at 24 hpf. 6 ng of morpholinos: Control-MO, SB-insra-MO and SB-insrb-MO were injected into the one-cell stage of zebrafish embryos respectively. WT, wild type; MO, morpholino; Morph: morpant.

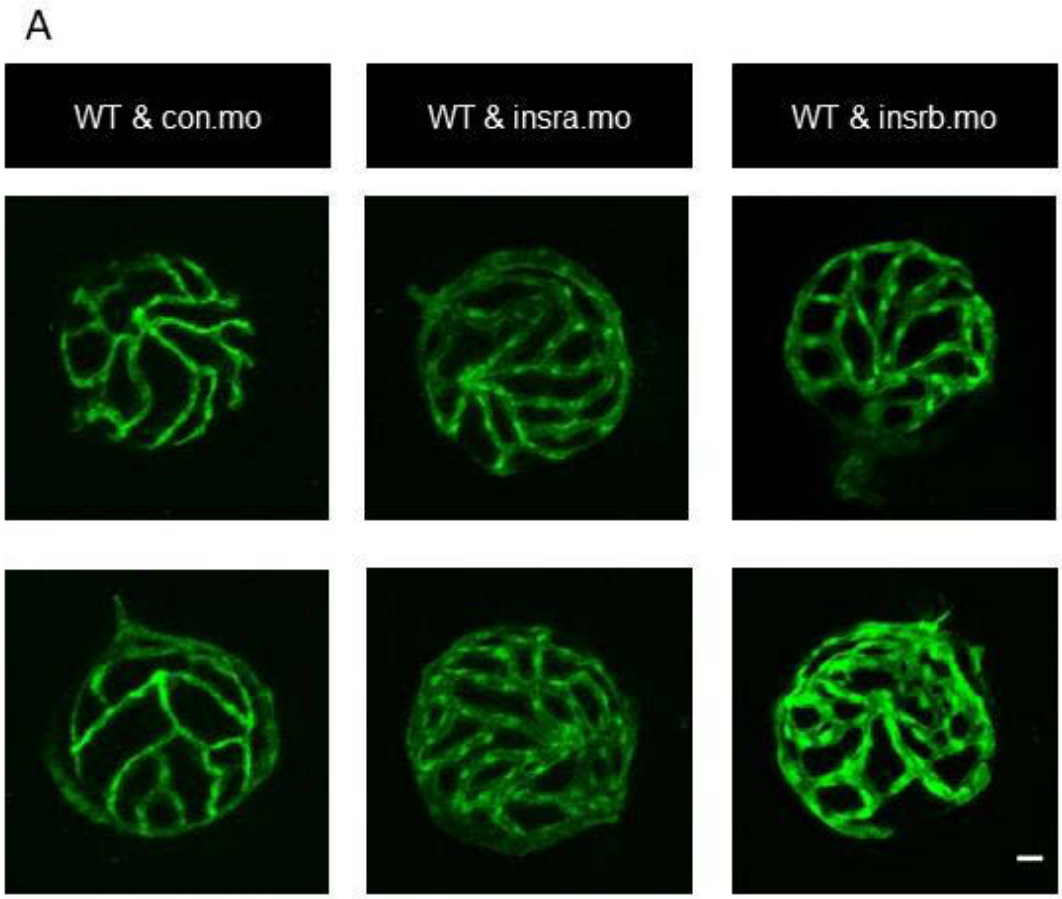

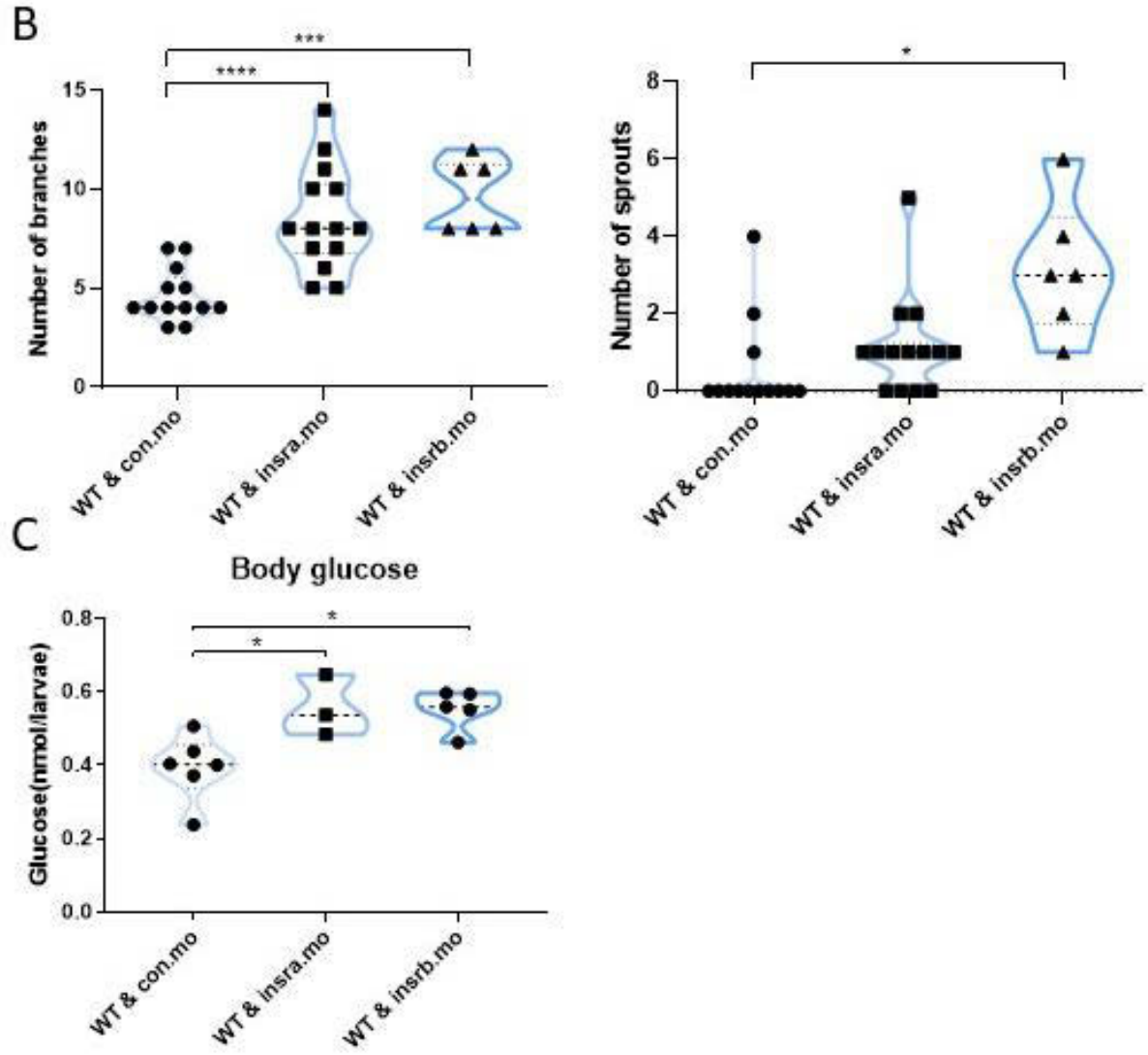

Fig.10 Hyaloid vasculature was impacted by *insra/insrb* silencing.
(A)Representative confocal images of hyaloid vasculature. White scale bar = 20 μm. (B)Quantification of the branches and sprouts formation, n=6-14 per group. (C) whole-body glucose increases significantly with *insra/insrb* silencing at 5dpf, n = 3-6 clutches with 20 larvae, Mean ± SD, for statistical analysis Student's t-test was applied. *p < 0.05. ***p<0.001. ****p<0.0001.

3.6 Acrolein but not AGEs precursors accumulated in *akr1a1a*$^{-/-}$ larvae

Up to now, the link between the loss of Akr1a1a and reduced *insra/insrb* mRNA is still missing. In order to find the potential mechanism, a couple of reactive carbonyl species (RCS) which were reported as substrates of Akr1a1, including glyoxal, methylglyoxal (MG), 3-Deoxyglucosone (3-DG), and acrolein were determined in both *akr1a1a*$^{+/+}$ and *akr1a1a*$^{-/-}$ larvae at 4dpf. The results showed that 3-DG and MG have no difference among both groups, while glyoxal has a slight elevating tendency

in *akr1a1a*$^{-/-}$ larvae but not statistically significant. Nevertheless, *akr1a1a*$^{-/-}$ larvae showed a significant increment of internal acrolein (Fig.11). Furthermore, AKR activity was determined again by treating acrolein as the substrate, and the result showed the AKR activity reduced significantly in *akr1a1a*$^{-/-}$ larvae, which confirmed Akr1a1a is a principal enzyme to metabolize acrolein in zebrafish (Fig.12).

Since Glo1 and ALDH enzyme systems have similar functions as the AKR enzyme system in detoxifying RCS metabolites and AGEs precursors, both Glo1 and ALDH enzyme activity were measured in larvae. However, Glo1 and ALDH enzyme activity kept unchanging in *akr1a1a*$^{-/-}$ larvae at 4dpf (Fig.13).

These data indicate that Akr1a1a is a main metabolizing enzyme for internal acrolein, and its deficiency does not influence the metabolism of glyoxal, MG, and 3-DG but causes dramatic acrolein accumulation. Besides, Glo1 and ALDH enzyme activity do not show a compensatory elevation in *akr1a1a*$^{-/-}$ larvae suggesting Glo1 and ALDH enzyme systems may not be able to detoxify accumulated acrolein.

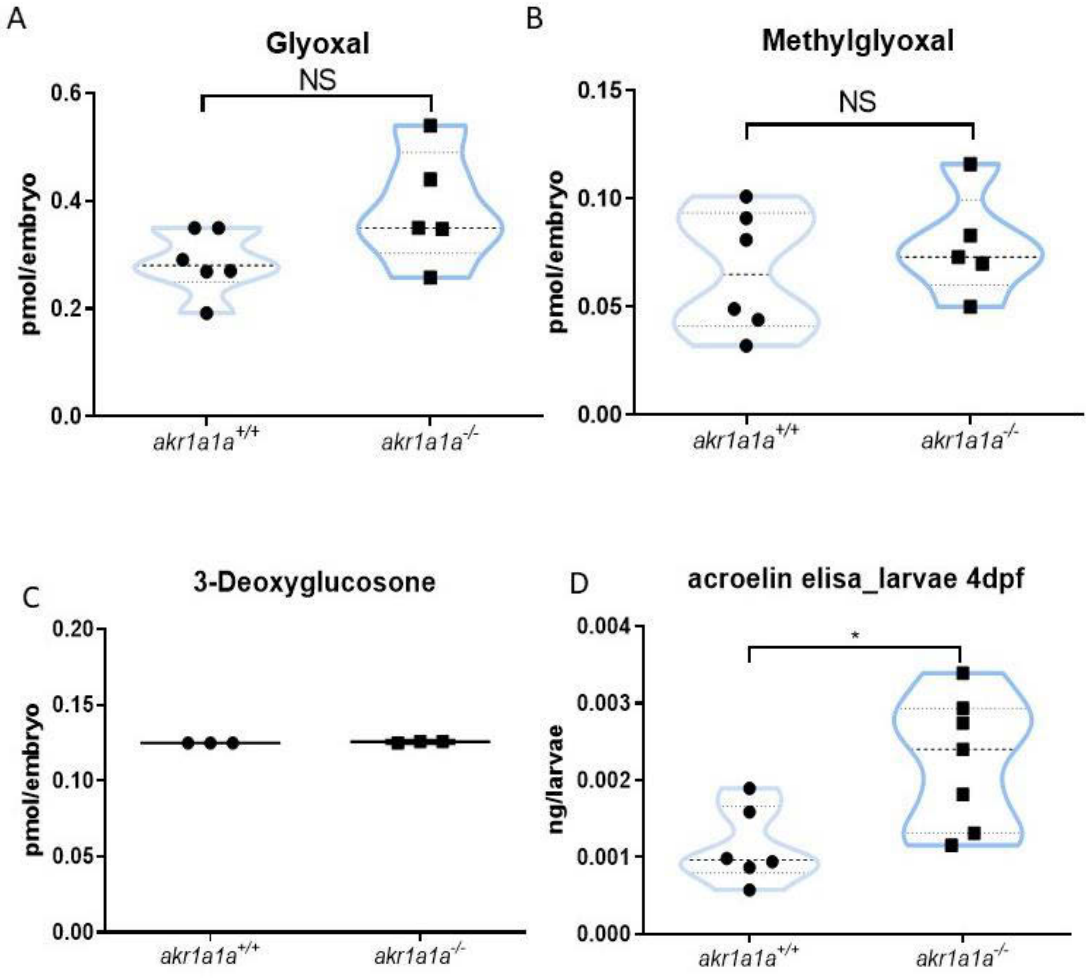

Fig.11 None of AGEs precursors but acrolein accumulated in *akr1a1a*$^{-/-}$ larvae at 4dpf

(A, B, C) *akr1a1a*$^{-/-}$ larvae at 96hpf showed stable glyoxal, methyglyoxal and 3-deoxyglucosone level, as compared with *akr1a1a*$^{+/+}$ larvae. n = 3-6 clutches with 50 larvae. (D) Internal acrolein exhibited a two-fold elevation in *akr1a1a*$^{-/-}$ larvae at 4dpf. Mean± SD, for statistical analysis Student's t-test was applied. *p < 0.05. NS, not significant.

Glyoxal, methylglyoxal and 3-deoxyglucosone were determined by Dr. Jakob Morgenstern/Dr. Tomas Fleming.

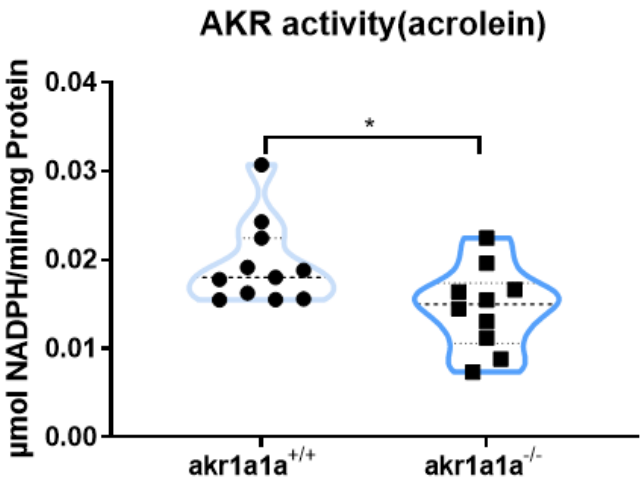

Fig.12 AKR activity decreased in *akr1a1a*$^{-/-}$ larvae by using acrolein as substrate

AKR activity decreased significantly in *akr1a1a*$^{-/-}$ larvae by using acrolein as substrate at 96hpf. n=10-11 clutches with 50 larvae. Mean± SD, for statistical analysis Student's t-test was applied. *p < 0.05.

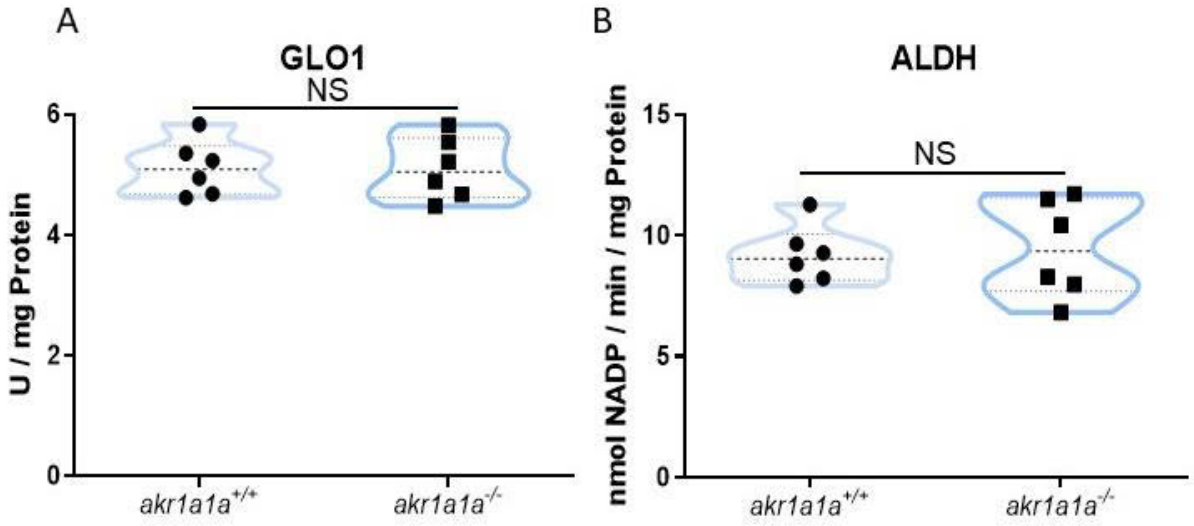

Fig.13 Measurement of Glo1 and ALDH enzyme activity.

(A, B) Both Glo1 and ALDH enzyme activity kept stable, as determined by LC-MS/MS. n = 6 clutches with 50 larvae. Mean± SD, for statistical analysis Student's t-test was applied. NS, not significant.

3.7 Acrolein cause alterations in hyaloid vasculature, higher whole-body glucose and reduced *insra/insrb* mRNA expression which can be rescued by L-carnosine and PK11195 treatment

To further investigate if acrolein is the missing point between the declined *insra/insrb* mRNA expression and the loss of Akr1a1a, wild-type larvae were incubated with artificially synthesized acrolein from 1dpf to 5dpf. Hyaloid vasculature was analyzed afterward. Interestingly, more branches can be observed in hyaloid vasculatures after the treatment (Fig.14A, B). Further experiments with acrolein intervention showed that treated larvae had elevated whole-body glucose level (Fig.14C), normal expression level of *ins* (Fig.14D) mRNA, but less expressed *insra/insrb* mRNA (Fig.14E) in contrast to the larvae without treatment. Since acrolein has been reported as a toxic antioxidant that can cause alterations in various tissues, I was wondering whether the alterations in hyaloid vasculature result from reduced *insra/insrb* expression or by acrolein directly. Therefore, the co-incubation experiment was performed on wild-type larvae with acrolein and scavenger–L-carnosine or hypoglycemic drug-PK11195. Surprisingly, both L-carnosine and PK11195 could rescue the alterations in hyaloid vasculature, suggesting acrolein induces alterations in hyaloid vasculature via adjusting glucose homeostasis instead of toxic effects caused by itself (Fig.15).

To sum up, these data furtherly prove via reducing *insra/insrb* mRNA expression, non-detoxified and accumulated internal acrolein could alter the hyaloid vasculature of zebrafish larvae. Moreover, successful reversion of the hyaloid phenotypes by applying hypoglycemic drug and acrolein-scavenger implies that these drugs are potential candidates for treating acrolein-induced vascular alterations.

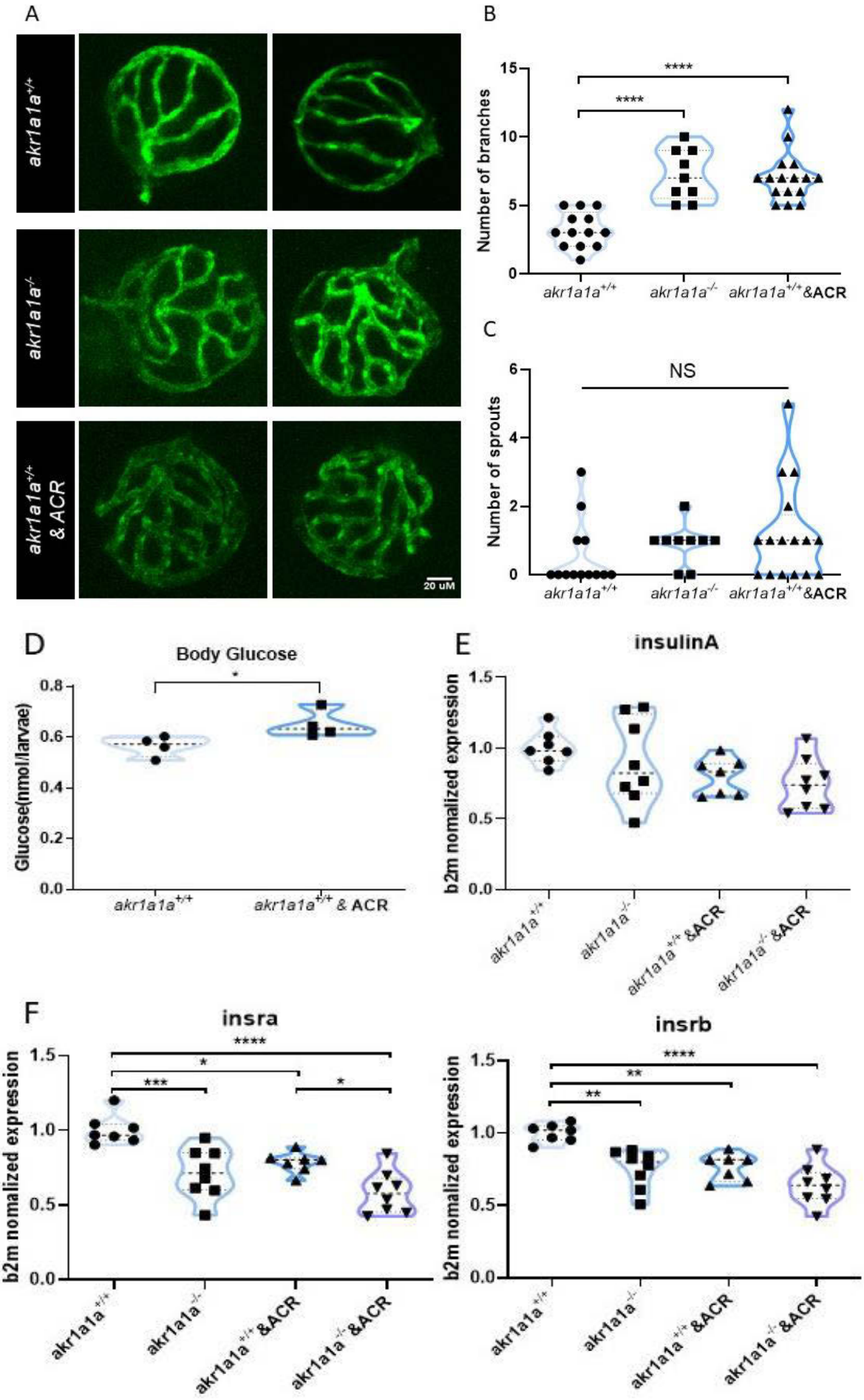
A
akr1a1a+/+
akr1a1a-/-
akr1a1a+/+ & ACR
20 uM
B
Number of branches
15
10
5
0
****
****
akr1a1a+/+
akr1a1a-/-
akr1a1a+/+&ACR
C
Number of sprouts
6
4
2
0
NS
akr1a1a+/+
akr1a1a-/-
akr1a1a+/+&ACR
D
Body Glucose
Glucose(nmol/larvae)
0.8
0.6
0.4
0.2
0.0
*
akr1a1a+/+
akr1a1a+/+ & ACR
E
insulinA
b2m nomalized expression
1.5
1.0
0.5
0.0
akr1a1a+/+
akr1a1a-/-
akr1a1a+/+ &ACR
akr1a1a-/- &ACR
F
insra
b2m nomalized expression
1.5
1.0
0.5
0.0
****
*
***
*
akr1a1a+/+
akr1a1a-/-
akr1a1a+/+ &ACR
akr1a1a-/- &ACR
insrb
b2m nomalized expression
1.5
1.0
0.5
0.0
****
**
**
akr1a1a+/+
akr1a1a-/-
akr1a1a+/+ &ACR
akr1a1a-/- &ACR

Fig.14 Acrolein induced alterations on retinal hyaloid vasculature and downregulation of *insra/insrb* mRNA expression at 5dpf.
(A)Representative confocal images of hyaloid vasculature. White scale bar:20uM. (B-C) Quantification of hyaloid vasculature showed significant increasing numbers of branches in *akr1a1a*$^{-/-}$ larvae and *akr1a1a*$^{+/+}$ larvae incubated with 10uM acrolein at 5dpf. n=9-16. White scale bar = 20 µm. (D) Whole-body glucose measurement showed higher glucose level in *akr1a1a*$^{+/+}$ larvae incubated with 10uM acrolein at 5dpf. n=4 clutches with 20 larvae. (E) *Insa* gene expression was unaltered in *akr1a1a*$^{-/-}$ larvae and *akr1a1a*$^{+/+}$ larvae with/without acrolein treatment. n=7-8 clutches with 30 larvae. (F) Both *insra* and *insrb* showed declined mRNA expression level in *akr1a1a*$^{-/-}$ larvae and *akr1a1a*$^{+/+}$ larvae incubated with 10uM acrolein. For statistical analysis one-way ANOVA followed by Tukey‘s multiple comparisons test and Student’s t-test was applied. n=7-8 clutches with 30 larvae. *p < 0.05. **p<0.01. ***p<0.001. ****p<0.0001.

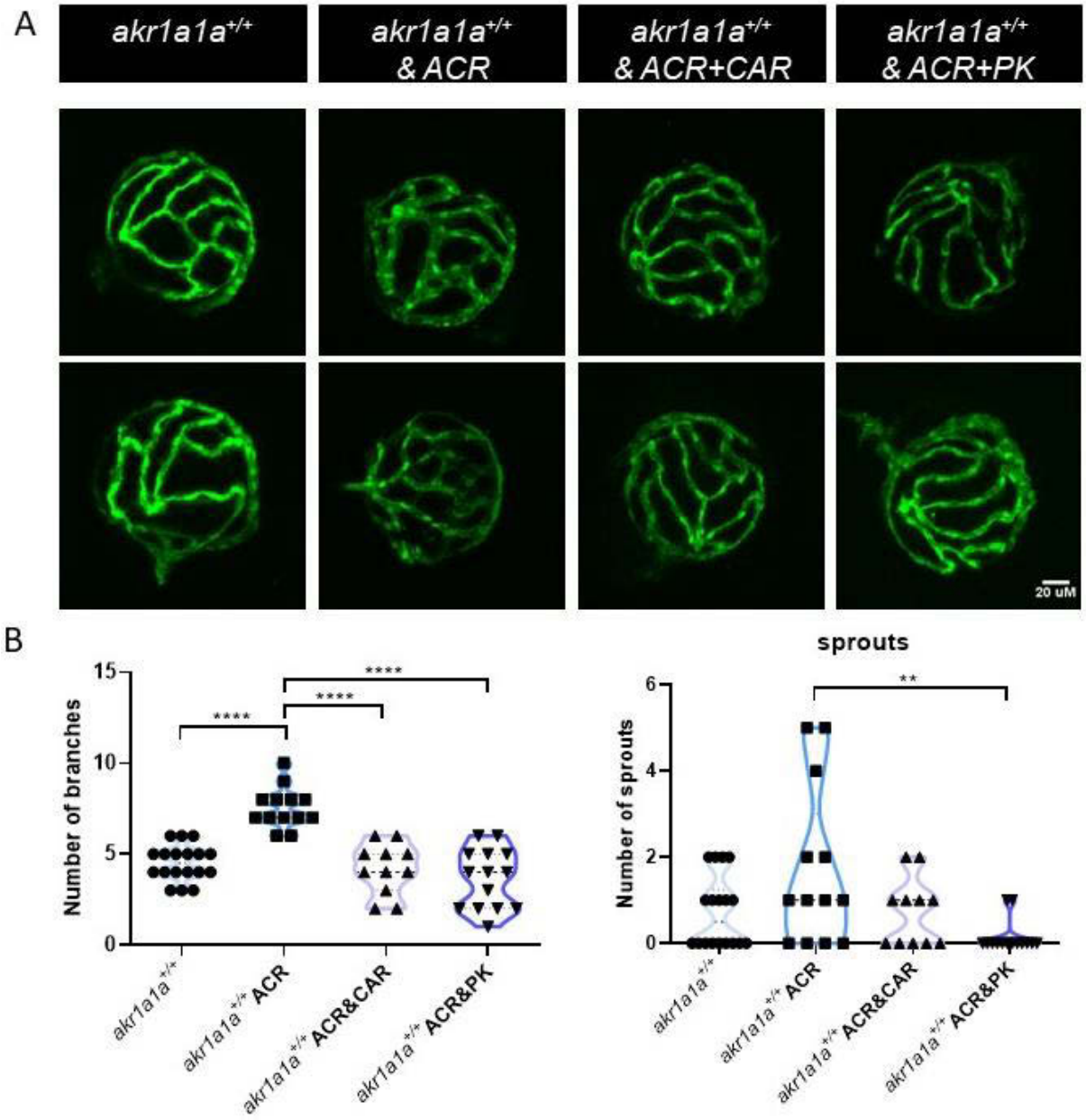

Fig.15 Carnosine and PK11195 can alleviate the effects caused by acrolein on retinal hyaloid vasculature at 5dpf.

(A)Representative confocal images of hyaloid vasculature. White scale bar: 20μm. (B) Quantification of hyaloid vasculature showed significant increasing numbers of branches in akr1a1a1+/+ larvae incubated with 10uM acrolein but rescued by carnosine and PK11195 at 5dpf. n=11-18. For statistical analysis one-way ANOVA followed by Tukey‘s multiple comparisons test was applied. **p<0.01. ****p<0.001.

3.8 Retina vascular and renal alterations in *akr1a1a*$^{-/-}$ adult zebrafish.

To evaluate if the alterations appearing in larval hyaloid vasculature also exist in adults, retina vessels of adult *akr1a1a*$^{-/-}$ zebrafish were assessed. Meanwhile, the blood glucose of adults at 2 hours postprandial and overnight fasting was determined. Results showed that, as same as larvae, adult *akr1a1a*$^{-/-}$ zebrafish also had increasing numbers of branches and sprouts in retina vessels in contrast to *akr1a1a*$^{+/+}$ adults (Fig.16A, B, C). Additionally, *akr1a1a*$^{-/-}$ adults exhibited postprandial hyperglycemia in both male and female, while overnight-fasting blood glucose kept unchanging (Fig.16D, E). Besides, although no apparent alterations in kidneys have been found with PAS staining under a light microscope (Fig.17), the thickening glomerular basement membrane (GBM) was observed with an electron microscope in adult *akr1a1a*$^{-/-}$ zebrafish (Fig.18-19).

Taken together, these results reveal that glucose homeostasis was destructed in *akr1a1a*$^{-/-}$ adults, which may further induce alterations in retina vessels. Besides, thickening GBM in *akr1a1a*$^{-/-}$ adults also suggest long-term imbalanced glucose level had already harmed the physiological structure of the kidney, which is in line with fundamental alterations existing in the early stage of diabetic nephropathy. Additionally, the transient hyperglycemia after feeding and the stable blood glucose level with overnight-fasting, implies that *akr1a1a*$^{-/-}$ adults have insulin resistance and potentially can be used as an attractive animal model for studying type 2 diabetes.

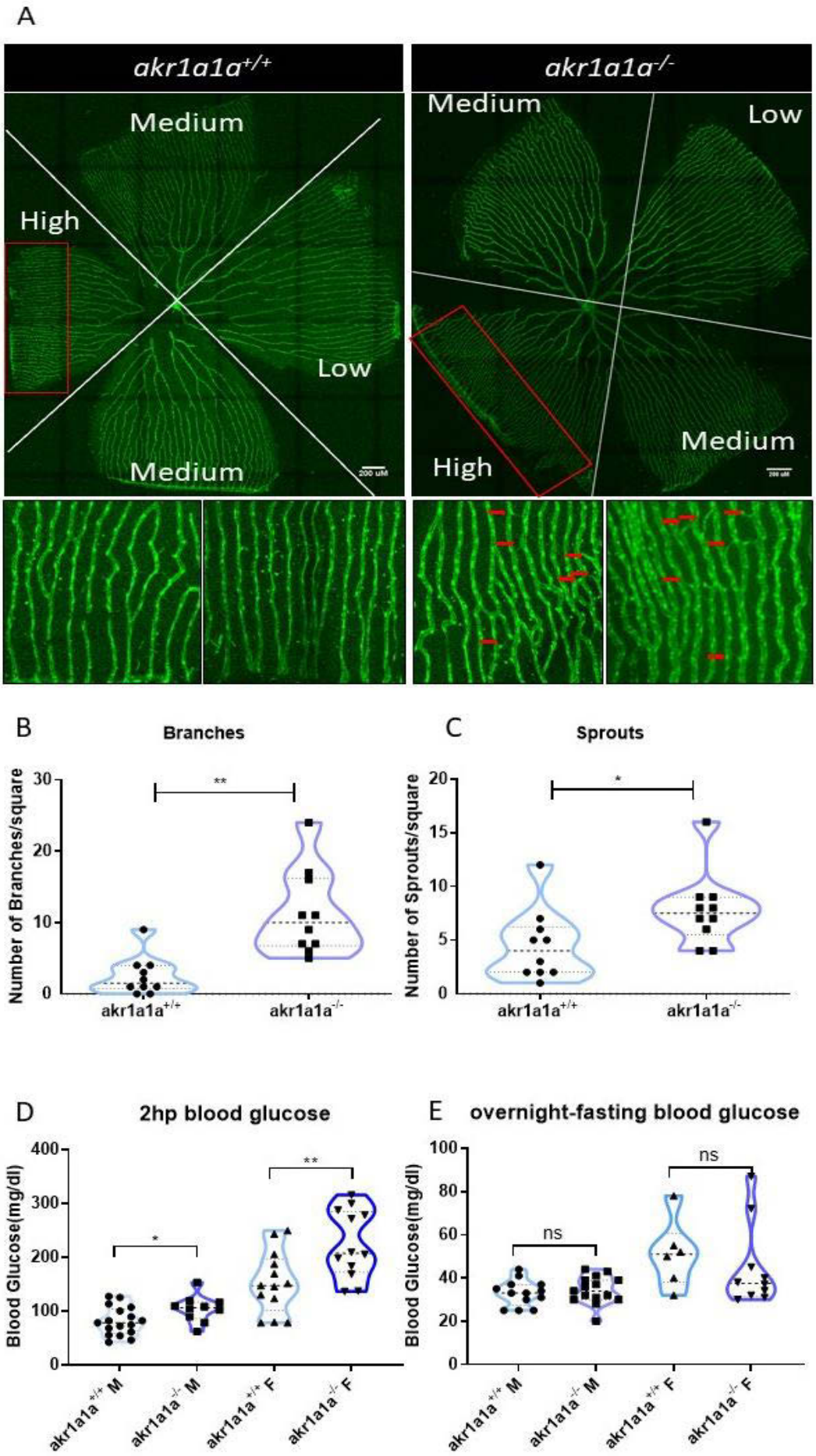
A
akr1a1a+/+
akr1a1a-/-
Medium
High
Low
Medium
Medium
Low
High
Medium
B
Branches
Number of Branches/square
30
20
10
0
**
akr1a1a+/+
akr1a1a-/-
C
Sprouts
Number of Sprouts/square
20
15
10
5
0
*
akr1a1a+/+
akr1a1a-/-
D
2hp blood glucose
Blood Glucose(mg/dl)
400
300
200
100
0
*
**
akr1a1a+/+ M
akr1a1a-/- M
akr1a1a+/+ F
akr1a1a-/- F
E
overnight-fasting blood glucose
Blood Glucose(mg/dl)
100
80
60
40
20
0
ns
ns
akr1a1a+/+ M
akr1a1a-/- M
akr1a1a+/+ F
akr1a1a-/- F

Fig.16 *akr1a1a*$^{-/-}$ adults showed more branches and sprouts and transient hyperglycemia at 2h postprandial.

(A) Representative confocal images of retinal vasculature. White scale bar:200uM. (B, C) Quantification of retinal vasculature showed significant increasing numbers of branches and sprouts in *akr1a1a*$^{-/-}$ adult zebrafish. n=10. (D, E) *akr1a1a*$^{-/-}$ adults zebrafish showed gender independent transient hyperglycemia at 2h postprandial, and normal blood glucose level after overnight-fasting. n=10-17. For statistical analysis Student's t-test was applied. *p < 0.05. **p<0.01. NS, not significant. M, male. F, female.

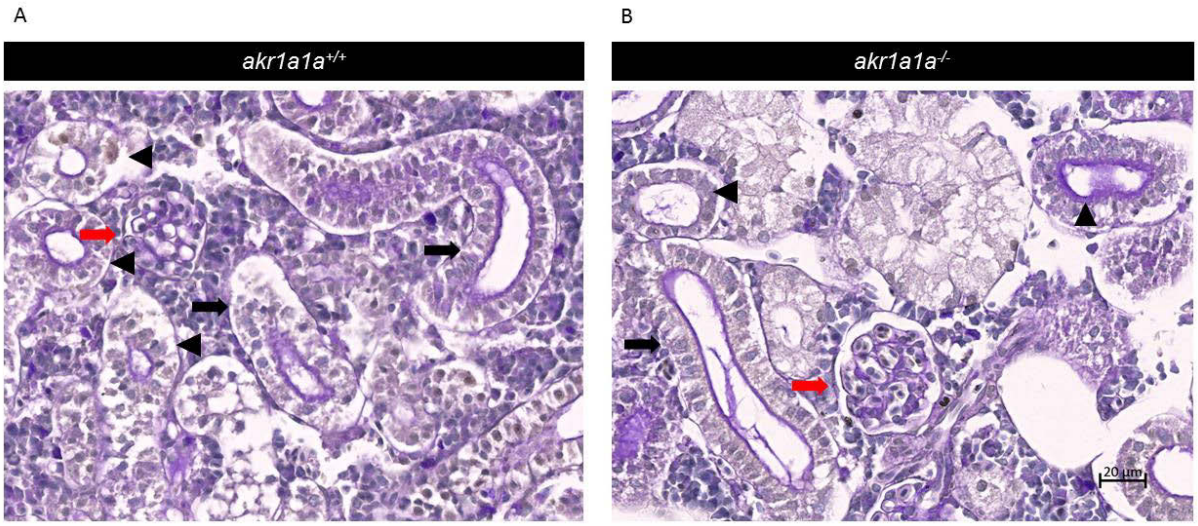

Fig.17 Renal general morphology of *akr1a1a*$^{+/+}$ and *akr1a1a*$^{-/-}$ adults with PAS staining.

(A) Representative Periodic acid–Schiff (PAS) staining slides showed gross structure of *akr1a1a*$^{+/+}$. (B) Representative PAS staining slides showed gross structure of *akr1a1a*$^{-/-}$. Red arrow: glomeruli. Black arrow: proximal tubule. Black triangle: distal tubule. Black scale bar: 20uM

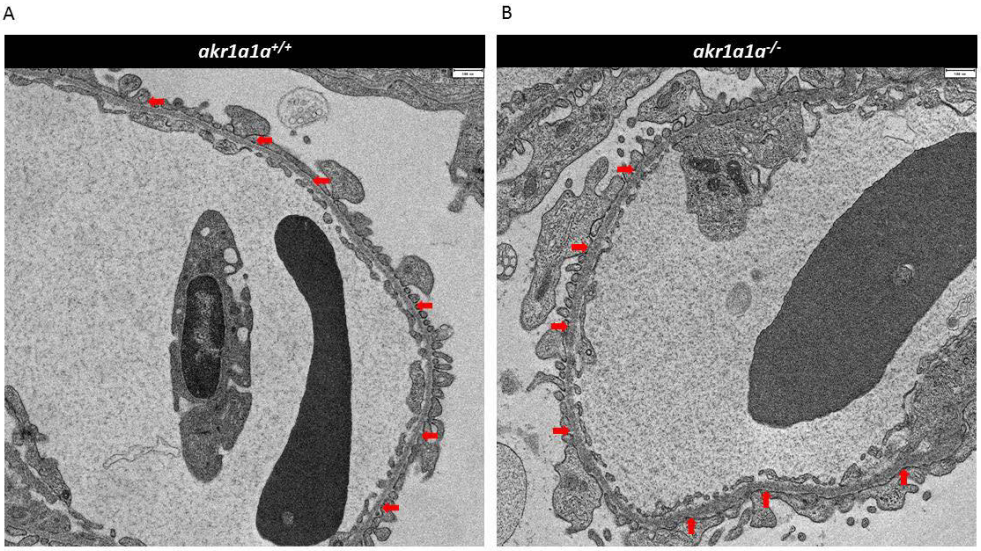

Fig.18 a*kr1a1a*$^{-/-}$ adults showed thicker glomerular basement membrane (GBM).

(A-B) Representative electronic microscopy images showed thicker GBM in *akr1a1a*$^{-/-}$ adult zebrafish. White scale bar: 500nM.
Electronic microscopy related experiments were performed by Dr. Ingrid Siller-Haußer.

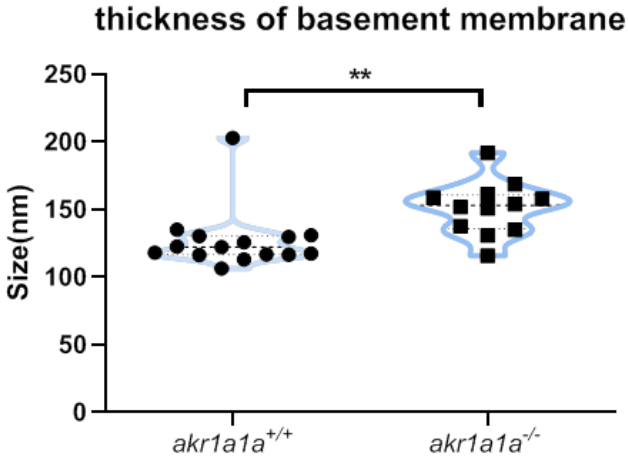

Fig.19 Quantification of glomerular basement membrane (GBM).
Average thickness of GBM in *akr1a1a*$^{-/-}$ adult zebrafish was thicker than *akr1a1a*$^{+/+}$ adult zebrafish. n=12-15. GBM: glomerular basement membrane. Mean± SD, for statistical analysis Student's t-test was applied. **p<0.01.

3.9 Adult *akr1a1a*$^{-/-}$ zebrafish exhibit insulin resistance and impaired glycolysis in liver accompanied with accumulated internal acrolein.

To further investigate if adult *akr1a1a*$^{-/-}$ zebrafish develop insulin resistance, phosphorylation of the p70-S6K, a downstream target of the insulin-signaling cascade, was determined by ELISA in livers. The result showed that p-p70-S6K significantly decreased in mutants (Fig.20A), which confirms insulin resistance existing in livers of adult mutants. Moreover, accumulated acrolein, reduced *insrb* mRNA expression, and decreasing *insra* mRNA expression tendency in mutants' livers (Fig.20B, C, D) indicate accumulated internal acrolein in *akr1a1a*$^{-/-}$ zebrafish can exert function and adjust *insra/insrb* expression over time and may cause insulin resistance in the end.

Widely known, several glucose transporters translocate to the cellular membrane from the cytoplasm to transport glucose after activated by an insulin cascade. Then glycolysis will get started as soon as glucose enters into the cytoplasm, which can be enhanced by insulin signal. Therefore, glucose transmembrane transportation and glycolysis could be recognized as a downstream process of the insulin cascade. To determine if these procedures are affected due to insulin resistance in adult *akr1a1a*$^{-/-}$ zebrafish, several relevant genes expression was tested by RT-qPCR. The result

showed that glucose transporter 2(*glut2*) mRNA reduced significantly in the livers of mutants at 2h postprandial (Fig.21), which implies impaired glucose uptake capability.

Furthermore, three rate-limiting enzymes in glycolysis process including phosphofructokinase (pfk), pyruvate kinase (pk) and hexokinase (hk) were determined on mRNA level. While *pfk* and *hk* mRNA showed a decreasing tendency, but *pk* mRNA increased (Fig.22A). Additionally, enzyme activity measurements showed that PFK activity but not PK and HK, decreased significantly in livers of mutants suggesting glycolysis procedure is also partially influenced. (Fig.22B)

Besides, primary metabolites in the liver were also determined by GC/MS. Most metabolites did not show a noticeable difference in contrast to wild-type while significantly declined pyruvic acid, the main product of glycolysis, shown in mutants indicating the inhibited glycolysis procedure again in mutants. (Fig.23)

In summary, these data prove that internal acrolein also accumulates in adult *akr1a1a*$^{-/-}$ zebrafish, and the insulin receptor gene expression was downregulated. Furthermore, both downstream pathways of insulin cascade encompassing glucose transmembrane transportation and glycolysis procedure were inhibited in mutants suggesting permanent loss of Akr1a1a may finally result in insulin resistance, which supports *akr1a1a*$^{-/-}$ zebrafish as a hopeful candidate for studying diabetes.

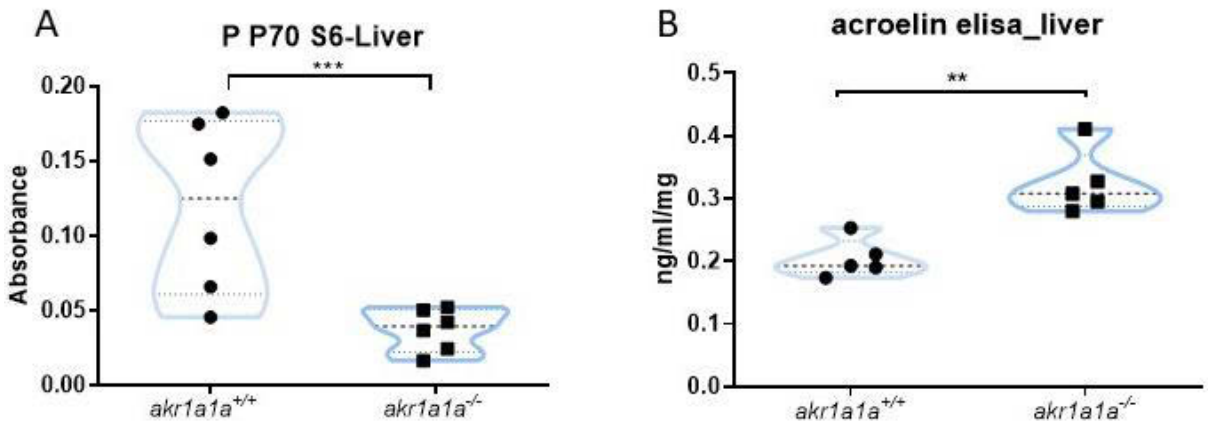

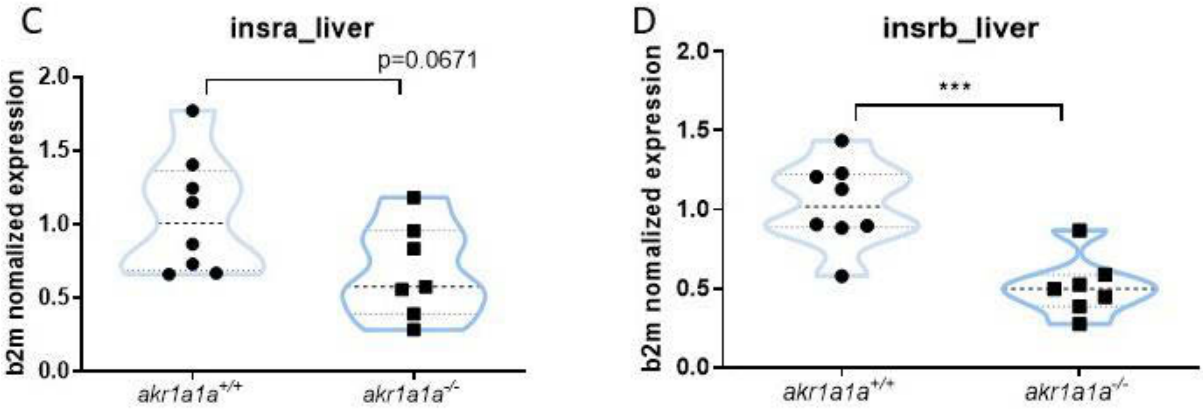

Fig.20 p-P70-S6K, acrolein level and *insra/insrb* expression level in adult livers. (A) p-P70-S6K protein showed a significant lower level in livers of *akr1a1a*$^{-/-}$ adults compared to *akr1a1a*$^{+/+}$ adults. n=6. (B) Acrolein increased significantly in livers of *akr1a1a*$^{-/-}$ adults. n=5-8. (C-D) *insra* gene expression showed decreasing tendency while *insrb* gene expression was downregulated significantly in livers of adult *akr1a1a*$^{-/-}$ zebrafish. n=7-8. Mean± SD, for statistical analysis Student's t-test was applied. **p<0.01. ***p<0.001. n=6-8.

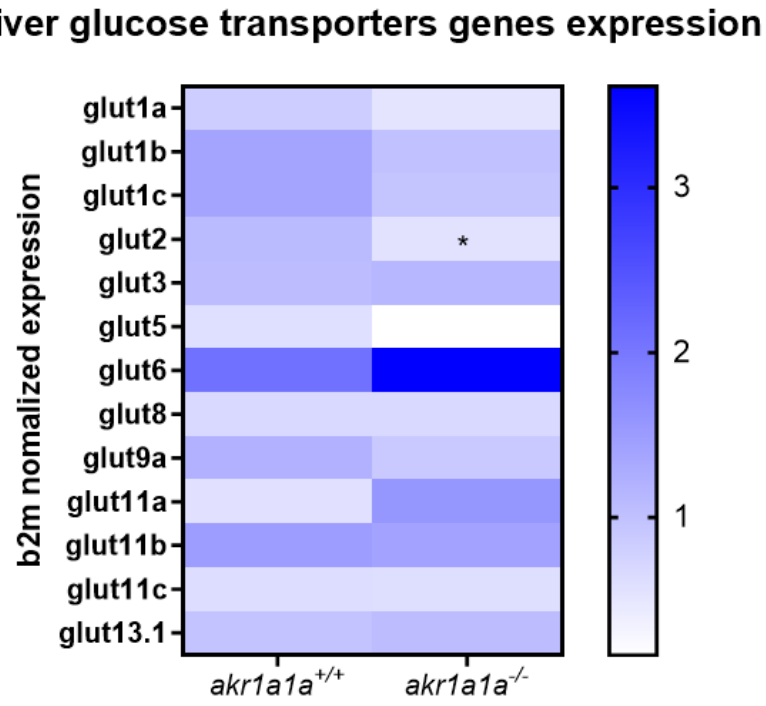

Fig.21 Glucose transporters genes expression in liver.
Heatmap of glucose transporters (*glut)* mRNA expression in liver showed a decreased trend for most *glut* (*glut 1a*, *glut1b, glut1c, glut5, glut9a, glut11b*) and *glut2* was downregulated significantly in *akr1a1a*$^{-/-}$ zebrafish. Higher and lower expression is displayed in blue and white, respectively. Expression of genes was determined by RT-qPCR and normalized to *b2m*. Mean± SD, for statistical analysis Student's t-test was applied. *$p < 0.05$. n=3

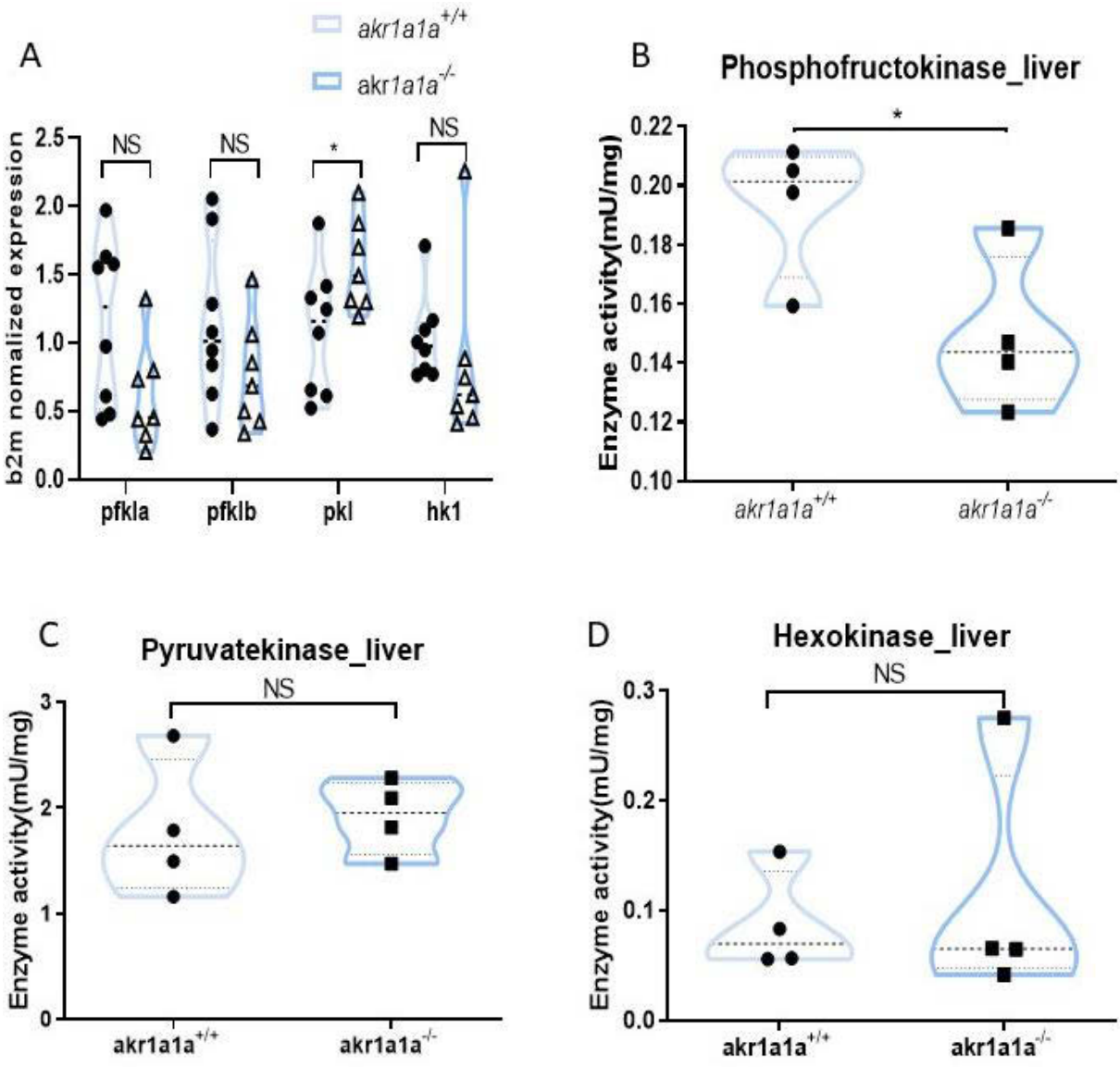

Fig.22 Glycolysis relevant genes expression, rate-limiting enzymes activity in livers

(A)Pfk and *hk* mRNA expression showed decreasing tendency while *pk* expression increased significantly in livers of mutants. n=7-8. (B-D) Activity of PFK reduced significantly in livers of mutants, while PK and HK did not show alteration. n=4 Mean± SD, for statistical analysis Student's t-test was applied. *$p < 0.05$. NS, not significant.

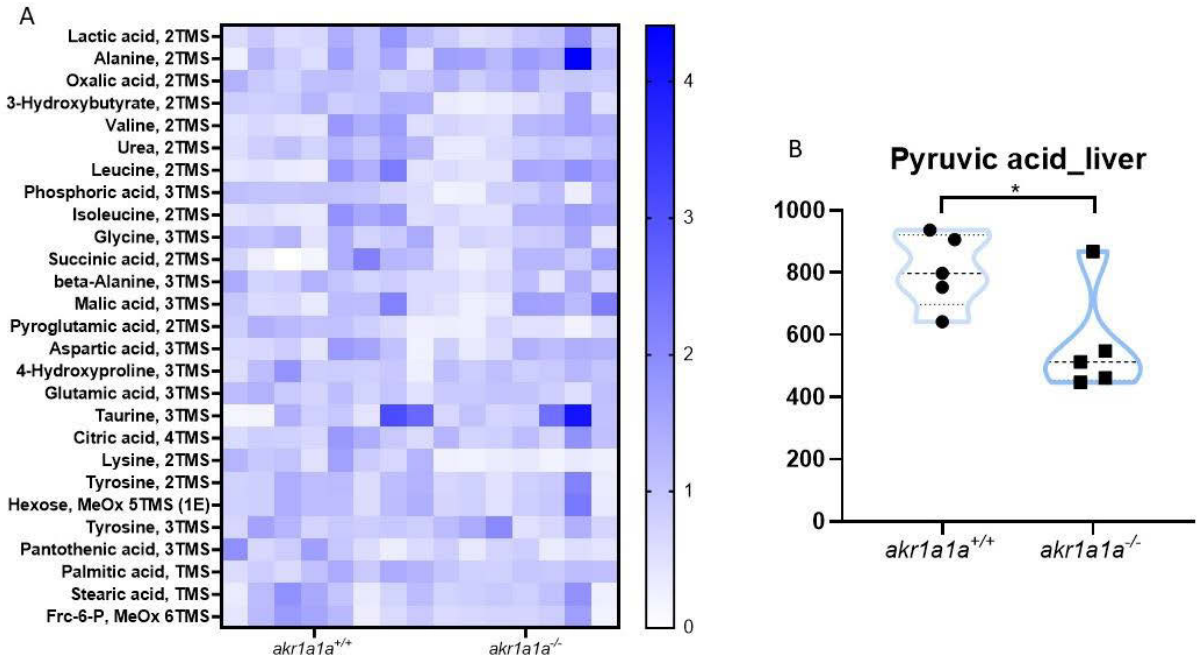

Fig.23 Primary metabolites and pyruvic acid in livers
(A) Primary metabolites did not show significant alterations in livers of mutants. n=7-8. (B) Pyruvic acid reduced significantly in livers of mutants. n=5. Mean± SD, for statistical analysis, Student's t-test was applied. *p < 0.05.

4 DISCUSSION

In this study, the physiological function of the Akr1a1a enzyme system was investigated by establishing an Akr1a1a knockout zebrafish model for the first time. The main findings are summarized in the following Fig.24. 1. Akr1a1a enzyme system in zebrafish is comparable to human and mouse by sharing a similar binding site and active site. Loss of Akr1a1a leads to declined AKR activity but does not impact on early morphological development and survival rate of zebrafish. 2. *akr1a1a*$^{-/-}$ larvae display normal trunk vasculature but aberrant retinal hyaloid vasculature accompanied with moderate hyperglycemia at 5dpf. 3. *akr1a1a*$^{-/-}$ larvae display reduced *insra/insrb* expression and downregulated insulin receptor signaling pathway. 4. Impaired detoxification and the accumulation of internal acrolein after Akr1a1a loss are responsible for abnormal hyaloid vasculature, reduced *insra/insrb* expression, and inhibited insulin receptor signaling pathway. 5. Acrolein scavenger-L-carnosine and hypoglycemic drug-PK11195 could reverse the alterations in hyaloid vasculature caused by exogeneous acrolein intervention. 6. Postprandial hyperglycemia, elevated internal acrolein, abnormal angiogenesis in the retinal vasculature, and thickening glomerular basement membrane can be found in *akr1a1a*$^{-/-}$ adults.

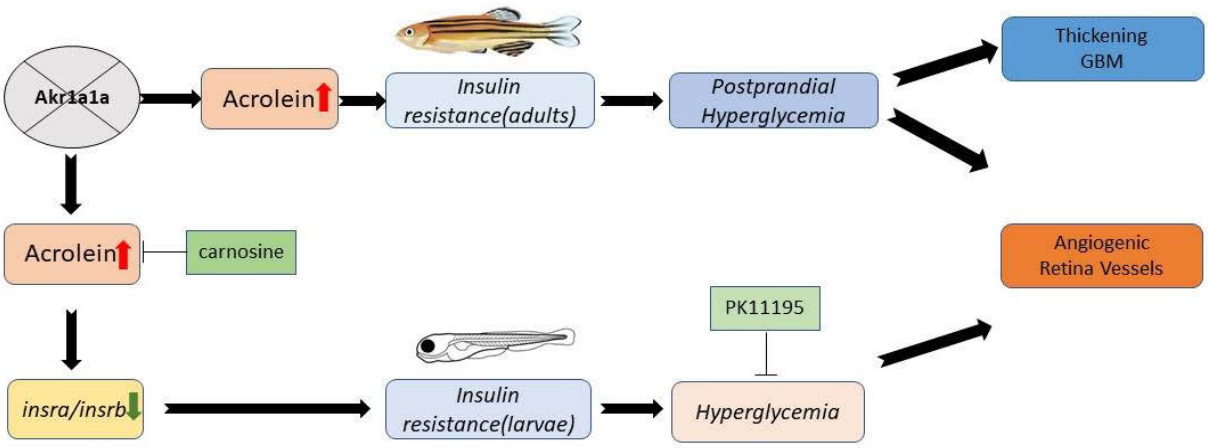

Fig.24 Model for the role of the Akr1a1a in zebrafish.
Permanent Akr1a1a loss causes accumulated internal acrolein which inhibits transcription of *insra/insrb* and downregulates insulin receptor signaling pathway, moreover, leads to insulin resistance and results in hyperglycemia afterwards. Elevated glucose level causes increased angiogenetic formation in retinal hyaloid vasculature and can be reversed by RCS-scavenger, carnosine and hypoglycemic drug, PK11195. Accumulated internal acrolein in adults results in insulin resistance

and postprandial hyperglycemia which leads to thickening GBM and angiogenic retina vessels.

4.1 The Akr1a1a enzyme system in zebrafish

Akr1a1, one of the first discovered AKRs, is widely believed to be involved in multiple metabolic procedures relying on its capacity in metabolizing carboxyl-group containing negatively charged substrates(Barski et al., 2008; Wermuth & Monder, 1983). Several studies have reported that Akr1a1 can reduce methylglyoxal and 3-deoxyglucosone, which are present at elevated levels under hyperglycemic conditions and are cytotoxic(O'Connor, Ireland, Harrison, & Hayes, 1999). It is also involved in the detoxification of lipid-derived aldehydes like acrolein(Kurahashi et al., 2014). In addition, Mano, Y et al. proved that Akr1a1 is involved in ascorbic acid biosynthesis in rodents and displays broad substrate activity(Mano, Suzuki, Yamada, & Shimazono, 1961; Wermuth & Monder, 1983). Nevertheless, humans and fish are prone to harvest ascorbic acid from food. Therefore, the persistence of functional akr1a1 gene in humans and fish indicates that the protein may prefer to exert enzyme-induced functions or some effects unknown in these two species. Besides, recently, Akr1a1 was also identified as a novel SNO-CoA reductase protecting against kidney injury via adjusting S-nitrosylation level, which offers new insight for the role of Akr1a1 in vivo(Zhou et al., 2019).

Worth to emphasize, varying from mammals with only one protein-coding gene, akr1a1, there are two homologs, akr1a1a and akr1a1b, appearing in zebrafish. Although both of them display high similarity in protein sequence alignment compared with Akr1a1 in human and mouse, the biological role is still unclear in zebrafish, which sparked our interest. The physiological functions of Akr1a1b in zebrafish has been addressed in another project from our lab in which Akr1a1b displayed the capability to participate in gluconeogenesis via regulating the S-nitrosylation level of cPEPCK *in vivo*(X. Li et al., 2020).

In our results, the protein sequence alignment of Akr1a1a showed identical binding site, active site, and comparable peptide sequence among zebrafish, human, and mouse, suggesting zebrafish Akr1a1a may behave similar features as mammals Akr1a1 in physiological and pathological aspects. It also implies that *akr1a1a*

knockout zebrafish might be a potent and appropriate animal model for studying human Akr1a1.

To get basic knowledge about Akr1a1a, the distribution of the protein needs to be clarified at first. Therefore, mRNA expression of *akr1a1a* was determined by RT-qPCR in various organs and different time points in early developmental stage of zebrafish. The expression of *akr1a1a* was elevated at the early stage of embryonic zebrafish, and *akr1a1a* expressed widely in adult organs and mostly in the liver. The result was consistent with a study that reported that the expression of Akr1a1 is restricted primarily to the brain, kidney, liver, and small intestine(O'Connor et al., 1999). Since the liver is the center for substance metabolism and detoxification, we can preliminarily hypothesize that Akr1a1a may exert essential functions in multiple metabolic and detoxifying procedures.

4.2 *Akr1a1a*$^{-/-}$ larvae display high-level body glucose and alterations in retinal hyaloid vasculature but regular trunk vasculature

So far, *akr1a1a* mutant has not been reported in zebrafish and rare studies investigated physiological and pathological function of Akr1a1a in zebrafish. Therefore, Akr1a1a knockout zebrafish line was generated in our lab for the first time by my colleague Dr. Felix Schmöhl. Two mutants were then identified, including one base-pair insertion and five base-pair deletion in *Tg(fli1: EGFP)* and *Tg(wt1b: EGFP)* lines separately for further exploration. The subsequent western-blot experiment confirmed the successful establishment of *akr1a1a*$^{-/-}$ zebrafish line. Additionally, both DL-Glyceraldehyde-dependent and acrolein-dependent AKR activity declined notably in *akr1a1a* mutants, proving the critical role of Akr1a1a for aldoses and aldehydes detoxifying among AKR superfamily.

In my results, hyaloid vasculature of *akr1a1a*$^{-/-}$ larvae showed increasing amounts of branches and sprouts in comparison with wild-type larvae while no noticeable alterations were observed in trunk vasculature. This result is consistent with a previous study, which aimed to screen new anti-angiogenic compounds potentially involved in blood vessel development(Rezzola et al., 2014). The researchers found that SU5416 treatment causes severe hyaloid vessel developmental lesions without impairing embryonic trunk vasculature in zebrafish(Rezzola et al., 2014). Additionally, among various genes that have been identified to modulate angiogenesis in

embryonic zebrafish, several ones were verified as selective hyaloid vasculature determinants that had rare effects on trunk vasculature development(Alvarez et al., 2007). Therefore, all these proofs demonstrate the heterogeneity of the mechanisms contributing to the angiogenic process in different organs in zebrafish, and hyaloid vasculature may be more sensitive and vulnerable to the alterations *in vivo* than trunk vasculature(Alvarez et al., 2007).

Based on the previous studies from our lab, my colleagues illustrated that exogenous glucose treatment alters intersomitic blood vessels (ISVs) in zebrafish via methylglyoxal (MG) targeting the VEFGR signaling cascade(Jorgens et al., 2015). While in further exploration following by knockout of Glo1, the main detoxification enzyme of MG, increased MG was confirmed in *glo1*$^{-/-}$ larvae as expected. However, alterations in ISVs were not seen. Besides, abnormal angiogenesis in retinal vessels, fasting hyperglycemia, and an average MG level was seen in adult *glo1*$^{-/-}$ zebrafish after overfed-treatment, which suggests hyperglycemia may induce angiogenic retinal vessels directly(Lodd et al., 2019). Meanwhile, hyperglycemia caused by the permanent loss of pancreatic and duodenal homeobox 1 (Pdx1), one of the earliest pancreatic transcription factors, results in angiogenic hyaloid vasculature was also seen in another study from our lab(Wiggenhauser et al., 2020). Taken together, all these proofs support that hyperglycemia is more likely to affect retinal vasculature directly and be responsible for abnormal angiogenesis.

My results showed that loss of Akr1a1a results in a moderate increment of whole-body glucose in larvae, implying glucose is responsible for the alterations in hyaloid vasculatures in mutants. In addition, based on our RNA-seq data, *notch1b*, *notch2*, *notch3*, and *vegfba* but not *vegfa*, showed significant alterations in *akr1a1a*$^{-/-}$ larvae, which demonstrates these factors might be the molecular mediators and contribute to abnormal hyaloid vasculature in embryonic mutants.

4.3 *Akr1a1a*$^{-/-}$ larvae exhibit downregulated insulin receptor signaling pathway

For better understanding the potential mechanisms behind high-level glucose and abnormal hyaloid vasculature appearing in *akr1a1a*$^{-/-}$ larvae, an RNA-seq approach was performed. Intriguingly, according to the RNA-seq data, the insulin receptor signaling pathway and several downstream pathways such as transmembrane

receptor protein tyrosine kinase signaling pathway, MAPK cascade, and protein autophosphorylation pathway were significantly downregulated in *akr1a1a*$^{-/-}$ larvae. Further RT-qPCR-based experiments confirmed that *insra/insrb* but not *ins* mRNA expression was significantly reduced in mutant larvae at 5dpf.

In zebrafish, knockout of *insra* or *insrb* does not affect survival, growth and breeding, but cause higher glucose level via the increased gluconeogenesis and decreased glycolysis at 3-5dpf(Yang et al., 2018). In addition, both *insra*$^{-/-}$ and *insrb*$^{-/-}$ zebrafish also showed postprandial hyperglycemia in adults(Yang et al., 2018). Besides, the elevated plasma insulin and lowered phosphorylated AKT were observed in *insra*$^{-/-}$ fish and *insrb*$^{-/-}$ fish, suggesting an insulin resistance in *insra*$^{-/-}$ and *insrb*$^{-/-}$ fish(Gong et al., 2018). However, whether downregulated *insra/insrb* would also destruct glucose homeostasis and induce altered hyaloid vasculature is still unknown. Therefore, an antisense approach was performed to reduce *insra/insrb* expression in larvae partially. Surprisingly, altered hyaloid vasculature was identified after injection of *insra/insrb* morpholinos, suggesting that reduced *insra/insrb* expression would be the reason why the mutant larvae showed abnormal hyaloid vasculature.

Up to now, *akr1a1a*$^{-/-}$ larvae exhibited alterations in hyaloid vasculature, which resulted from an increasing level of glucose caused by reduced *insra/insrb* expression. In order to explore the possible connection between the loss of Akr1a1a and reduced *insra/insrb* expression, I shift the focus to the physiological functions of Akr1a1a.

4.4 Accumulated internal acrolein leads to angiogenic hyaloid vasculature and high-level glucose in *akr1a1a*$^{-/-}$ larvae

Several potential substrates of Aka1a1 were determined as the next step. Intriguingly, the amount of AGEs precursors, including MG, glyoxal, and 3-DG, did not change, while the lipid peroxidation product, acrolein, showed significant elevation in mutants. Additionally, by utilizing acrolein as substrate, *akr1a1a*$^{-/-}$ larvae displayed lowering AKR activity, suggesting Akr1a1a might be the main metabolizing enzyme of acrolein in zebrafish.

Rafael et al. found the formation of the insulin-acrolein adduct modifies the structure of insulin and decreases its hypoglycemic effect in rat and glucose uptake by 3T3

adipocytes(Medina-Navarro, Guzman-Grenfell, et al., 2007). Additionally, by exploring the mouse embryonic fibroblasts (MEFs) from wild-type (WT) and human Akr1a-transgenic (Tg) mice, it has been confirmed that one of the principal roles of Akr1a1 in primates is the reductive detoxification of acrolein(Kurahashi et al., 2014). The same result also showed up in our findings, in which *akr1a1a*$^{-/-}$ larvae showed the accumulation of internal acrolein.

To further confirm the impacts of acrolein on zebrafish, extraneous acrolein was used for the external treatment assay. After exposed to acrolein for five days, hyaloid vessels of wild-type zebrafish larvae showed increasing numbers of branches. Incremental whole-body glucose was also seen in larvae with acrolein treatment. Additionally, *insra/insrb* expression was also reduced in the larvae exposed to acrolein. Furthermore, acrolein-scavenger and hypoglycemic drug, carnosine and PK11195 were able to alleviate the abnormalities in hyaloid vasculature in larvae exposed to acrolein. These pieces of evidences approve that non-detoxified acrolein due to the loss of Akr1a1a impairs *insra/insrb* expression and destructs glucose homeostasis and suggest the destructed glucose homeostasis is responsible for acrolein-induced abnormal hyaloid vasculature. Additionally, L-carnosine and PK11195 would be powerful and hopeful candidates to prevent acrolein-induced vascular alterations.

Several clinical studies indicated that acrolein is tightly linked to insulin resistance, diabetes and relevant complications(Feroe et al., 2016; Medina-Navarro, Guzmán-Grenfell, et al., 2007; Stevens & Maier, 2008). But the fundamental mechanism is still missing. Here we first prove acrolein could directly downregulate *insra/insrb* expression, destruct glucose homeostasis and result in angiogenic alterations in hyaloid vasculature. Additionally, this study has confirmed Akr1a1a as a principal detoxifying enzyme to acrolein *in vivo*, therefore, keeping regular detection of AKR activity and internal acrolein in patients with high risk in developing diabetes in clinics would be a hopeful and helpful strategy in preventing insulin resistance at early stage.

4.5 Adult *akr1a1a*$^{-/-}$ zebrafish display abnormal retina vasculature, insulin resistance in liver and thickening GBM in kidney

Since angiogenic hyaloid vasculature and impaired glucose homeostasis was seen in *akr1a1a*$^{-/-}$ larvae, how does the deficiency of Akr1a1a effect on adult zebrafish drew my attention. Thus, a series of explorations were then performed on adults.
In my results, *akr1a1a*$^{-/-}$ adults also showed more branches and sprouts in retinal vessels as similar as the phenotypes in larvae, and thickening glomerular basement membrane (GBM) in kidneys in parallel with elevated postprandial hyperglycemia. Additionally, declined *insra* expression tendency, significantly reduced *insrb* expression, more acrolein, and less p-P70-S6K were also determined in livers of mutants. These data reveal that long-term over-loaded internal acrolein has driven insulin resistance in liver and induced organic damage in retina vessels and kidney.

A previous study has indicated insulin receptor A(IR-A) functions primarily as a growth-promoting isoform during fetal life, while insulin receptor B(IR-B) functions mainly as moderating hepatocyte sensitivity to insulin in the adult liver(Moller, Yokota, Caro, & Flier, 1989). This may explain the decreasing trend of *insra* expression but significantly reduced *insrb* expression in liver of adult mutants. However, how does acrolein down-regulate the transcription of *insra/insrb* is still unknown, which is worth further exploration.

As approved in several previous studies regarding diabetic retinopathy, less controlled glucose has a positive correlation with the development of retinopathy characterized by the growth of new, abnormal blood vessels in the retina of patients. Besides, thickening GBM is recognized as an early feature for diabetic nephropathy(Cusumano et al., 2002; Uil et al., 2018; Zhang et al., 2018). Thus, the phenotypes appearing in *akr1a1a*$^{-/-}$ adults are highly conserved as diabetic retinopathy and nephropathy symptoms in diabetic patients suggesting adult *akr1a1a*$^{-/-}$ zebrafish as a potential and promising animal model for studying diabetic complications.

To date, in terms of harmful effects on glucose homeostasis and subsequent phenotypes in *akr1a1a*$^{-/-}$ larvae and adults supports acrolein as a “maker” more than a “marker” for insulin resistance. Moreover, the appearance of tissue damage

including retina vessels and kidney accompanied with loss of Akr1a1a, accumulated acrolein and postprandial hyperglycemia furtherly confirm the comprehensive contribution of two/multi metabolic hits to diabetic complications. However, more efforts are still needed for studying comprehensive effects of accumulated internal acrolein in *akr1a1a*$^{-/-}$ adults since molecular mechanism behind acrolein-induced downregulation of *insra/insrb* expression remains unknown. In addition, whether acrolein has dose-dependent or tissue preference *in vivo* also needs more exploration to address.

4.6 Glucose transport and glycolysis are impaired in adult *akr1a1a*$^{-/-}$ zebrafish

Glucose transport and glycolysis are the downstream biological procedures after successful insulin signaling transduction, aiming to take glucose from the circulation system into various cells by a series of glucose transporters and produce vital energy for the body. Therefore, abnormal insulin signaling transduction would undoubtedly influence these two relevant processes.

Gong et al. found glucose level of both adult *insra*$^{-/-}$ and *insrb*$^{-/-}$ zebrafish increased markedly at 1.5hpp (hours postprandial), meanwhile, increased plasma insulin and decreased phosphorylated AKT indicated that there is insulin resistance both in *insra*$^{-/-}$ fish and *insrb*$^{-/-}$ fish. Additionally, glycolysis genes *gck*, *pklr*, *pfklb*, *hk1*, and *ldha* as well as GCK concentration and PK activity, were uniformly down-regulated in the liver and muscle of *insra*$^{-/-}$ and *insrb*$^{-/-}$ fish(Gong et al., 2018). While in our results, *pfk* and *hk* expression only showed a decreasing tendency, but PFK activity and pyruvic acid amount decreased significantly in the liver of *akr1a1a*$^{-/-}$ mutants. It implies heterogeneity between permanent loss of *insra/insrb* and transient downregulation of *insra/insrb* caused by acrolein. Besides, it is no doubt that the glycolysis process is partially inhibited in adult *akr1a1a*$^{-/-}$ zebrafish. However, whether PFK activity could be reduced by acrolein directly via posttranslational modification or downregulated gene expression is worth addressing in the near future.

In addition to glycolysis, the glucose transport process was also analyzed by determining the related gene expression level of multiple glucose transporters.

Among them, *glut2* is the unique gene which remarkably reduced in the liver of mutants compared with wild-type.

Glucose enters the cells by facilitated diffusion driven by a family of glucose transporter proteins comprising 14 members in human(Mueckler & Thorens, 2013). In general, each glucose transporter plays a specific role in glucose metabolism as it relied on its pattern of tissue preference, transport kinetics, and various physiological conditions(Uldry & Thorens, 2004). GLUT2 has been verified in mammals to be expressed in many organs, predominantly the liver(Thorens, Sarkar, Kaback, & Lodish, 1988). Alignment of the amino acid sequences of zebrafish GLUT2 and human GLUT2 revealed a high degree of structural and functional conservation(Castillo et al., 2009). Further studies revealed that GLUT2 is also highly expressed in the liver and intestine of zebrafish and has similar glucose transport properties as mammalian GLUT2(Castillo et al., 2009). Therefore, down-regulated *glut2* suggests less glucose uptake by the liver and explains the transient hyperglycemia after feeding in *akr1a1a* mutants.

Unlike GLUT4, which is responsible for most glucose transport into muscle and adipose cells in an insulin-dependent way, GLUT2 functions insulin-independently in mammals(Olson, Trumbly, & Gibson, 2001). Nevertheless, the correlation between GLUT2 and insulin in zebrafish is still an open question that needs further investigation. Furthermore, whether acrolein directly influences *glut2* expression is also unknown so far, which might be a new direction for studying shortly.

Notably, adult *akr1a1a-/-* zebrafish displayed impaired glucose transport and glycolysis, which implies AKR1a1 playing a critical role in glucose metabolism. Furthermore, lack of AKR1a1 or reduced AKR enzyme activity might be promising biomarkers to predict impaired glucose tolerance and insulin resistance. However, more evidence from clinics is necessary in the near future.

5 SUMMARY

Diabetes mellitus is a worldwide disease with increasing prevalence globally. Type 2 diabetes is considered the primary subtype that occupies vast amounts of cases and is characterized by insulin resistance. Therefore, early diagnosis and insulin resistance intervention are more than necessary in treating diabetes and relevant complications. However, up to now, there is still a lack of influential factor for predicting the onset of insulin resistance and molecular mechanisms behind insulin resistance is also far away from clarity.

In my study, by using CRISPR/CAS9 technology, Akr1a1a knockout zebrafish model was generated. A series of experiments were performed regarding the vasculature, glucose homeostasis, and metabolism after Akr1a1a loss. The main discoveries of this dissertation are: *akr1a1a*$^{-/-}$ larvae and adults exhibit impaired ACR detoxification ability and increased internal ACR concentration, which induces the downregulation of *insra/insrb* expression and leads to insulin resistance and hyperglycemia. Impaired glucose homeostasis causes abnormal angiogenesis in retina hyaloid vasculature and can be reversed by L-carnosine and PK11195 application in larvae. Meanwhile, prolonged and impaired glucose homeostasis in *akr1a1a*$^{-/-}$ adults results in angiogenic retina vessels and thickening GBM in the kidney, parallel with an early pathological appearance in diabetic retinopathy and nephropathy.

Although this study successfully linked a loss of Akr1a1a to an elevation of ACR to impaired glucose homeostasis, there are some limitations. First, due to the lack of specific and commercial antibodies for zebrafish, our conclusion on how ACR regulates *insra/insrb* expression as well as relevant downstream pathways are based on qPCR data and RNA-seq, which are on mRNA level. It would be interesting to explore the potential pathways based on the alterations of protein levels. Second, although it has been confirmed that acrolein cause reduced *insra/insrb* expression, the detailed mechanism remains unknown. Third, whether the impaired glycolysis and glucose transport process appearing in *akr1a1a*$^{-/-}$ adults caused by reduced PFK activity and declined *glut2* expression results from insulin resistance or partially caused by accumulated internal acrolein is still controversial.

At last, in my study, a clear connection between acrolein and insulin resistance has been confirmed in zebrafish, suggesting acrolein as a promising candidate to predict insulin resistance in clinics. It also implies that acrolein would be a target for early intervention for insulin resistance. However, it surely needs more assessment with clinical samples. Moreover, since L-carnosine and PK11195 could rescue the vascular effects caused by acrolein, indicating these drugs as hopeful candidates to treat acrolein-induced vascular diseases. In another perspective, it also supports the onset of organ damage requires two/multiple metabolic alterations, emphasizing the importance of pluralism in diabetic complications and offering a new insight for us to develop new drugs.

Overall, this dissertation provided patent evidence for the contribution of poor acrolein detoxification and subsequently increased acrolein concentration to the development of hyperglycemia via insulin receptor signaling dysfunction in akr1a1a mutants, as a novel direction for future research regarding diabetic pathophysiology and therapy.

6 REFERENCE

Ahlqvist, E., Storm, P., Karajamaki, A., Martinell, M., Dorkhan, M., Carlsson, A., . . . Groop, L. (2018). Novel subgroups of adult-onset diabetes and their association with outcomes: a data-driven cluster analysis of six variables. *Lancet Diabetes Endocrinol, 6*(5), 361-369. doi:10.1016/S2213-8587(18)30051-2

Ahmed, M. M., Wang, T., Luo, Y., Ye, S., Wu, Q., Guo, Z., . . . Yang, J. Y. (2011). Aldo-keto reductase-7A protects liver cells and tissues from acetaminophen-induced oxidative stress and hepatotoxicity. *Hepatology, 54*(4), 1322-1332. doi:10.1002/hep.24493

Aldini, G., Orioli, M., & Carini, M. (2011). Protein modification by acrolein: relevance to pathological conditions and inhibition by aldehyde sequestering agents. *Mol Nutr Food Res, 55*(9), 1301-1319. doi:10.1002/mnfr.201100182

Alvarez, Y., Cederlund, M. L., Cottell, D. C., Bill, B. R., Ekker, S. C., Torres-Vazquez, J., . . . Kennedy, B. N. (2007). Genetic determinants of hyaloid and retinal vasculature in zebrafish. *BMC Dev Biol, 7*, 114. doi:10.1186/1471-213x-7-114

Amaro, R., Tajkhorshid, E., & Luthey-Schulten, Z. (2003). Developing an energy landscape for the novel function of a (beta/alpha)8 barrel: ammonia conduction through HisF. *Proc Natl Acad Sci U S A, 100*(13), 7599-7604. doi:10.1073/pnas.1331150100

Avruch, J., Hara, K., Lin, Y., Liu, M., Long, X., Ortiz-Vega, S., & Yonezawa, K. (2006). Insulin and amino-acid regulation of mTOR signaling and kinase activity through the Rheb GTPase. *Oncogene, 25*(48), 6361-6372. doi:10.1038/sj.onc.1209882

Bahrami, B. F., Ataie-Kachoie, P., Pourgholami, M. H., & Morris, D. L. (2014). p70 Ribosomal protein S6 kinase (Rps6kb1): an update. *J Clin Pathol, 67*(12), 1019-1025. doi:10.1136/jclinpath-2014-202560

Barski, O. A., Papusha, V. Z., Ivanova, M. M., Rudman, D. M., & Finegold, M. J. (2005). Developmental expression and function of aldehyde reductase in proximal tubules of the kidney. *Am J Physiol Renal Physiol, 289*(1), F200-207. doi:10.1152/ajprenal.00411.2004

Barski, O. A., Tipparaju, S. M., & Bhatnagar, A. (2008). The aldo-keto reductase superfamily and its role in drug metabolism and detoxification. *Drug Metab Rev, 40*(4), 553-624. doi:10.1080/03602530802431439

Belfiore, A., Malaguarnera, R., Vella, V., Lawrence, M. C., Sciacca, L., Frasca, F., . . . Vigneri, R. (2017). Insulin Receptor Isoforms in Physiology and Disease: An Updated View. *Endocr Rev, 38*(5), 379-431. doi:10.1210/er.2017-00073

Bellier, J., Nokin, M. J., Larde, E., Karoyan, P., Peulen, O., Castronovo, V., & Bellahcene, A. (2019). Methylglyoxal, a potent inducer of AGEs, connects between diabetes and cancer. *Diabetes Res Clin Pract, 148*, 200-211. doi:10.1016/j.diabres.2019.01.002

Boucher, J., Kleinridders, A., & Kahn, C. R. (2014). Insulin receptor signaling in normal and insulin-resistant states. *Cold Spring Harb Perspect Biol, 6*(1). doi:10.1101/cshperspect.a009191

Bourne, R. R., Stevens, G. A., White, R. A., Smith, J. L., Flaxman, S. R., Price, H., . . . Vision Loss Expert, G. (2013). Causes of vision loss worldwide, 1990-2010: a systematic analysis. *Lancet Glob Health, 1*(6), e339-349. doi:10.1016/S2214-109X(13)70113-X

Brownlee, M. (2001). Biochemistry and molecular cell biology of diabetic complications. *Nature, 414*(6865), 813-820. doi:10.1038/414813a

Byfield, M. P., Murray, J. T., & Backer, J. M. (2005). hVps34 is a nutrient-regulated lipid kinase required for activation of p70 S6 kinase. *J Biol Chem, 280*(38), 33076-33082. doi:10.1074/jbc.M507201200

Capitao, M., & Soares, R. (2016). Angiogenesis and Inflammation Crosstalk in Diabetic Retinopathy. *J Cell Biochem, 117*(11), 2443-2453. doi:10.1002/jcb.25575

Castillo, J., Crespo, D., Capilla, E., Diaz, M., Chauvigne, F., Cerda, J., & Planas, J. V. (2009). Evolutionary structural and functional conservation of an ortholog of the GLUT2 glucose transporter gene (SLC2A2) in zebrafish. *Am J Physiol Regul Integr Comp Physiol, 297*(5), R1570-1581. doi:10.1152/ajpregu.00430.2009

Chang, T., & Wu, L. (2006). Methylglyoxal, oxidative stress, and hypertension. *Can J Physiol Pharmacol, 84*(12), 1229-1238. doi:10.1139/y06-077

Cheung, N., Mitchell, P., & Wong, T. Y. (2010). Diabetic retinopathy. *Lancet, 376*(9735), 124-136. doi:10.1016/S0140-6736(09)62124-3

Cogan, D. G., Kinoshita, J. H., Kador, P. F., Robison, G., Datilis, M. B., Cobo, L. M., & Kupfer, C. (1984). NIH conference. Aldose reductase and complications of diabetes. *Ann Intern Med, 101*(1), 82-91. doi:10.7326/0003-4819-101-1-82

Cohen, S. R., & Gardner, T. W. (2016). Diabetic Retinopathy and Diabetic Macular Edema. *Dev Ophthalmol, 55*, 137-146. doi:10.1159/000438970

Csosz, E., Deak, E., Kallo, G., Csutak, A., & Tozser, J. (2017). Diabetic retinopathy: Proteomic approaches to help the differential diagnosis and to understand the underlying molecular mechanisms. *J Proteomics, 150*, 351-358. doi:10.1016/j.jprot.2016.06.034

Cusi, K., Maezono, K., Osman, A., Pendergrass, M., Patti, M. E., Pratipanawatr, T., . . . Mandarino, L. J. (2000). Insulin resistance differentially affects the PI 3-kinase- and MAP kinase-mediated signaling in human muscle. *J Clin Invest, 105*(3), 311-320. doi:10.1172/JCI7535

Cusumano, A. M., Bodkin, N. L., Hansen, B. C., Iotti, R., Owens, J., Klotman, P. E., & Kopp, J. B. (2002). Glomerular hypertrophy is associated with hyperinsulinemia and precedes overt diabetes in aging rhesus monkeys. *Am J Kidney Dis, 40*(5), 1075-1085. doi:10.1053/ajkd.2002.36348

Daimon, M., Sugiyama, K., Kameda, W., Saitoh, T., Oizumi, T., Hirata, A., . . . Kato, T. (2003). Increased urinary levels of pentosidine, pyrraline and acrolein adduct in type 2 diabetes. *Endocr J, 50*(1), 61-67. doi:10.1507/endocrj.50.61

De Meyts, P. (2000). The Insulin Receptor and Its Signal Transduction Network. In K. R. Feingold, B. Anawalt, A. Boyce, G. Chrousos, W. W. de Herder, K. Dungan, A. Grossman, J. M. Hershman, H. J. Hofland, G. Kaltsas, C. Koch, P. Kopp, M. Korbonits, R. McLachlan, J. E. Morley, M. New, J. Purnell, F. Singer, C. A. Stratakis, D. L. Trence, & D. P. Wilson (Eds.), *Endotext*. South Dartmouth (MA).

Diez-Dacal, B., Gayarre, J., Gharbi, S., Timms, J. F., Coderch, C., Gago, F., & Perez-Sala, D. (2011). Identification of aldo-keto reductase AKR1B10 as a selective target for modification and inhibition by prostaglandin A(1): implications for antitumoral activity. *Cancer Res, 71*(12), 4161-4171. doi:10.1158/0008-5472.CAN-10-3816

Draznin, B. (2006). Molecular mechanisms of insulin resistance: serine phosphorylation of insulin receptor substrate-1 and increased expression of

p85alpha: the two sides of a coin. *Diabetes, 55*(8), 2392-2397. doi:10.2337/db06-0391

El-Kabbani, O., & Podjarny, A. (2007). Selectivity determinants of the aldose and aldehyde reductase inhibitor-binding sites. *Cell Mol Life Sci, 64*(15), 1970-1978. doi:10.1007/s00018-007-6514-3

Feroe, A. G., Attanasio, R., & Scinicariello, F. (2016). Acrolein metabolites, diabetes and insulin resistance. *Environ Res, 148*, 1-6. doi:10.1016/j.envres.2016.03.015

Forman, H. J., Fukuto, J. M., Miller, T., Zhang, H., Rinna, A., & Levy, S. (2008). The chemistry of cell signaling by reactive oxygen and nitrogen species and 4-hydroxynonenal. *Arch Biochem Biophys, 477*(2), 183-195. doi:10.1016/j.abb.2008.06.011

Freedman, B. I., Bostrom, M., Daeihagh, P., & Bowden, D. W. (2007). Genetic factors in diabetic nephropathy. *Clin J Am Soc Nephrol, 2*(6), 1306-1316. doi:10.2215/CJN.02560607

Fuloria, S., Subramaniyan, V., Karupiah, S., Kumari, U., Sathasivam, K., Meenakshi, D. U., . . . Fuloria, N. K. (2020). A Comprehensive Review on Source, Types, Effects, Nanotechnology, Detection, and Therapeutic Management of Reactive Carbonyl Species Associated with Various Chronic Diseases. *Antioxidants (Basel), 9*(11). doi:10.3390/antiox9111075

Furuhata, A., Ishii, T., Kumazawa, S., Yamada, T., Nakayama, T., & Uchida, K. (2003). N(epsilon)-(3-methylpyridinium)lysine, a major antigenic adduct generated in acrolein-modified protein. *J Biol Chem, 278*(49), 48658-48665. doi:10.1074/jbc.M309401200

Furuhata, A., Nakamura, M., Osawa, T., & Uchida, K. (2002). Thiolation of protein-bound carcinogenic aldehyde. An electrophilic acrolein-lysine adduct that covalently binds to thiols. *J Biol Chem, 277*(31), 27919-27926. doi:10.1074/jbc.M202794200

Gnudi, L., Coward, R. J. M., & Long, D. A. (2016). Diabetic Nephropathy: Perspective on Novel Molecular Mechanisms. *Trends Endocrinol Metab, 27*(11), 820-830. doi:10.1016/j.tem.2016.07.002

Gong, Y., Zhai, G., Su, J., Yang, B., Jin, J., Liu, H., . . . Han, D. (2018). Different roles of insulin receptor a and b in maintaining blood glucose homeostasis in zebrafish. *Gen Comp Endocrinol, 269*, 33-45. doi:10.1016/j.ygcen.2018.08.012

Grigsby, J., Betts, B., Vidro-Kotchan, E., Culbert, R., & Tsin, A. (2012). A possible role of acrolein in diabetic retinopathy: involvement of a VEGF/TGFbeta signaling pathway of the retinal pigment epithelium in hyperglycemia. *Curr Eye Res, 37*(11), 1045-1053. doi:10.3109/02713683.2012.713152

Gugliucci, A. (2000). Glycation as the glucose link to diabetic complications. *J Am Osteopath Assoc, 100*(10), 621-634. Retrieved from http://www.ncbi.nlm.nih.gov/pubmed/11105451

Haberzettl, P., Vladykovskaya, E., Srivastava, S., & Bhatnagar, A. (2009). Role of endoplasmic reticulum stress in acrolein-induced endothelial activation. *Toxicol Appl Pharmacol, 234*(1), 14-24. doi:10.1016/j.taap.2008.09.019

He, J., Gao, H. X., Yang, N., Zhu, X. D., Sun, R. B., Xie, Y., . . . Wang, G. J. (2019). The aldose reductase inhibitor epalrestat exerts nephritic protection on diabetic nephropathy in db/db mice through metabolic modulation. *Acta Pharmacol Sin, 40*(1), 86-97. doi:10.1038/s41401-018-0043-5

Heng, L. Z., Comyn, O., Peto, T., Tadros, C., Ng, E., Sivaprasad, S., & Hykin, P. G. (2013). Diabetic retinopathy: pathogenesis, clinical grading, management and future developments. *Diabet Med, 30*(6), 640-650. doi:10.1111/dme.12089

Hengstermann, A., & Muller, T. (2008). Endoplasmic reticulum stress induced by aqueous extracts of cigarette smoke in 3T3 cells activates the unfolded-protein-response-dependent PERK pathway of cell survival. *Free Radic Biol Med, 44*(6), 1097-1107. doi:10.1016/j.freeradbiomed.2007.12.009

Jorgens, K., Stoll, S. J., Pohl, J., Fleming, T. H., Sticht, C., Nawroth, P. P., . . . Kroll, J. (2015). High tissue glucose alters intersomitic blood vessels in zebrafish via methylglyoxal targeting the VEGF receptor signaling cascade. *Diabetes, 64*(1), 213-225. doi:10.2337/db14-0352

Jung, S. H., Kim, Y. S., Lee, Y. R., & Kim, J. S. (2016). High glucose-induced changes in hyaloid-retinal vessels during early ocular development of zebrafish: a short-term animal model of diabetic retinopathy. *Br J Pharmacol, 173*(1), 15-26. doi:10.1111/bph.13279

Kaminskas, L. M., Pyke, S. M., & Burcham, P. C. (2007). Michael addition of acrolein to lysinyl and N-terminal residues of a model peptide: targets for cytoprotective hydrazino drugs. *Rapid Commun Mass Spectrom, 21*(7), 1155-1164. doi:10.1002/rcm.2945

Kasuga, M., Karlsson, F. A., & Kahn, C. R. (1982). Insulin stimulates the phosphorylation of the 95,000-dalton subunit of its own receptor. *Science, 215*(4529), 185-187. doi:10.1126/science.7031900

Kitaguchi, Y., Taraseviciene-Stewart, L., Hanaoka, M., Natarajan, R., Kraskauskas, D., & Voelkel, N. F. (2012). Acrolein induces endoplasmic reticulum stress and causes airspace enlargement. *PLoS One, 7*(5), e38038. doi:10.1371/journal.pone.0038038

Konermann, S., Brigham, M. D., Trevino, A. E., Joung, J., Abudayyeh, O. O., Barcena, C., . . . Zhang, F. (2015). Genome-scale transcriptional activation by an engineered CRISPR-Cas9 complex. *Nature, 517*(7536), 583-588. doi:10.1038/nature14136

Kowalski, A., Krikorian, A., & Lerma, E. V. (2015). Diabetes and chronic kidney disease. *Dis Mon, 61*(9), 378-386. doi:10.1016/j.disamonth.2015.07.002

Kurahashi, T., Kwon, M., Homma, T., Saito, Y., Lee, J., Takahashi, M., . . . Fujii, J. (2014). Reductive detoxification of acrolein as a potential role for aldehyde reductase (AKR1A) in mammals. *Biochem Biophys Res Commun, 452*(1), 136-141. doi:10.1016/j.bbrc.2014.08.072

Kusuhara, S., Fukushima, Y., Ogura, S., Inoue, N., & Uemura, A. (2018). Pathophysiology of Diabetic Retinopathy: The Old and the New. *Diabetes Metab J, 42*(5), 364-376. doi:10.4093/dmj.2018.0182

Lawson, N. D., & Weinstein, B. M. (2002). In vivo imaging of embryonic vascular development using transgenic zebrafish. *Dev Biol, 248*(2), 307-318. doi:10.1006/dbio.2002.0711

Li, J., Huang, B., Wang, S., Ji, X., Yin, J., Yang, N., . . . Ma, X. (2019). [Effect of diabetic management modes on diabetic nephropathy: a prospective study]. *Zhonghua Wei Zhong Bing Ji Jiu Yi Xue, 31*(12), 1497-1500. doi:10.3760/cma.j.issn.2095-4352.2019.12.012

Li, Q. R., Wang, Z., Zhou, W., Fan, S. R., Ma, R., Xue, L., . . . Yang, H. Y. (2016). Epalrestat protects against diabetic peripheral neuropathy by alleviating oxidative stress and inhibiting polyol pathway. *Neural Regen Res, 11*(2), 345-351. doi:10.4103/1673-5374.177745

Li, X., Schmohl, F., Qi, H., Bennewitz, K., Tabler, C. T., Poschet, G., . . . Kroll, J. (2020). Regulation of Gluconeogenesis by Aldo-keto-reductase 1a1b in Zebrafish. *iScience, 23*(12), 101763. doi:10.1016/j.isci.2020.101763

Liu, J., Wen, G., & Cao, D. (2009). Aldo-keto reductase family 1 member B1 inhibitors: old drugs with new perspectives. *Recent Pat Anticancer Drug Discov, 4*(3), 246-253. doi:10.2174/157489209789206931

Lodd, E., Wiggenhauser, L. M., Morgenstern, J., Fleming, T. H., Poschet, G., Buttner, M., . . . Kroll, J. (2019). The combination of loss of glyoxalase1 and obesity results in hyperglycemia. *JCI Insight, 4*(12). doi:10.1172/jci.insight.126154

Lou, M. F., Xu, G. T., Zigler, S., Jr., & York, B., Jr. (1996). Inhibition of naphthalene cataract in rats by aldose reductase inhibitors. *Curr Eye Res, 15*(4), 423-432. doi:10.3109/02713689608995833

Lovell, M. A., Xie, C., & Markesbery, W. R. (2001). Acrolein is increased in Alzheimer's disease brain and is toxic to primary hippocampal cultures. *Neurobiol Aging, 22*(2), 187-194. doi:10.1016/s0197-4580(00)00235-9

Mano, Y., Suzuki, K., Yamada, K., & Shimazono, N. (1961). Enzymic studies on TPN L-hexonate dehydrogenase from rat liver. *J Biochem, 49*, 618-634. doi:10.1093/oxfordjournals.jbchem.a127352

McCarthy, M. I. (2010). Genomics, type 2 diabetes, and obesity. *N Engl J Med, 363*(24), 2339-2350. doi:10.1056/NEJMra0906948

Medina-Navarro, R., Guzman-Grenfell, A. M., Diaz-Flores, M., Duran-Reyes, G., Ortega-Camarillo, C., Olivares-Corichi, I. M., & Hicks, J. J. (2007). Formation of an adduct between insulin and the toxic lipoperoxidation product acrolein decreases both the hypoglycemic effect of the hormone in rat and glucose uptake in 3T3 adipocytes. *Chem Res Toxicol, 20*(10), 1477-1481. doi:10.1021/tx7001355

Medina-Navarro, R., Guzmán-Grenfell, A. M., Díaz-Flores, M., Duran-Reyes, G., Ortega-Camarillo, C., Olivares-Corichi, I. M., & Hicks, J. J. (2007). Formation of an adduct between insulin and the toxic lipoperoxidation product acrolein decreases both the hypoglycemic effect of the hormone in rat and glucose uptake in 3T3 adipocytes. *Chem Res Toxicol, 20*(10), 1477-1481. doi:10.1021/tx7001355

Mohammad, M. K., Avila, D., Zhang, J., Barve, S., Arteel, G., McClain, C., & Joshi-Barve, S. (2012). Acrolein cytotoxicity in hepatocytes involves endoplasmic reticulum stress, mitochondrial dysfunction and oxidative stress. *Toxicol Appl Pharmacol, 265*(1), 73-82. doi:10.1016/j.taap.2012.09.021

Moller, D. E., Yokota, A., Caro, J. F., & Flier, J. S. (1989). Tissue-specific expression of two alternatively spliced insulin receptor mRNAs in man. *Mol Endocrinol, 3*(8), 1263-1269. doi:10.1210/mend-3-8-1263

Moretto, N., Volpi, G., Pastore, F., & Facchinetti, F. (2012). Acrolein effects in pulmonary cells: relevance to chronic obstructive pulmonary disease. *Ann N Y Acad Sci, 1259*, 39-46. doi:10.1111/j.1749-6632.2012.06531.x

Mueckler, M., & Thorens, B. (2013). The SLC2 (GLUT) family of membrane transporters. *Mol Aspects Med, 34*(2-3), 121-138. doi:10.1016/j.mam.2012.07.001

Noiri, E., Yamada, S., Nakao, A., Tsuchiya, M., Masaki, I., Fujino, K., . . . Uchida, K. (2002). Serum protein acrolein adducts: utility in detecting oxidant stress in hemodialysis patients and reversal using a vitamin E-bonded hemodialyzer. *Free Radic Biol Med, 33*(12), 1651-1656. doi:10.1016/s0891-5849(02)01138-3

O'Connor, T., Ireland, L. S., Harrison, D. J., & Hayes, J. D. (1999). Major differences exist in the function and tissue-specific expression of human aflatoxin B1

aldehyde reductase and the principal human aldo-keto reductase AKR1 family members. *Biochem J, 343 Pt 2*, 487-504. Retrieved from https://www.ncbi.nlm.nih.gov/pubmed/10510318

Olson, A. L., Trumbly, A. R., & Gibson, G. V. (2001). Insulin-mediated GLUT4 translocation is dependent on the microtubule network. *J Biol Chem, 276*(14), 10706-10714. doi:10.1074/jbc.M007610200

Penning, T. M. (2015). The aldo-keto reductases (AKRs): Overview. *Chem Biol Interact, 234*, 236-246. doi:10.1016/j.cbi.2014.09.024

Perner, B., Englert, C., & Bollig, F. (2007). The Wilms tumor genes wt1a and wt1b control different steps during formation of the zebrafish pronephros. *Dev Biol, 309*(1), 87-96. doi:10.1016/j.ydbio.2007.06.022

Ramana, K. V. (2011). ALDOSE REDUCTASE: New Insights for an Old Enzyme. *Biomol Concepts, 2*(1-2), 103-114. doi:10.1515/BMC.2011.002

Rezzola, S., Belleri, M., Gariano, G., Ribatti, D., Costagliola, C., Semeraro, F., & Presta, M. (2014). In vitro and ex vivo retina angiogenesis assays. *Angiogenesis, 17*(3), 429-442. doi:10.1007/s10456-013-9398-x

Saeedi, P., Petersohn, I., Salpea, P., Malanda, B., Karuranga, S., Unwin, N., . . . Committee, I. D. F. D. A. (2019). Global and regional diabetes prevalence estimates for 2019 and projections for 2030 and 2045: Results from the International Diabetes Federation Diabetes Atlas, 9(th) edition. *Diabetes Res Clin Pract, 157*, 107843. doi:10.1016/j.diabres.2019.107843

Sakata, K., Kashiwagi, K., Sharmin, S., Ueda, S., Irie, Y., Murotani, N., & Igarashi, K. (2003). Increase in putrescine, amine oxidase, and acrolein in plasma of renal failure patients. *Biochem Biophys Res Commun, 305*(1), 143-149. doi:10.1016/s0006-291x(03)00716-2

Sano, H., Kane, S., Sano, E., Miinea, C. P., Asara, J. M., Lane, W. S., . . . Lienhard, G. E. (2003). Insulin-stimulated phosphorylation of a Rab GTPase-activating protein regulates GLUT4 translocation. *J Biol Chem, 278*(17), 14599-14602. doi:10.1074/jbc.C300063200

Schlondorff, D., & Banas, B. (2009). The mesangial cell revisited: no cell is an island. *J Am Soc Nephrol, 20*(6), 1179-1187. doi:10.1681/ASN.2008050549

Schmohl, F., Peters, V., Schmitt, C. P., Poschet, G., Buttner, M., Li, X., . . . Kroll, J. (2019). CNDP1 knockout in zebrafish alters the amino acid metabolism, restrains weight gain, but does not protect from diabetic complications. *Cell Mol Life Sci, 76*(22), 4551-4568. doi:10.1007/s00018-019-03127-z

Shah, O. J., Wang, Z., & Hunter, T. (2004). Inappropriate activation of the TSC/Rheb/mTOR/S6K cassette induces IRS1/2 depletion, insulin resistance, and cell survival deficiencies. *Curr Biol, 14*(18), 1650-1656. doi:10.1016/j.cub.2004.08.026

Steckelings, U. M., Rompe, F., Kaschina, E., & Unger, T. (2009). The evolving story of the RAAS in hypertension, diabetes and CV disease: moving from macrovascular to microvascular targets. *Fundam Clin Pharmacol, 23*(6), 693-703. doi:10.1111/j.1472-8206.2009.00780.x

Stevens, J. F., & Maier, C. S. (2008). Acrolein: sources, metabolism, and biomolecular interactions relevant to human health and disease. *Mol Nutr Food Res, 52*(1), 7-25. doi:10.1002/mnfr.200700412

Stomberski, C. T., Anand, P., Venetos, N. M., Hausladen, A., Zhou, H. L., Premont, R. T., & Stamler, J. S. (2019). AKR1A1 is a novel mammalian S-nitroso-glutathione reductase. *J Biol Chem, 294*(48), 18285-18293. doi:10.1074/jbc.RA119.011067

Sultana, R., Perluigi, M., & Butterfield, D. A. (2013). Lipid peroxidation triggers neurodegeneration: a redox proteomics view into the Alzheimer disease brain. *Free Radic Biol Med, 62*, 157-169. doi:10.1016/j.freeradbiomed.2012.09.027

Summary of revisions for the 2010 Clinical Practice Recommendations. (2010). *Diabetes Care, 33 Suppl 1*, S3. doi:10.2337/dc10-S003

Suzen, S., & Buyukbingol, E. (2003). Recent studies of aldose reductase enzyme inhibition for diabetic complications. *Curr Med Chem, 10*(15), 1329-1352. doi:10.2174/0929867033457377

Tang, M. S., Wang, H. T., Hu, Y., Chen, W. S., Akao, M., Feng, Z., & Hu, W. (2011). Acrolein induced DNA damage, mutagenicity and effect on DNA repair. *Mol Nutr Food Res, 55*(9), 1291-1300. doi:10.1002/mnfr.201100148

Thomas, R. L., Halim, S., Gurudas, S., Sivaprasad, S., & Owens, D. R. (2019). IDF Diabetes Atlas: A review of studies utilising retinal photography on the global prevalence of diabetes related retinopathy between 2015 and 2018. *Diabetes Res Clin Pract, 157*, 107840. doi:10.1016/j.diabres.2019.107840

Thorens, B., Sarkar, H. K., Kaback, H. R., & Lodish, H. F. (1988). Cloning and functional expression in bacteria of a novel glucose transporter present in liver, intestine, kidney, and beta-pancreatic islet cells. *Cell, 55*(2), 281-290. doi:10.1016/0092-8674(88)90051-7

Toyoda, F., Tanaka, Y., Ota, A., Shimmura, M., Kinoshita, N., Takano, H., . . . Kakehashi, A. (2014). Effect of ranirestat, a new aldose reductase inhibitor, on diabetic retinopathy in SDT rats. *J Diabetes Res, 2014*, 672590. doi:10.1155/2014/672590

Toyoshima, Y., Monson, C., Duan, C., Wu, Y., Gao, C., Yakar, S., . . . LeRoith, D. (2008). The role of insulin receptor signaling in zebrafish embryogenesis. *Endocrinology, 149*(12), 5996-6005. doi:10.1210/en.2008-0329

Tsukahara, H., Sekine, K., Uchiyama, M., Kawakami, H., Hata, I., Todoroki, Y., . . . Mayumi, M. (2003). Formation of advanced glycosylation end products and oxidative stress in young patients with type 1 diabetes. *Pediatr Res, 54*(3), 419-424. doi:10.1203/01.PDR.0000076662.72100.74

Uchida, K. (2000). Role of reactive aldehyde in cardiovascular diseases. *Free Radic Biol Med, 28*(12), 1685-1696. doi:10.1016/s0891-5849(00)00226-4

Uchida, K., Kanematsu, M., Morimitsu, Y., Osawa, T., Noguchi, N., & Niki, E. (1998). Acrolein is a product of lipid peroxidation reaction. Formation of free acrolein and its conjugate with lysine residues in oxidized low density lipoproteins. *J Biol Chem, 273*(26), 16058-16066. doi:10.1074/jbc.273.26.16058

Uchida, K., Kanematsu, M., Sakai, K., Matsuda, T., Hattori, N., Mizuno, Y., . . . Osawa, T. (1998). Protein-bound acrolein: potential markers for oxidative stress. *Proc Natl Acad Sci U S A, 95*(9), 4882-4887. doi:10.1073/pnas.95.9.4882

Uil, M., Scantlebery, A. M. L., Butter, L. M., Larsen, P. W. B., de Boer, O. J., Leemans, J. C., . . . Roelofs, J. (2018). Combining streptozotocin and unilateral nephrectomy is an effective method for inducing experimental diabetic nephropathy in the 'resistant' C57Bl/6J mouse strain. *Sci Rep, 8*(1), 5542. doi:10.1038/s41598-018-23839-9

Uldry, M., & Thorens, B. (2004). The SLC2 family of facilitated hexose and polyol transporters. *Pflugers Arch, 447*(5), 480-489. doi:10.1007/s00424-003-1085-0

Vega, M. C., Lorentzen, E., Linden, A., & Wilmanns, M. (2003). Evolutionary markers in the (beta/alpha)8-barrel fold. *Curr Opin Chem Biol, 7*(6), 694-701. doi:10.1016/j.cbpa.2003.10.004

Wang, G., Ouyang, J., Li, S., Wang, H., Lian, B., Liu, Z., & Xie, L. (2019). The analysis of risk factors for diabetic nephropathy progression and the construction of a prognostic database for chronic kidney diseases. *J Transl Med, 17*(1), 264. doi:10.1186/s12967-019-2016-y

Wermuth, B., & Monder, C. (1983). Aldose and aldehyde reductase exhibit isocorticosteroid reductase activity. *Eur J Biochem, 131*(2), 423-426. doi:10.1111/j.1432-1033.1983.tb07280.x

Whitehead, M., Wickremasinghe, S., Osborne, A., Van Wijngaarden, P., & Martin, K. R. (2018). Diabetic retinopathy: a complex pathophysiology requiring novel therapeutic strategies. *Expert Opin Biol Ther, 18*(12), 1257-1270. doi:10.1080/14712598.2018.1545836

Wiggenhauser, L. M., Kohl, K., Dietrich, N., Hammes, H. P., & Kroll, J. (2017). Studying Diabetes Through the Eyes of a Fish: Microdissection, Visualization, and Analysis of the Adult tg(fli:EGFP) Zebrafish Retinal Vasculature. *J Vis Exp*(130). doi:10.3791/56674

Wiggenhauser, L. M., Qi, H., Stoll, S. J., Metzger, L., Bennewitz, K., Poschet, G., . . . Kroll, J. (2020). Activation of Retinal Angiogenesis in Hyperglycemic pdx1 (-/-) Zebrafish Mutants. *Diabetes, 69*(5), 1020-1031. doi:10.2337/db19-0873

Wise, E., Yew, W. S., Babbitt, P. C., Gerlt, J. A., & Rayment, I. (2002). Homologous (beta/alpha)8-barrel enzymes that catalyze unrelated reactions: orotidine 5'-monophosphate decarboxylase and 3-keto-L-gulonate 6-phosphate decarboxylase. *Biochemistry, 41*(12), 3861-3869. doi:10.1021/bi012174e

Yang, B. Y., Zhai, G., Gong, Y. L., Su, J. Z., Peng, X. Y., Shang, G. H., . . . Xie, S. Q. (2018). Different physiological roles of insulin receptors in mediating nutrient metabolism in zebrafish. *Am J Physiol Endocrinol Metab, 315*(1), E38-E51. doi:10.1152/ajpendo.00227.2017

Yau, J. W., Rogers, S. L., Kawasaki, R., Lamoureux, E. L., Kowalski, J. W., Bek, T., . . . Meta-Analysis for Eye Disease Study, G. (2012). Global prevalence and major risk factors of diabetic retinopathy. *Diabetes Care, 35*(3), 556-564. doi:10.2337/dc11-1909

Zhang, J., Gao, Z., Yin, J., Quon, M. J., & Ye, J. (2008). S6K directly phosphorylates IRS-1 on Ser-270 to promote insulin resistance in response to TNF-(alpha) signaling through IKK2. *J Biol Chem, 283*(51), 35375-35382. doi:10.1074/jbc.M806480200

Zhang, J., Wang, Y., Gurung, P., Wang, T., Li, L., Zhang, R., . . . Liu, F. (2018). The relationship between the thickness of glomerular basement membrane and renal outcomes in patients with diabetic nephropathy. *Acta Diabetol, 55*(7), 669-679. doi:10.1007/s00592-018-1128-9

Zhang, L., Lee, J. J., Tang, H., Fan, Y. H., Xiao, L., Ren, H., . . . Mao, L. (2008). Impact of smoking cessation on global gene expression in the bronchial epithelium of chronic smokers. *Cancer Prev Res (Phila), 1*(2), 112-118. doi:10.1158/1940-6207.CAPR-07-0017

Zhang, X., Lai, Y., McCance, D. R., Uchida, K., McDonald, D. M., Gardiner, T. A., . . . Curtis, T. M. (2008). Evaluation of N (epsilon)-(3-formyl-3,4-dehydropiperidino)lysine as a novel biomarker for the severity of diabetic retinopathy. *Diabetologia, 51*(9), 1723-1730. doi:10.1007/s00125-008-1071-3

Zheng, Y., Ley, S. H., & Hu, F. B. (2018). Global aetiology and epidemiology of type 2 diabetes mellitus and its complications. *Nat Rev Endocrinol, 14*(2), 88-98. doi:10.1038/nrendo.2017.151

Zhou, H. L., Zhang, R., Anand, P., Stomberski, C. T., Qian, Z., Hausladen, A., . . . Stamler, J. S. (2019). Metabolic reprogramming by the S-nitroso-CoA

reductase system protects against kidney injury. *Nature, 565*(7737), 96-100. doi:10.1038/s41586-018-0749-z

Zimmet, P., Alberti, K. G., & Shaw, J. (2001). Global and societal implications of the diabetes epidemic. *Nature, 414*(6865), 782-787. doi:10.1038/414782a.

7 PUBLICATION LIST

Some parts of the experimental work, although not included in this written thesis, has been published in the following journal:

Activation of Retinal Angiogenesis in Hyperglycemic *pdx1*$^{-/-}$ Zebrafish Mutants
Lucas M. Wiggenhauser, **Haozhe Qi**, Sandra J. Stoll, Lena Metzger, Katrin Bennewitz, Gernot Poschet, Guido Krenning, Jan-Luuk Hillebrands, Hans-Peter Hammes, and Jens Kroll
Diabetes, 2020 May;69(5):1020-1031. DOI: 10.2337/db19-0873. Epub 2020 Mar 5.

Regulation of Gluconeogenesis by Aldo-keto-reductase 1a1b in Zebrafish
Xiaogang Li, Felix Schmöhl, **Haozhe Qi**, Katrin Bennewitz, Christoph T. Tabler, Gernot Poschet, Rüdiger Hell, Nadine Volk, Tanja Poth, Ingrid Hausser, Jakob Morgenstern, Thomas Fleming, Peter Paul Nawroth and Jens Kroll
iScience, 2020 Nov 3;23(12):101763. DOI: 10.1016/j.isci.2020.101763.
eCollection 2020 Dec 18.

The main parts of this thesis are currently in preparation for publication:

The accumulated acrolein in *akr1a1a* zebrafish mutants promotes insulin resistance leading to hyperglycemia and retina vessels alteration
Haozhe Qi, Felix Schmöhl, Xiaogang Li, Katrin Bennewitz, Thomas Fleming, Jakob Morgenstern, Nadine Volk, Tanja Poth, Poschet Gernot, Elena Heidenreich, Carsten Sticht, Peter Paul Nawroth, Jens Kroll

Planned for submission in March 2021

8 CURRICULUM VITAE

Personal Information

Name:	Haozhe Qi
Date of birth:	12.07.1992
Place of birth:	Xining, Qinghai, China
Marital status:	married
Father:	Zhen Qi, civil servant
Mother:	Limei Mu, civil servant
Wife:	Wei He

Primary School Education

09.1998 – 06.2004	Qilianshan Primary School, Haibei, Qinghai
09.2004 – 06.2007	Hutai Junior High School, Xining, Qinghai
09.2007 – 06.2010	Huangchuan High School, Xining, Qinghai

University Education

09.2010–06.2015	Bachelor of Medicine, Xiangya Medical school, Central South University, Hunan Province, China
09.2015–06.2018	Master of Medicine, Medical School, Shanghai Jiao Tong University, Shanghai, China
10.2018 – Present	Medical Faculty Mannheim, Heidelberg University, Germany

9 ACKNOWLEGEMENT

I thank everyone who contributed to the successful completion of this work.

At first, my deepest gratitude goes to Prof. Dr. Jens Kroll, my supervisor, who made it possible for me to accomplish my MD/Dr.med study, for his constant guidance, great encouragement and useful advice he has provided throughout my research.

Then, I would like to express my heartfelt gratitude to the whole Kroll-Lab team, which has accompanied and assisted me in the past three years. Katrin Bennewitz, Xiaogang Li, Dr. Bowen Lou, Mike Boger, David Wohlfart, Christoph T. Table, Lena Metzger, Middel Chiara, Huehn Bjoern, Xin Qian and everyone else, who has brought the laboratory to life, thank you.

I also thank, Dr. Gernot Poschet, Elena Heidenreich, Dr. Carsten Sticht, Dr.Carolina De La Torre, Dr. Thomas Flemming, Dr. Jakob Morgenstern, Prof. Dr. Peter Paul Nawroth, Prof. Dr. Hans-Peter Hammes and Live Cell Imaging Mannheim, for all the technical sustentation, excellent instruction and cooperation.

Furthermore, I would like to thank all the support from the SFB1118, the GRK 1874 DIAMICOM and China Scholarship Council (CSC).

Last, I would like to say thanks to my beloved family, my parents and my wife, for their loving consideration and great confidence in me all through these years. As well, thanks for being all the things that make you.